# Sol-gel derived nano-silica suspensions for inclusion in cement paste

**Dulani Pankaja Abeysing Kodippili**

A Thesis
In the Department
of
Building, Civil and Environmental Engineering

Presented in Partial Fulfillment of the Requirements
For the Degree of
Doctor of Philosophy (Building Engineering) at
Concordia University
Montreal, Quebec, Canada
July 2020

**CONCORDIA UNIVERSITY**

**SCHOOL OF GRADUATE STUDIES**

This is to certify that the thesis prepared

By: Dulani Pankaja Abeysing Kodippili

Entitled: Sol-gel derived nano-silica suspensions for inclusion in cement paste

and submitted in partial fulfillment of the requirements for the degree of

Doctor Of Philosophy (Building Engineering)

complies with the regulations of the University and meets the accepted standards with respect to originality and quality.

Signed by the final examining committee:

_____ Chair
Dr. Ahmed Kishk

_____ External Examiner
Dr. Karl W. Peterson

_____ External to Program
Dr. Martin D. Pugh

_____ Examiner
Dr. Catherine Mulligan

_____ Examiner
Dr. Ahmed Soliman

_____ Thesis Co-Supervisor
Dr. Michelle Nokken

_____ Thesis Co-Supervisor
Dr. Robin Drew

Approved by _____
Dr. Michelle Nokken, Graduate Program Director

August 25, 2020

_____

Dr. Mourad Debbabi, Dean
Gina Cody School of Engineering and Computer Science

## ABSTRACT

**Sol-gel derived nano-silica suspensions for inclusion in cement paste**

**Dulani P. A. Kodippili, Ph.D.**

**Concordia University, 2020**

Nano-silica (NS) is one of the most widely used nanomaterials in the cement industry, the addition of which delivers many advantages in improving the properties of hardened cement. It has been proven that NS can increase the strength, reduce the permeability, increase the durability, and reduce the $CO_2$ emissions by lessening the usage of cement. However, the associated problems such as the agglomeration of NS and uneven dispersion of NS in the cement pastes limit its potential benefits.

These problems were addressed in this research by optimizing the method of NS incorporation. NS was synthesized by the sol-gel method and was utilized in cement as a suspension of calcium hydroxide. The hydration of cement with the sol-gel derived NS was studied using various techniques such as isothermal calorimetry, differential scanning calorimetry, mercury intrusion porosimetry, scanning electron microscopy, non-evaporable water content measurements, and X-ray diffraction with Rietveld refinement as well as mechanical properties. The optimum amount of NS was determined to be approximately 4% and perhaps as low as 2% if ultra sonification is utilized. It was shown that the NS synthesized by this method increased the rate of hydration by 12% in two days in terms of energy. Calcium hydroxide consumption and refinement of the microstructure and pore structure improved until this optimum amount. Moreover, the mechanical strength was improved up 35% in two days and 50% in seven days. The limitations of the NS usage can be minimized by this novel approach of NS incorporation.

**Acknowledgement**

I wish to thank Dr. Michelle Nokken and Dr. Robin Drew for supervising me during my PhD work. Moreover, I wish to thank Dr. Ehsan Rezabeigi for his kind mentoring. Also, I wish to acknowledge, my colleagues and friends for all their help.

I would like to extend my thanks to all the technical staff in the BCEE and MIAE departments for their assistance for the experiment set ups. Moreover, I wish to acknowledge the technical staff of the facility for electron microscope research for providing access to their facility. Also, I wish to thank Lafarge and Levasil for providing cement and nano-silica for the research.

I am also grateful to my family for supporting me all the time.

# Table of Contents

# List of Figures

# List of Tables

# Chapter 1

# Introduction

Concrete is one of the most widely used materials. This is especially true in the construction industry within which concrete has been a material of choice for a number of years. The annual worldwide production of concrete is approximately 20 billion tons [1,2]. It is a composite material composed of amorphous and crystalline phases ranging in size from nanometers to micrometers, and bound water [3]. Cement is one of the main components of the widely used construction material, concrete. As production of cement is an energy consuming and expensive process, supplementary cementitious materials (SCM) have been researched in order to reduce the usage of cement and to enhance the properties of concrete. However, the concrete produced with supplementary materials such as fly ash has a lower early strength and delayed setting times. This issue becomes worse during the cold weather seasons [4]. Therefore, nanoparticles which have the potential of avoiding those drawbacks have attracted attention in the concrete industry. Nanoparticles have also gained much interest in the concrete industry due to many reasons including the enhancement of performance of hardened concrete, fresh and rheological properties, and durability. Some nanoparticles can impart not only these properties but also can give a photocatalytic nature which results in the self-cleaning property and self-consolidating features in concrete [5].

There are many nanoparticles that have been researched for incorporation in concrete. Nano silica, nano $CaCO_3$, nano $Fe_2O_3$, nano $ZrO_2$, nano $TiO_2$, nano $ZnO_2$, nano $Al_2O_3$, carbon nano tubes, nano clays, nano cement particles of $C_2S$ (alite) and $C_3S$ (belite). Nanoparticles can enhance the performance of concrete by means of both physical and chemical mechanisms. The physical mechanism is that nanoparticles fill up voids making denser concrete. In chemical manner, nanoparticles can provide seeds for the nucleation of hydration products thus accelerating cement hydration. This nuclei formation not only occurs on the surface of cement grains but also within the pores of cement paste due to nanoparticles [6].

Although NS has many advantages, there are also several drawbacks which hinder their wide deployment in concrete. Being in nano size, the nanoparticles have a larger surface area compared to micro, or other larger scale materials. Thus, their surface energy is very high. As a result, they tend to agglomerate themselves to reduce the energy. Also, as the particle size decreases, the interparticle attractive forces (specially Van der Waals) increases compared to the gravitational forces [7]. Therefore, if the attractive forces exceed the repulsive forces, the particles will agglomerate. When the nanoparticles are in a dispersion, they have random motions which are called Brownian motion which cause collisions of particles. As the particle size decreases, the distance between the particles in a constant volume reduces [7]. Therefore, the probability of the collisions increases with the particle size reduction [7]. This also leads to formation of agglomerates in the nanoparticle dispersions.

When the agglomeration occurs, the nanoparticles cannot deliver their maximum beneficial effects on the cement paste/ concrete due to the reduction of the effective surface area. The larger agglomerates can remain in the cement paste without reacting. Moreover, a homogeneous dispersion of NS throughout the cement paste is impossible when agglomeration is present. Unreacted NS particles which are the result of agglomeration could cause minute areas of low strength and voids by leaching the particles. The optimum NS amount that might be introduced to cement has not yet been well identified. Many researchers reported different quantities which

depended on the overall properties of NS and its production route. The bulk production of NS economically for concrete is another issue which should be resolved.

## 1.1. Research scope and objectives

As such, a proper mechanism is required to disperse nano-silica particles in concrete and to achieve the effect of reactivity of NS. While some researchers have used high energy mixing in order to disperse nanoparticles in cementitious matrices [8], it is questionable that the proper dispersion is achievable by this method in bulk concrete production. Therefore, production of NS in liquid state, application of surfactants, ultrasonication and microwave drying have been suggested to eliminate agglomerated NS products [9]. From the sol-gel method, it is possible to obtain NS in the gelled state which can be useful to ensure proper dispersion of NS within concrete while achieving the required consistency.

### 1.1.1 The research objectives in this thesis

1. ***Optimize NS particle production***

In order to address the agglomeration and high-water demand issues of NS, this research suggests using sol-gel derived NS as a suspension in calcium hydroxide. By this method, it was hypothesized that calcium hydroxide, which is a strong base, would be able to reduce the agglomeration of NS while maintaining the same pH (11-12) of the cement gel. Moreover, some processing steps of the sol-gel method such as drying and stabilization, can be eliminated by using sol-gel derived NS added directly as a suspension.

2. ***Investigate incorporation into cement pastes as a suspension***

Another problem of using NS in cement is the difficulty of even dispersion of particles throughout the cement paste. This occurs when NS is being used in powdered form. To overcome this problem, using NS as a suspension is studied in this research.

3. ***Investigate hydration and strength***

The characteristics of NS depend on its production route. When including NS in concrete, these characteristics can affect the hydration of cement which consequently affects the properties of concrete. In this research, the hydration of cement with sol-gel derived silica is studied using different methods. As well, mechanical properties are examined.

4. ***Determine optimum NS additions***

Due to the agglomeration of nanoparticles, the quantity of nanoparticles which can be used in concrete is currently limited. The optimum amount of NS which can be used as a replacement of cement has not yet been well understood. Many researchers could not use NS beyond 4% of cement while improving the properties of cement [10–13]. Exceeding these amounts of NS have caused a reduction in the expected properties of hardened cement paste. In this research, it is investigated if it is possible to increase the NS amount used in cement by using NS produced by this method. In this research, NS suspensions were tested up to 8% to determine the performance.

## Outline

The contents of this thesis are outlined as below.

**Chapter 2**

Chapter 2 presents a thorough literature review on the current research on the incorporation of NS in cement/concrete. This includes the NS production methods that are used by other researchers for the association of cement/concrete and how the production method would affect the properties of NS and ultimately the properties of concrete which includes NS. Moreover, the techniques that the researchers use to characterize the NS included cement paste are reviewed. Furthermore, the gaps and issues in the present research on this subject are discussed.

**Chapter 3**

Chapter 3 discusses the experimental program utilized to achieve the objectives of this research. The materials, the procedures, the techniques, the theories behind the techniques, the instruments used in this study are explained in detail in this section.

**Chapter 4**

This chapter presents the results obtained by the experimental program. The separate results obtained by each technique and procedure are explained individually. Furthermore, the outcomes obtained by each variable are illustrated here.

**Chapter 5**

To draw the complete picture, the relationships, and the co-relations of individual results are analyzed in Chapter 5. The results are analyzed and compared with other researchers' findings. Besides, the possible errors and the efforts to avoid them are discussed here.

**Chapter 6**

This chapter explains the conclusions drawn by the results and the discussion. Moreover, it discusses possible future research avenues after this project and potential improvements that can be studied on the incorporation of the sol-gel synthesized NS in cement/concrete.

# Literature Review

Chapter 2

Research regarding manufacturing nano-silica (NS) for the purpose of improving cement hydration and hardened properties has been receiving significant attention within the research community over the past few years. In this chapter, the concepts and the background theories will be discussed. Also the work related to different types of NS, the methods of NS production, the sol-gel method in NS production, the properties of NS including hardened cement/mortar/concrete, and the techniques that can be utilized to evaluate those properties will be reviewed.

## Concrete

2.1

Concrete is a material which is comprised of cement, water, sand, and rock, where the sand and rock are bound by the hardened hydrated cement. Concrete is one of the most common man-made composite materials and has become very popular in the construction industry due to its ease of use and higher reasonable compressive strength. Yet, the tensile strength of concrete is very poor, so that steel bars are used in the concrete structures to reinforce them to withstand tensile loads. Concrete is also an inert material to many chemicals and can be fabricated into many shapes. Concrete can be designed in numerous ways by varying the main ingredients and sometimes adding additional ingredients to achieve different compressive strengths and other desired properties. There are some nominal mixing ratios set by different standardization authorities for the main ingredients in order to achieve different compressive strengths. However, the resulting strength can vary depending on the quality of the main ingredients even if the nominal mixing ratios are used. The additional chemicals, minerals, and surfactants that are used in concrete are called admixtures. The admixtures are incorporated in concrete to obtain the fresh (wet) properties and the properties of the hardened concrete that cannot be achieved by concrete itself (e.g. longer flowability, air entrainment, etc.).

2.2.

## Cement

Cement is the material that provides the binding ability to the concrete. Cement reacts and holds the sand, the rock, the steel, etc. in the matrix of concrete by binding this inhomogeneous multiscale mixture of materials. The cement can be categorized into two types depending on their basis of hardening, hydraulic or non-hydraulic. The hardening of hydraulic cement is called hydration. The hydration of hydraulic cement requires water which reacts with cement and this process continues over a long period of time. The main resultant products formed by hydration are calcium silicate hydrate (CSH) gel and calcium hydroxide (CH). The non-hydraulic cement does not harden in water but hardens by reacting with the carbon dioxide in the air. Portland cement is the mostly used hydraulic cement.

The Portland cement is made of minerals that contain mainly the oxides of Calcium, Silicon, Aluminum, and Iron. As such, there are two types of raw materials which are used in cement manufacturing. The first is lime containing materials which provide calcium oxide and the other is clay which provides the silica, alumina, and iron oxides while providing less lime. The lime is obtained by extracting limestone, chalk, and marl which have calcium carbonate as the main constituent. Clay, shale, slags, and other such raw materials also provide the hydrates of aluminum silicates, iron hydroxides, sand, and calcium. These raw materials are heated up to around 1400℃ – 1500℃ in a kiln to break down into the required oxides. However, the correct mixture of raw materials should be fed to the kiln to achieve the product called clinker. The clinker

is formed like lumps or nodules. The clinker is cooled down and then ground to a very fine powder form (approximately 150 μm) after mixing with gypsum. Gypsum is added to the cement to control the setting of the cement.

Due to the large amount of energy required to heat the raw materials, cement manufacturing is an energy intensive process. Also, this process releases a large quantity of greenhouse gases, especially carbon dioxide, by decomposing limestone (calcium carbonate – $CaCO_3$) to obtain lime (calcium oxide - CaO). As this process requires a large amount of energy, the requirement of burning fuels which releases another large quantity of greenhouse gases is necessary. Therefore, the usage of supplementary cementing materials (SCMs) to reduce the greenhouse gases is essential.

## Materials used in construction industry to replace cement

SCMs are the materials that are being used in the construction industry to replace cement and which contribute to form the hardened concrete structure because of their hydraulic or pozzolanic nature. The pozzolanic nature can be explained as the ability of a siliceous or aluminous material which are not cementitious to form the cementitious compounds in the presence of calcium hydroxide and moisture. The pozzolanic reaction is as follows;

**2.3.**

$$SiO_2 + Ca(OH)_2 \rightarrow C\text{-}S\text{-}H$$

The reactions of SCMs range from mainly hydraulic and to mainly pozzolanic. Fly ash, slag, metakaolin, and silica fume are some of the common SCMs used in the construction industry. They are usually added to concrete as a replacement instead of an addition. Silica fume, or microsilica, is a by-product of silicon metal production as has an average particle size of approximately 0.1 microns (100 nm). Microsilica has been used in concrete for decades and produces notable increases in strength and durability at relatively low replacement levels (5-10%). As silica fume consists of mainly $SiO_2$, the reaction is pozzolanic.

**2.4.**

## Nanoparticles

Nanoparticles have one or more dimensions between 1 – 100 nm in size. Therefore, nanoparticles have a larger surface which gives higher reactivity to the material and therefore its behaviour is different from the bulk cement particles. When nanoparticles are incorporated into cement pastes, the cement hydration reactions can be altered owing to the mentioned facts. Thus, a thorough study of the behavior of nanoparticles is essential to the construction industry. This thesis investigates the production and the incorporation of one such type of promising nanoparticles in cement paste to suit the construction industry, namely nano-silica.

**2.5.**

## Nanotechnology in concrete

Nanotechnology came into the interest of the scientists after the famous talk by physicist, Richard Feynman, titled “There’s plenty of room at the bottom” in 1959 [14]. In his talk, he explained processes and the possibilities of controlling and changing things on a small scale [14]. Also, he explained the possibilities of manipulating atoms and molecules to obtain marvellous differences in bulk [14]. According to Iqbal et al. “Nanotechnology involves the study, imaging, measuring, modeling, or manipulation of matter at scales falling in the range of 1–100 nanometers (nm)” [15]. The fabrication techniques in nanotechnology can be categorized into two approaches;

which are top – down and bottom – up [15]. In the top – down approach, the bulk materials are modified to obtain small structures. In contrast to that, atoms and molecules are used as the building blocks to organize the bulk structures in the bottom – up approach [15]. Many chemical synthesis processes are involved in the bottom – up approach. In this research, the bottom – up approach is used to synthesize the nano-silica.

As the properties vary over time, concrete is a complex material. The bulk properties of this complex material can be improved by nano level modifications to its composition. The gel structure of the cement paste in concrete has nano pores which is a nanostructure itself. Therefore, extensive research is being carried out to build up the bridge between nanotechnology and concrete. Nanotechnology can be utilized in concrete in the areas of cement hydration, influence of nanoparticles in concrete and coatings [16]. Birgisson et al. [17] identified some outcomes such as high performance concrete, sustainable and safe concrete materials, intelligent concrete, and novel concrete materials by processing cement and cement pastes wherein nanotechnology can be employed to develop concrete.

## Nano-silica (NS)

2.6. Nano-silica (NS) is nanoparticles of the oxide of silicon namely, silica ($SiO_2$). Silica can be found both in amorphous and crystalline forms. The most abundant form of silica in nature is quartz as sand. Quartz has a crystalline structure of silica. The volcanic ashes are one of the naturally occurring silicas in the amorphous form. The amorphous silica has the pozzolanic nature which can be utilized to form cementitious materials.

Similarly, nano-silica has pozzolanic behavior attributed to its amorphous structure. When it comes to nano scale, the amorphousness dominates over the crystallinity of the particles as there are a fewer number of molecules in a particle. This in turn increases the reactivity of the nanoparticles. Thus, the nano-silica can be considered as a SCM. To this end, nano-silica is investigated in this research as a replacement for the cement taking that fact into account.

$SiO_2$ is one of the most promising among available nano materials which has been investigated for its performance with cement. Nano-silica (NS) can improve the properties of both fresh and hardened concrete in many aspects. In general, research studies have been carried out to improve properties of concrete such as workability, hydration, and mechanical strength, resistance to water penetration and durability. Moreover, NS was used to increase the effectiveness of cementitious additive materials in cement such as fly ash and silica fume. These aspects will be discussed in later sections.

2.7.

## Comparison of Cementitious material with NS and silica fume

The study of Sharma et al. [18] showed the effects of two different sizes of NS on mortar. They investigated 8 -15 nm and 100 – 300 nm size NS in their study. The latter had particle sizes similar to silica fume. Their study revealed that smaller NS had higher reactivity during the first 24 hours of hydration by lime reaction analysis. Furthermore, according to their study, the reactivity was ~60% higher.

The work of Haruehansapong et al.[19] also showed that the cement mortar with NS had higher compressive strength than the cement mortar with silica fume. In their investigation, 12 nm, 20 nm, and 40 nm NS were incorporated in the mortar to compare the compressive strength of

mortar with silica fume. Moreover, they found that associating 40 nm NS could result in more compressive strength than associating 12 nm or 20 nm NS. Their work was also supported by having denser and compact micrographs obtained by scanning electron microscopy for the cement pastes with 12 nm, 20 nm, and 40 nm NS, and silica fume.

## Production methods of NS

There are many methods available to produce NS. The properties of the NS vary with the technique that has been used to produce NS. The particle size and the size distribution, the particle shape, the purity of NS, the hydrophobicity, the crystallinity, etc. are some of the properties that were influenced by the technique used.

Thus, the ultimate resulting properties of nano-modified concrete depend on the features of the NS being used for the production, which itself depends on the NS production routes and conditions [3]. In addition, the dispersion method of NS also affects the final properties of concrete [3]. Thus, several methods have been explored in order to produce NS. The main methods of NS production include the sol-gel method, vaporization of silica, biological methods, and the precipitation method. Alternative production routes are: plasma, flame pyrolysis, chemical vapor deposition, electrodeposition, and mechanical attrition [20,21]. However, the sol gel method is advantageous over the other methods due to the ability of synthesizing monodispersed NS with a narrow-size distribution under simple conditions such as ambient temperatures and ambient pressure [22].

NS has been widely used for many applications such as an addition to cement, ceramics, chromatography, catalytic applications, and production of other advanced material and thus has been widely researched. For example, in Sarikaya et al. [23], the authors synthesized highly pure NS by alkaline treatments from pyrophyllite deposits, which is a mineral that is important within the mineral industry. The authors obtained the morphological structures and properties of the raw pyrophyllite, and conducted the X-ray fluorescence (XRF), X-ray diffraction (XRD), Fourier-transform infrared spectroscopy with attenuated total reflectance (FTIR-ATR), Scanning Electron Microscopy (SEM), and Energy dispersive X-ray spectroscopy (EDS) tests on the synthesized $SiO_2$. It was shown that a highly pure form of NS having nano-sizes of less than 50 nm could be obtained with a purity of 98%.

The effect of cationic surfactants on the particle size of NS which had been produced to investigate cement hydration was researched by Singh et al. [24]. The authors used tetraethyl orthosilicate (TEOS) as the precursor and dodecyltrimethylammonium bromide (DTAB), tetradecyltrimethylammonium bromide (TTAB) and cetyltrimethylammonium bromide (CTAB) as surfactants. Further, they investigated how the chain length of the surfactants affected the particle size of NS and found out that the particle size decreases with increasing chain length of the surfactants. It was possible for them to adjust the particle size of NS in the ~50 – 100 nm range by using the cationic surfactants. The XRD spectra of cement paste with 5% NS produced using the cationic surfactants showed that the intensity of the peaks related to CH in the paste had reduced when compared with the plain cement and the cement paste with 5% silica fume [24] indicated improved reactions with NS.

NS with a high specific surface area of ~260 $m^2/g$ were produced by Concha Real et al. using rice husk ash [25]. Their studies by Transmission Electron Microscopy (TEM) confirmed

that the silica produced by their method were in the nanometric scale. Moreover, they were able to obtain a homogeneously distributed ~99.5% pure NS by this.

The dissolution of olivine is another method to produce NS. Lazaro et al. [26] investigated this synthesis method and assessed its processing conditions on the properties of the NS product. The particle size of the produced NS was in 10-25 nm range and the particles were agglomerated resulting a mesoporous silica structure where the pore sizes were 17-28 nm according to their findings. The purity of NS was higher than 95% which is comparatively less than the other methods mentioned previously. Further they stated that this method was more feasible than the other techniques because of its lower energy requirement compared with the other method.

The precipitation method is one of the most common methods of NS synthesis. It involves producing alkaline silicate and then precipitating silica by adding an acid. Using this method, Thuadaij and Nuntiya [27] and Jal et al. [28] produced 50 nm NS using two different raw materials. Figure 2.1 shows a TEM image of the NS synthesized by Thuadaij and Nuntiya [27]. The first authors used rice husk ash and the latter used silica gel as the raw materials. The work of Nittaya et al. developed a NS which was uniformly distributed in shape and had a specific surface area of 656 $m^2/g$ to associate in cement. Their findings showed that the compressive strength of NS included cement paste were higher than that of without NS. The NS synthesized by Jal et al. was in spherical shape and had a specific surface area of 560 $m^2/g$ measured by BET.

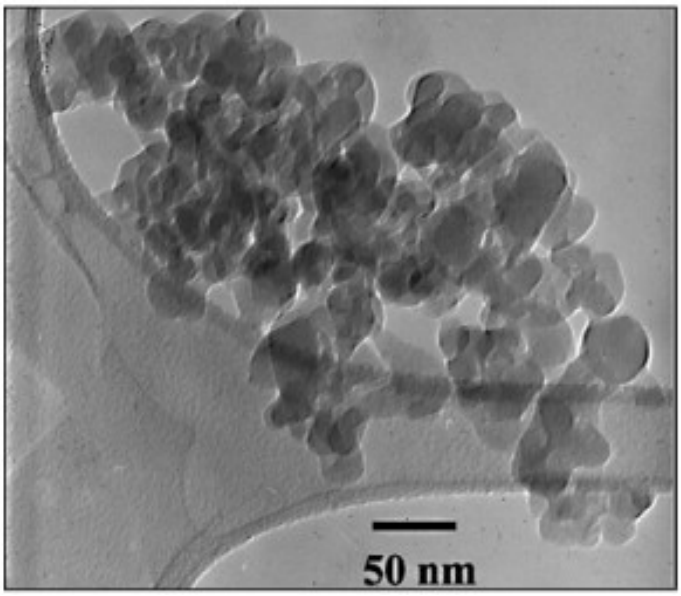


2.9.
**Figure 2.1: TEM image of NS produced by the precipitation method to associate in cement paste [27]**

## Sol-gel method

In 1640, “water glass” was discovered by van Helmont [29,30]. He observed the formation of alkali silicate by dissolving silicates in alkali and precipitation of silica by acidification [29,30]. During mid 1800s, the sol-gel terminology and the technique developed after the work on silica sols and silica gels by Ebelman and Graham [29–31]. The sol-gel involves a process where molecules in a sol (colloidal suspension) are linked to form a network which would then become

a gel-like material. The sol-gel method is used to synthesize metal oxides which has applications in a wide range of industries such as coatings, catalysts, and bio medical. The sol gel method is attractive in producing nano materials as homogeneous particles and multicomponent compounds can be produced [32].

In 1968, Stöber et al. [33] developed the process called "Stöber process" to synthesize NS by the sol-gel method [30,31]. It is one of the widely used methods to synthesize NS. With the sol-gel process, it is possible to tailor the parameters of NS which itself can affect the properties of concrete [20]. The properties of NS such as the particle size, surface conditions, and porosity can be engineered using sol-gel synthesis and these properties are reproducible at the same time [34]. When the processing parameters are accurately controlled, spherical NS with the size of 1 nm – 100 nm can be synthesized from the sol-gel method [20].

## 2.10. Hydration of cement

It is important to understand the mechanisms of cement hydration before studying the effects of nanoparticles on hydration. Cement chemists use a different notation to simplify the compounds in cementitious systems. This thesis will use this notation from here onwards. Cement consists of four main minerals: tricalcium silicate/alite ($3CaO.SiO_2$ – $C_3S$), dicalcium silicate/belite ($2CaO.SiO_2$ – $C_2S$), Tricalcium aluminate ($3CaO.Al_2O_3$ - $C_3A$), and Tetracalcium aluminoferrite ($4CaO.Al_2O_3.Fe_2O_3$ – $C_4AF$). Another mineral gypsum is present in cement to control the hydration rate of the aluminates. When these minerals come into contact with water, they dissolve and produce ionic species of the compounds. Once they are saturated the ionic species combine and form new solid phases.

$C_3S$ and $C_2S$ react with water to produce a hydrated calcium silicate structure (CSH). But the amounts of calcium hydroxide ($Ca(OH)_2$ - CH) formed vary for $C_3S$ and $C_2S$.

$$2C_3S + 6H \rightarrow C_3S_2H_3 + 3CH$$

$$2C_2S + 4H \rightarrow C_3S_2H_3 + CH$$

The rapid reaction of $C_3A$ with association of water and the sulphate ions ($\overline{S}$) from gypsum ($C\overline{S}H_2$) dissolution is as follows;

$$C_3A + 3C\overline{S}H_2 + 26H \rightarrow C_3A(C\overline{S})_3H_{32}$$

$$C_3A + C\overline{S}H_2 + 10H \rightarrow C_3AC\overline{S}H_{12}$$

$C_4AF$ also produces similar compounds like above substituting iron for the alumina component.

In the absence of sulphate $C_3A$ forms $C_3AH_6$ or $C_4AH_{19}$

$$C_3A + 6H \rightarrow C_3AH_6$$

$$C_3A + CH + 18H \rightarrow C_4AH_{19}$$

The chemical processes of these reactions can be categorized as follows [35];

1. Dissolution/dissociation - detachment of molecular units of solid cement particles in the presence of water
2. Diffusion - transportation of dissolved ions into the bulk solution
3. Growth – saturation of molecular units into the structure of crystalline or amorphous solid
4. Nucleation - initiation of precipitation
5. Complexation - formation of ion complexes or adsorbed molecular complexes on solid surfaces by reactions.
6. Adsorption - accumulation of ions or molecular units

Hydration of cement is a combination of the above chemical processes in series, parallel or other complex combinations. The rate of cement hydration varies with time, and can be divided in to five stages namely [36],

1. Rapid initial process
2. Dormant period (Period of slow reaction)
3. Acceleration period
4. Retardation/deceleration period
5. Long term reactions

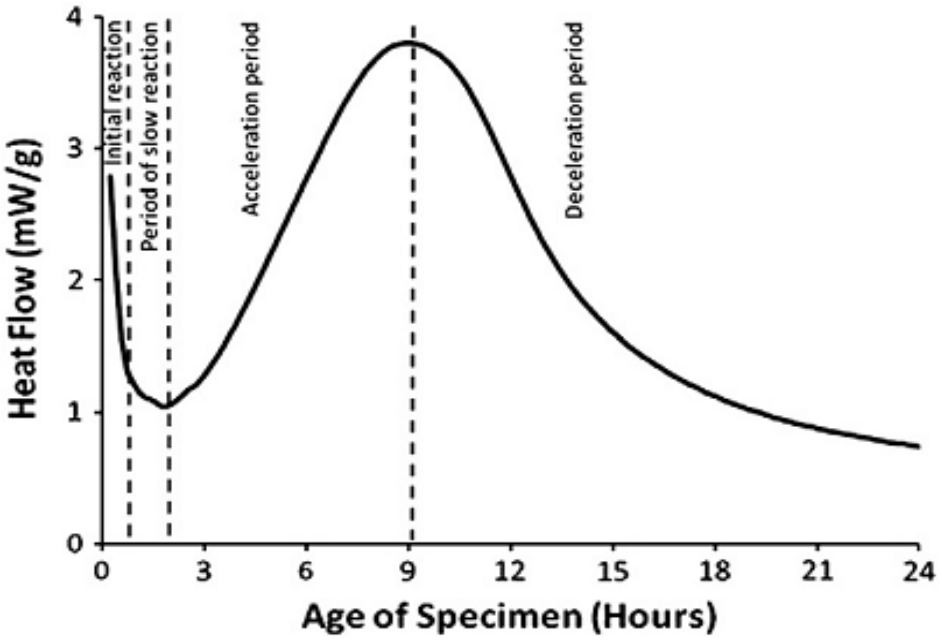


**Figure 2.2: Rate of alite hydration as a function of time given by isothermal calorimetry [36]**

The reaction of cement minerals with water is an exothermic process. Therefore, the hydration of cement can be observed through calorimetry. The first four stages are plotted on Figure 2.2, the heat flow vs. age curve from calorimetry. However, the exact points of starting or ending of each stage cannot be located. The initial period is mainly attributable to wetting of cement and some heat generated by dissolution of $C_3S$. This stage is followed by the dormant stage or the slow reaction stage. The reason for this stage is debatable and many hypotheses were proposed. However, formation of a metastable layer of calcium silicate hydrate which limits the diffusion of detaching ions was hypothesized by Gartner et al. [36]. In the acceleration period, nucleation and growth of the hydration products occur contributing around 30% of cement hydration [37]. During the deceleration period, the hydration occurs by a diffusion process which decelerates as the hydration products become thicker. The hydration will not stop at the end of this point but will continue further over years. The hydration of cement is affected by the composition of cement, cement type, sulphate content, fineness which is proportional to Blaine fineness value [38], water/cement ratio, curing temperature, the effects of SCMs, and admixtures. This typical curve is taken to compare the hydration of cement with other supplementary materials.

The adiabatic calorimeter, isothermal calorimeter, solution calorimeter, conduction calorimeter and differential calorimeter are some calorimeters used to measure hydration. The isothermal calorimeter is better than the adiabatic calorimeter because it can give high resolution quantitative data [39]. Apart from calorimetry, there are many other methods to observe the hydration of cement. They are X-ray diffraction (XRD), measurement of non-evaporable water as lost on ignition and by thermogravimetry (TG), measurement of continuous chemical shrinkage which has a direct proportional trend to heat of hydration within 4 hours – 50 hours of curing [40], SEM (Scanning Electron Microscopy) observations of the residual quantity of calcium hydroxide, and nuclear magnetic resonance spectroscopy to assess the degree of hydration [36].

## 2.11. Review of nanotechnology in concrete

As reviewed by Sanchez and Sobolev, there are two avenues in which nanotechnology can be brought to concrete research [3]. The first is understanding the nano level structure of cement-based materials, their characteristics, and how this structure affects the properties of the bulk material. This includes advanced characterization techniques and molecular level modeling with regards to the analysis of the cement-based materials' structure. The second is controlling the nano structure of the material using nano materials and enhancing the performance of concrete, which is the focus of this thesis which will be discussed later. Modern characterization techniques have created a path to understand the nano scale structure of calcium silicate hydrate (CSH), which is the major component of hardened cement. Understanding the features and characteristics of the structure at this level helps scientists and engineers to improve the performance of concrete [3]. These techniques include nanoindentation, small angle neutron scattering, ultra small angle x-ray scattering, quasi elastic neutron scattering, nuclear magnetic resonance spectroscopy (NMR), nuclear resonance reaction analysis (NRRA), and atomic force microscopy (AFM). Atomic microscopy (AFM) is a technique used for investigating the surface morphology of cement phases. AFM has revealed that calcium silicate hydrate structure (CSH) of hardened cement has an ordered structure and it is formed by agglomerating identical elementary clusters with sizes on the order of 60 x 30 x 5 $nm^3$ [3,41,42]. Figure 2.3 is an AFM image which reveals the ordered CSH crystallite nanostructure of concrete.

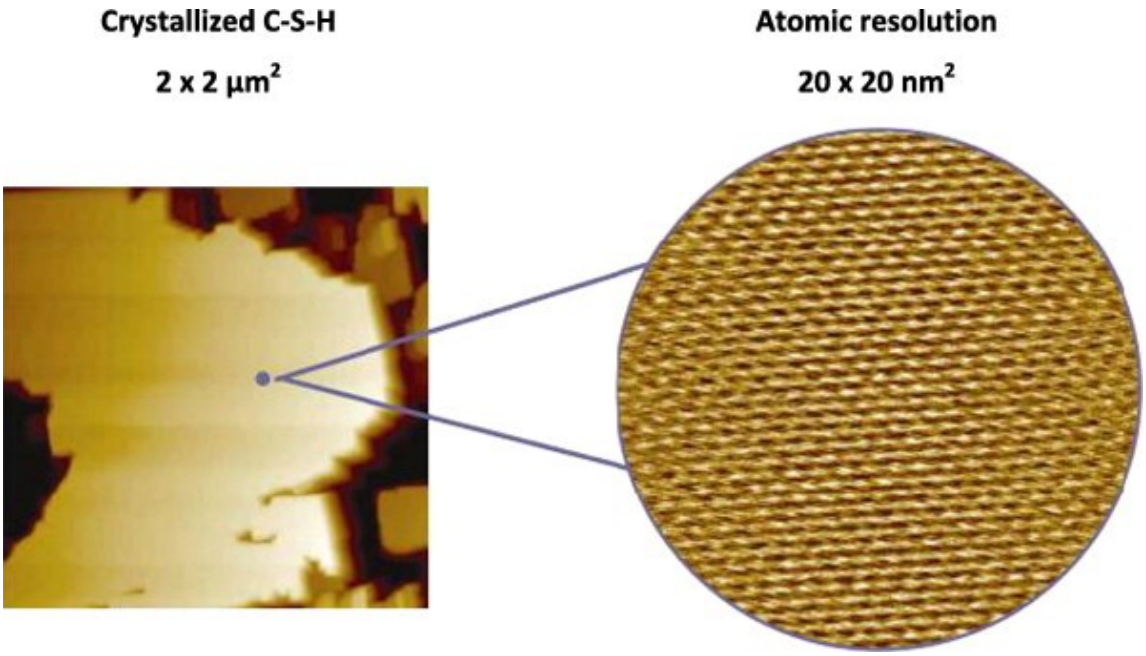


**Figure 2.3: Nanoscale structure of CSH crystallized on calcite substrate and revealed by AFM (Ca/Si = 0.9) [3]**

Nanoparticles in cement/concrete have gained much research interest due to their remarkable contribution to enhance the properties of concrete. As illustrated, the calcium silicate hydrate structure (CSH) of the hardened cement has an ordered structure at the nano scale [20]. Therefore, this structure can be improved with respect to hydration properties, mechanical properties, durability, and others by introducing nano materials [20].

### 2.11.1 Nanoparticles used in cement

Association of nanoparticles in cement-based systems dates back to 1964, where amorphous silica, which had a high surface area equivalent to prevailing nano-silica products, had been utilized to accelerate the hydration of $C_3S$ [43,44]. However, the recent studies on nanoparticle incorporation in cement-based materials after 2004 are described in [44]. $SiO_2$, $TiO_2$, $Al_2O_3$, $Fe_2O_3$, and clay are some of the nanoparticles that have been studied in the recent years [44]. All the types of nanoparticles provide nucleation seeds and densify the material by filling the larger gaps. In addition to them, $SiO_2$ nanoparticles [1,3,20] ,some clay nanoparticles [45,46], and $Al_2O_3$ nanoparticles [47,48] have shown pozzolanic activities to form the cementitious phases such as CSH and CAH. Santra et al. [49] investigated different nanoparticles and accelerators by isothermal calorimetry to examine the behavior of nanoparticles as accelerators in oilwell cement hydration. They discovered that 0.9% nano-silica, 0.45% nano-silica and 2% nano-alumina accelerated the hydration of cement pastes in the descending order compared to a control cement paste. Furthermore, they reported that nano-alumina had shown fewer chemical effects than nano-silica. Reches [44] reviewed that $TiO_2$, $SiO_2$, bentonite, and $CaCO_3$ have been investigated up to 5% of the binder mass in cement paste, up to 7.5% $SiO_2$ of the binder mass in mortar, and up to 4% several types of nanoparticles in concrete for mechanical properties. This review also included studies that had utilized 10% nanoparticles of binder mass to investigate compressive strength. Overall, strength improvements with these nanoparticles content were reported while the opposite

was observed in some cases. Also, the article revealed that the peak in the strength for most of the studies was achieved by 1% or lower nanoparticles contents. Moreover, these effects were noticeable within 1-7 days.

## Synthesis of NS

Although there are many methods to produce NS, the economy and the repeatability of the method are crucial for the construction industry. The sol-gel method has advantages for the construction industry over the other methods such as vaporization of silica, biological methods, the precipitation method, plasma, flame pyrolysis, chemical vapor deposition, electrodeposition, and mechanical attrition. The characteristics of such techniques which limit their use for construction industry are tabulated in 2.12.

Table 2.1.

The suitability of the sol-gel method for preparing NS for inclusion in concrete is based on the ability to control the size and shape, simple processing conditions like ambient temperature and ambient pressure, and the ability to produce mono-dispersed particles with a narrow size distribution.

Bagheri et al. [50] have investigated the influence of pyrogenic NS in concrete. Their studies show that even though it is possible to synthesize very fine NS from this route, the particles are aggregated and monodispersed in concrete due to their fineness.

Quercia et al. [51] characterized several types of amorphous NS used in concrete prepared using different methods. Their studies showed that the specific surface area, the micro pore volume, and the average size of the primary particles affect the slump flow (workability) and the final mechanical properties of cement mortar. Furthermore, they discovered that there is no direct effect from nano-silica's (NS') the pore diameter and the pore size distribution on the mortar properties. These characteristics of NS also vary with production route.

The investigations of Land and Stephen [34] showed using calorimetry that acceleration of $C_3S$ hydration in cement is controlled by the surface area of NS added into the cement paste. In this study, they had used NS synthesized by the sol-gel method and commercial NS synthesized by the precipitation (water glass) method. As the particle sizes of NS used for this research were quite comparable in each case, and because their focus was not on the production method of NS, there was no distinct revelation about the effect of the sol-gel synthesized NS on cement hydration. However, they reported an early formation of the sulphate type AFm and accelerations of $C_3S$ hydration due the sol-gel synthesized NS.

Flores et al. [20] examined the performance of cement with the sol-gel synthesized NS. This study did not explain about the drying method which had been used to synthesize NS and the method of dispersion of NS in cement. For deagglomeration techniques, the use of superplasticizer and high-speed mixing were used, and they were proven to be effective. They reported that even a miniscule quantity (such as 0.25%) of sol-gel derived NS addition had increased the compressive strength of cement mortar. They also suggested further research on the modification of the sol-gel method to overcome the formation of xerogel agglomerates. The suggested methods include: the

production of NS products in liquid state, application of surfactants, ultrasonication, and microwave drying.

**Table 2.1: The features of NS production techniques**

| Method of NS production | Characteristics |
|---|---|
| Vaporization | High processing temperature [51] |
| Hydrothermal method | Time consuming as the concentration of reaction species must be low [52] |
| Homogeneous precipitation method | Time consuming as the concentration of reaction species must be low [52] |
| Chemical vapour deposition,<br>Physical vapour deposition, Electrodeposition | Deposition techniques<br>Difficulty of bulk production due the formation of hard agglomerates [52]<br>Expensive |
| Precipitation method | Difficulty to control the particle size and the agglomeration of particles [53] |
| Plasma | Complex equipment |
| Flame pyrolysis | Difficulty in large scale production<br>Need of sophisticated equipment such as reactors |
| Pyrogenic methods | Difficulty to control agglomeration [54] |
| Mechanical attrition | Less purity due to contamination [55]<br>Difficulty to control particle size |

**2.13.**

## The sol-gel method - steps

In the sol-gel method, a starting compound, which is called a precursor, is hydrolyzed to form a colloidal suspension. The next step of the method is condensation and polymerization. Then, the monomers form particles, and thereafter, the growth of particles occurs. It forms a gel structure by the agglomeration of the particles. The gel is then dried to remove the solvents and surface functional groups. The final size and the shape of the synthesized particle depend on the type of the precursor, type of the solvent, the $H_2O$ to Si molar ratio, type of catalyst, pH of the solution and temperature [56].

Unlike traditional ceramic processing routes, the sol-gel method requires low processing temperatures for drying the gel [56]. Hence by definition: “A sol (Figure 2.4) is a suspension of colloidal particles in a liquid or a solution of polymer molecules”[56]. Colloidal particles are solid

particles whose diameters are in the range of 1 – 100 nm. Gel (Figure 2.4) is a semi rigid mass formed when the colloidal particles are linked to form a network or when the polymer molecules are cross-linked or interlinked [56].

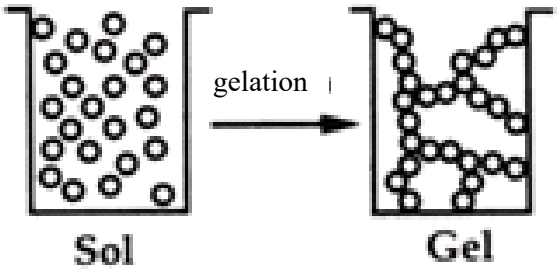


**Figure 2.4: A sol and a gel**

In the sol-gel method, a starting compound, which is called a precursor, is hydrolyzed to form a colloidal suspension. The next step of the method is condensation and polymerization. Then, the monomers form particles, and thereafter, the growth of particles occurs. It forms a gel structure by the agglomeration of the particles. The gel is then dried to remove the solvents and surface functional groups. The final size and the shape of the synthesized particle depend on the type of the precursor, type of the solvent, the $H_2O$ to Si molar ratio, type of catalyst, pH of the solution and temperature [56].

### 2.13.1 Precursors

Inorganic salts or metal organic compounds are the precursors for the sol-gel method but metal alkoxides and semi metal alkoxides are the most extensively used class of precursors. Metal alkoxides readily react with water which is called hydrolysis. The general formula of metal alkoxide is $M(OR)_Z$, where M is the metal, R is the alkyl group, and Z is the valence of the metal, M.

### 2.13.2 Hydrolysis and condensation

Hydrolysis and condensation reactions of silicon-based alkoxides take place with an acid or base catalyst which controls the structure and morphology of the resulting gel network [57]. The condensation reaction occurs soon after the hydrolysis reaction takes place that results in many reaction products within the solution [58]. The following equation gives the hydrolysis reaction of a metal alkoxide.

$$M(OR)_z + H_2O \rightarrow M(OH)(OR)_{z-1} + ROH$$

Thereafter the condensation reactions take place as follows;

$$M(OH)(OR)_{z-1} + M(OR)_z \rightarrow (RO)_{z-1}M\text{-}O\text{-}M(OR)_{z-1} + ROH$$

$$2M(OH)(OR)_{z-1} \rightarrow (RO)_{z-1}M\text{-}O\text{-}M(OR)_{z-1} + H_2O$$

The final structure of the gel depends on the relative rates of hydrolysis and condensation [31]. The relative rate constant of hydrolysis increases when the concentration of $H^+/H_3O^+$ in an acidic media or the concentration of $OH^-$ in a basic media increase [31]. However, under basic

conditions, the hydrolysis reaction is limited and OH- ions favour the condensation reaction [59]. In addition, the nature of the alkoxy group on the silicon atom affects the rate constant [31]. Bulky groups give slow reaction rates as per Schmidt's findings [58]. The pH of the solution and the reactant concentration (i.e. $H_2O$:Si ratio) affect the size of the sol particles and the cross-linking within the particles [31].

Silicon alkoxide has slower hydrolysis and condensation reactions when compared with other metal alkoxides like Ti, Zr, B and Al [60]. Therefore, by controlling the hydrolysis reaction, various shapes of sol-gel materials can be produced [60].

### 2.13.3 Gelation

Hench and West [31] have defined the gelation point or gelation time as the point when a stress elastically can be supported or alternately when the sol becomes a gel. Even though measuring this point analytically is difficult, the gelation time has been analyzed by measuring the viscoelastic response of the gel as a function of shear rate [31].

The structural evolution during the sol-gel transition can be investigated by several techniques which include small angle X-Ray scattering (SAXS), small angle neutron scattering (SANS), light scattering, nuclear magnetic resonance spectroscopy (NMR), Raman, and infrared spectroscopy [3]. In the sol structure, the individual particles show a few interactions, but after gelation, the structure becomes a continuous network.

As reviewed by Hench and West [31], the gelation can be explained by three theories, namely, classical, percolation, and fractal theory. Even though the gel point of the sol-gel structure can be explained by classical theory, the polymer growth does not match with the realistic situation. Percolation theory gives a good description of the gelling system which is in agreement with the practical observations. However, it is not possible to obtain much information analytically. Therefore, computer simulations are required to investigate this theory. The fractal theory employs fractal concepts to explain the growth of the sol-gel particles. A fractal is a paradigm in order to describe the morphology of some random shapes and growth processes [61]. A fractal (See Figure 2.5) has a symmetry that does not change with the level of detail chosen [31] and the density of a fractal decreases with its size. From SAXS experiments, the fractal nature of gelation has been proven [31].


**Figure 2.5: Fractal Growth [15]**

### 2.13.4 Aging

The change of the structure and properties of the gel when it is preserved with the pore liquid after the gel point is called aging [31]. As reviewed by Hench and West, polycondensation, syneresis, coarsening and phase transformation can occur individually or together during aging. When the formed gel is the pore liquid, it continues to form more and more bonds and keeps connecting with the neighbouring silanol groups. This continuous occurrence of this condensation reaction increases the fractal dimensions of the gel. Because the reactions are faster at higher temperatures, polycondensation can be made faster by hydrothermal treatments [31].

The expulsion of the pore liquid as a result of the shrinkage is called syneresis [31]. During the aging process, oxygen continues to bridge silica atoms by the condensation reactions. This results in shrinkage of the silica gel. Syneresis is slower where the rate of the condensation reactions is slower. With increasing time, the rate of syneresis falls. Hench and West suggested that this is due to the increase of the stiffness of the gel network during formation of more bridging bonds [31].

The convex surfaces are more soluble than the concave surfaces. Thus, convex surfaces tend to dissolve and make connections with other particles while the dissolved material precipitate on to the concave surfaces when the gel is in the pore liquid. This process reduces the surface area of the pore structure by creating necks between particles and filling up the pores. This process is called Ostwald ripening or coarsening. Coarsening is dependent on the pH of the solution because the solubility of silica gel increases with the pH value.

### 2.13.5 Drying

Drying can be explained in three stages (see Figure 2.6). During stage 1, the evaporation rate is almost constant and it is called the constant rate period (CRP) [31]. The evaporation rate per unit volume of the surface area is independent of time during this stage [31], and the evaporation occurs similarly to a free liquid surface [56]. During this stage, a volume of liquid

equalling the decrease of volume of the gel is evaporated [31]. At the end of this period, the shrinkage of the gel stops. A gel can be shrunk to one tenth of its original volume [56].

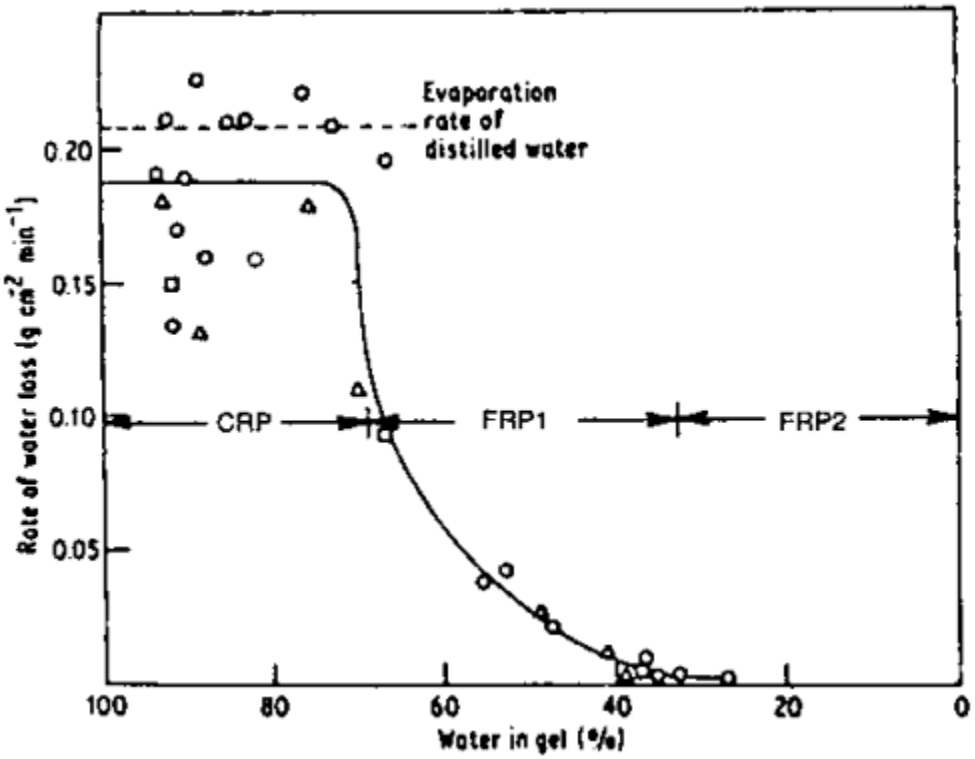


**Figure 2.6: Three stages of drying [56]**

After this period, the falling rate period starts. It is divided into two stages as first falling rate period (FRP1), which is the second stage of drying, and as the second falling rate period that is the third stage. Due to the shrinkage during stage 1, the gel becomes highly packed so that it cannot shrink anymore. As a result of the resistance to shrinkage, the radius of the meniscus of pore liquid decreases and ultimately becomes zero. Therefore, the gel network holds a great strength at this point which is called the critical point or leatherhard point [31]. At this critical point stage 2 begins. In the first falling rate period, the evaporation rate falls in an approximately linear manner with time [56]. The liquid in the partially empty pores flows to the exterior surface through surface films due to the gradient in capillary stress since the liquid in the pore is continuous with the liquid in the exterior surface. In the exterior surface, the evaporation occurs from the surface films.

When the pores are emptied by this evaporation, the flow of liquid to the exterior is not possible. After this stage 3, which is the second falling rate period, begins (FRP2). In this period, the evaporation takes place within the pores and vapour diffusion occurs to the surface [56]. Although no volume change occurs during this period, the weight of the gel decreases.

### 2.13.6 Stabilization

Due to the high concentration of silanol groups on the surface of porous material, it is not chemically and thermally stable at an ambient environment. By removing the surface silanol groups below a critical level, it can be chemically stabilized to avoid rehydroxilating while in use.

The surface area should be reduced in order to stabilize the material at a particular temperature so that reversible structural changes will not occur [31].

Dehydration, dilation, and contraction of the silica network with adsorption and desorption of water are important steps in stabilization. In a silica gel structure, water is present as free water within the porous structure and as hydroxyl groups associated with the gel structure. The free water can be removed, and surface hydroxyls can be condensed starting at about 170 °C. Dehydration is reversible up to 400 °C. This reversible dehydration occurs due to the removal of surface water and the formation of single and adjacent surface hydroxyl groups. Afterwards, the dehydration is irreversible due to the shrinkage and sintering in between pores. Above 400 °C, the adjacent hydroxyl groups are removed. Chlorine compounds can be used to dehydrate the gel. These compounds can react with surface hydroxyl groups completely by forming hydrochloric acid. This hydrochloric acid can be evaporated in the temperature range of 400 – 800 °C [31].

Viscous flow starts at above 850 °C. The temperature at which the viscous flow starts depends on the pore size of the gel. Voids are removed by connecting particles with each other through the reaction of isolated hydroxyl on the gel surface. The surface area of the gel decreases, and it depends on the time and the temperature. This elimination of single hydroxyl group takes place until the gel densification occurs between 850 – 1000 °C. When there are no further surface hydroxyl groups, the surface becomes hydrophobic as a result of the inability to absorb free water. Thus, although it converts to a stable gel, some single hydroxyl groups can still be trapped inside the densified gel. Therefore, foaming occurs with increasing temperature. The densification in atmospheric air causes this problem which can be avoided by using an atmosphere containing a chlorine compound such as $ClSi(CH_3)_3$, $Cl_2Si(CH_3)_2$, $Cl_3Si(CH_3)$, silica tetrachloride ($SiCl_4$), chlorine ($Cl_2$), and carbon tetrachloride ($CCl_4$). However, a dechlorination treatment is required to remove the incorporated chlorine atoms in the gel glass structure; chlorine is reduced under an oxygen atmosphere of 1000 -1100 °C [31].

**2.14.**

## Properties of concrete enhanced by NS

### 2.14.1 Workability

NS added to cement paste requires more water than the normal cement to achieve workability. The studies of Senff et al. [62] showed that the yield stress of cement paste with NS increased significantly when compared with normal cement paste. With 2.5% NS by weight, the paste had a reduction in flow diameter of fresh mortar by 19.6% and an increase in the yield stress of the cement paste of 157% [62]. The studies of Berra et al. [63] provided some solutions to avoid this matter without changing the water/binder ratio or adding superplasticizer. Without adding the required water content at once, the delayed addition of water in portions was proven to solve the reduction of workability. Moreover, delayed addition of superplasticizer was advised in order to not deteriorate the reactivity of NS.

### 2.14.2 Hydration

NS can impart better performance to concrete through both physical and chemical mechanisms [64]. By the chemical mechanism, NS creates nucleation sites to improve pozzolanic reactions that subsequently accelerate the hydration of cement (See Figure 2.7). In the physical mechanism, NS fills up the voids and thereby increases the density of the concrete [64]. Due to

the large surface area of NS particles which is very reactive, the hydration reactions of cement are accelerated.

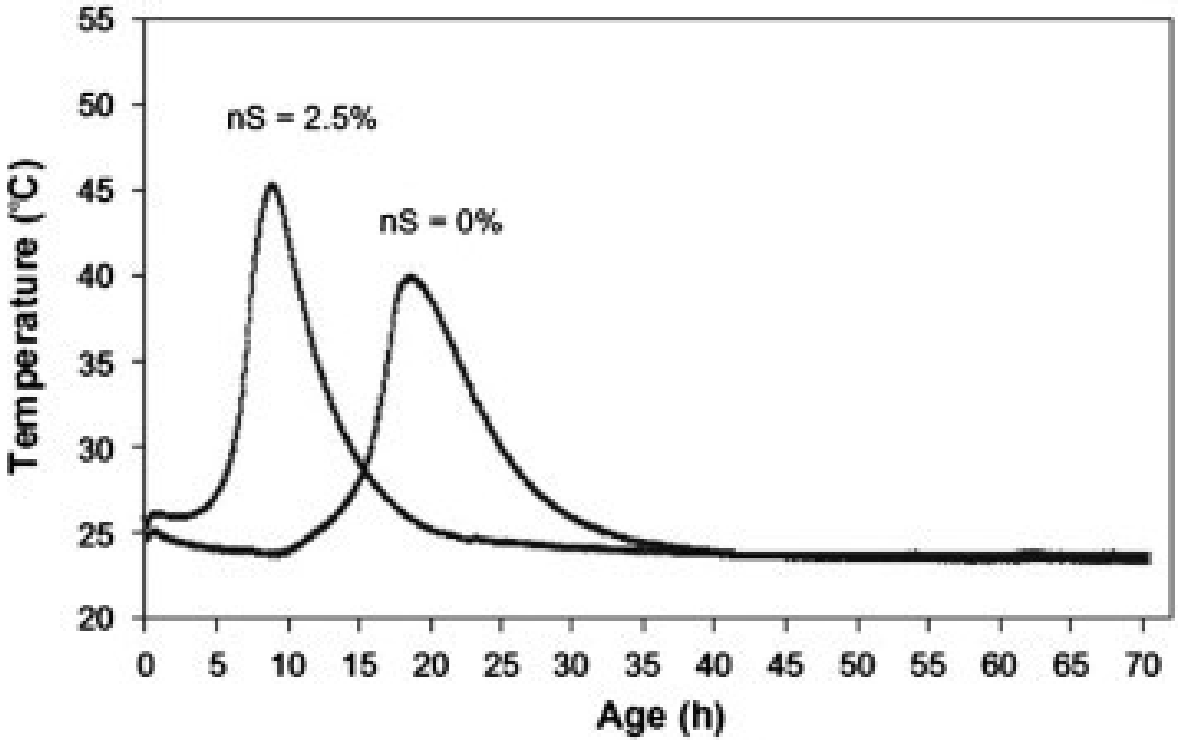


**Figure 2.7: Influence of NS on heat of hydration of cement paste [62]**

The studies of Thomas et al. [65] showed that NS can accelerate the hydration of tricalcium silicate which is the main component of cement (50%-70%). Hydration of cement pastes by differential calorimetric analysis [34] showed that the heat evolution during hydration was higher in NS added cement compared to normal Portland cement as shown in Figure 2.8. Their work showed that the maximum of the $C_3S$ hydration peak (the peak in between 2 – 4 hours) increased as the NS content in the paste increased. This behavior was visible in other series of calorimetric tests performed in the same way using 7, 18, 86, and 295 nm NS.

The formation of calcium hydroxide crystals is also lower in NS added cement [1]. The formation of larger CSH crystals with increasing NS percentages was reported [1,66]. Thomas et al. proposed that NS can provide seeds for the nucleation of hydration process by forming CSH particles which is the result from the reaction of NS and the dissolved calcium ions from cement or $C_3S$ [65]. They also reported that these CSH particles formed hydrated products not only on the surface of cement particles, but also within the pore space of particles [65].

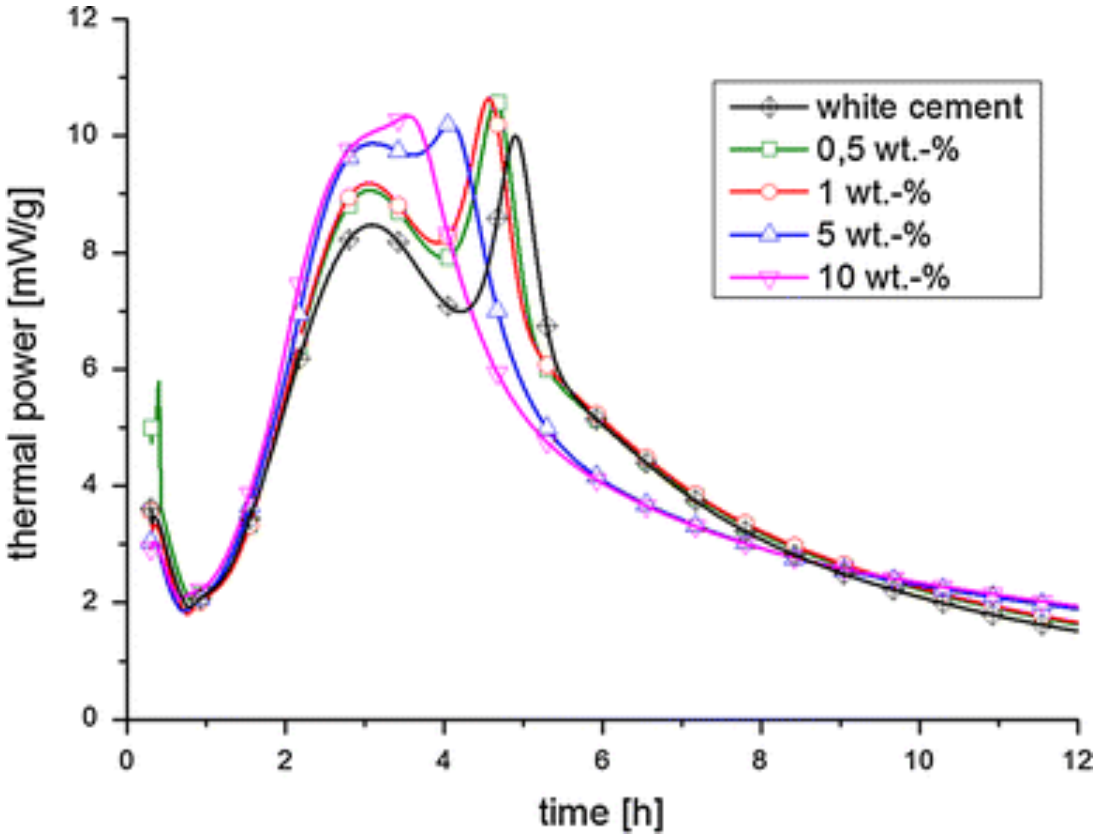


**Figure 2.8: Calorimetry of cement hydration with admixture of nano-silica of 86 nm in diameter [34]**

Björnstörm et al. [67] studied the hydration of $C_3S$ cement for the accelerating effects of colloidal silica. They found out that the colloidal silica increases the rate of the dissolution of $C_3S$ and forms more CSH in the binding phase. Kong et al. compared [68] the effect of NS and colloidal silica, and according to their findings, the agglomeration of NS make less effective in the accelerating effect than the colloidal silica.

Isfahani et al. [69] have investigated the early stages of hydration by isothermal calorimetry in which they found that the rate of hydration during the induction period, dormant period, and the acceleration period could be accelerated by 1.5 % and 2.5 % NS. They also found that the rate was decelerated during the period after the acceleration period and explained that as a result of the presence of the formed more compacted hydrates around the cement particles in the NS containing paste than the plain cement paste. However, their study did not reveal much changes in the porosity by having NS in the cement pastes.

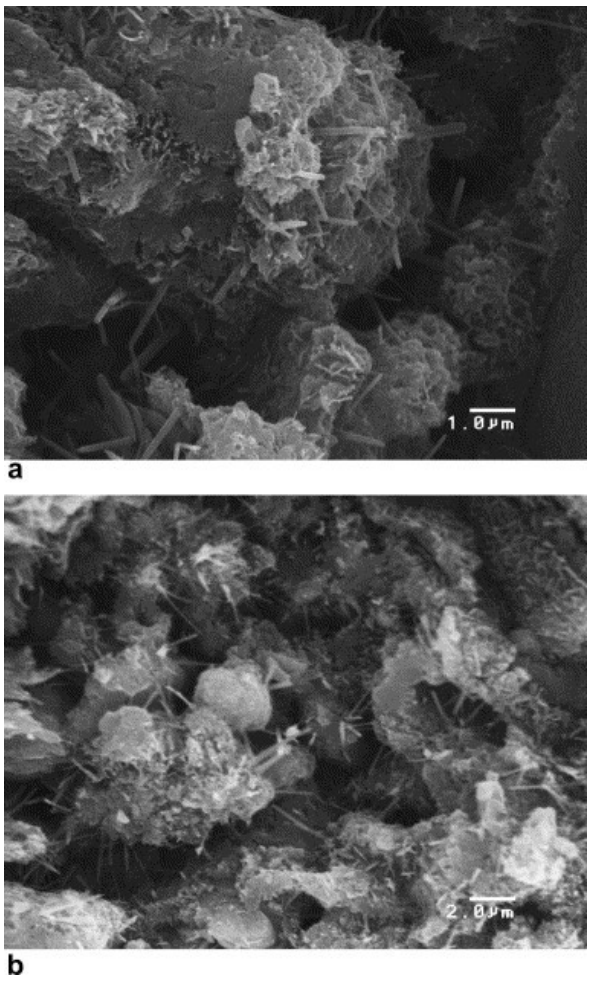


**Figure 2.9: SEM micrographs of OPC paste: (a) 10,000× and (b) 5000× [38]**

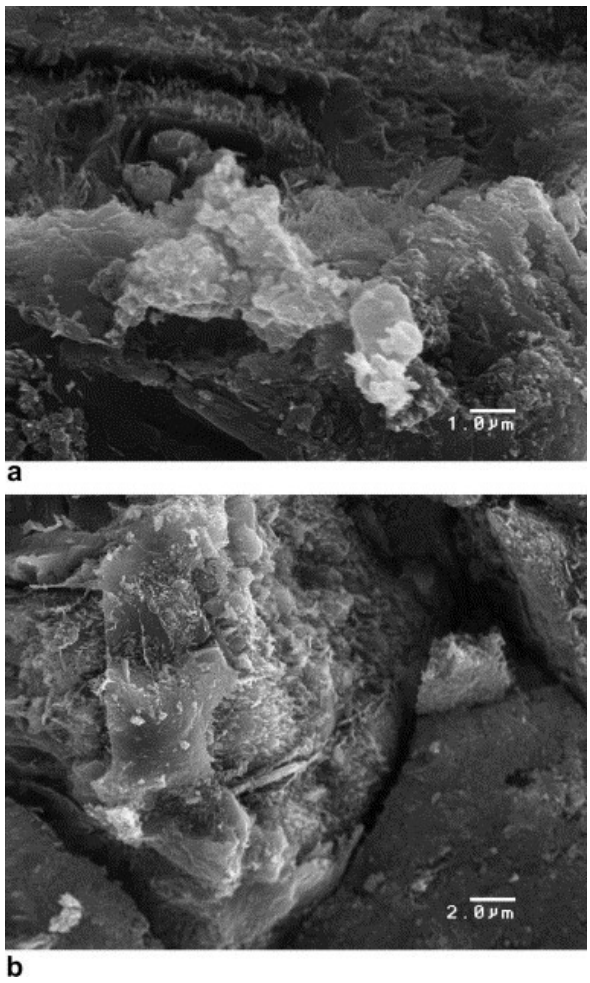


**Figure 2.10: SEM micrographs of paste containing NS particles (a) 10,000x and (b) 5000x [38]**

The hydration studies by Rupasinghe et al. [70] revealed that improvements in the rate of hydration by using NS up to 12%. However, their work showed that the improvements obtained by 8% and 12% are not significant indicating using NS beyond 8% was not effective in the early stages of hydration.

In [62] the work of Senff et al., the setting time of 2.5% NS incorporated cement showed a 60% reduction compared to that without no NS. Moreover, the time taken to achieve the maximum temperature was decreased by 51.3%. The dormant period during the hydration was reduced. Their findings revealed that an increase in CH formation during the early age in NS silica included cement than that without NS. However, this is contradictory with the work of some other researchers [3,13,70] where a less CH formation was discovered by them in NS included cement paste.

Due to differences of hydration behaviour of normal and NS added cement paste, the hardened paste of the NS containing cement shows a denser microstructure (Figure 2.10) with compacted hydration products and a lower number of $Ca(OH)_2$ crystals [38] compared to normal

cement paste (Figure 2.9). Figure 2.9 shows the SEM of hardened cement paste made without NS which contains isolated C–S–H gel and needle-like hydrate products.

### 2.14.3 Mechanical properties

As reviewed by Sanchez and Sobolev, even a minute amount of NS such as 0.25% increased the flexural and compressive strength by significant percentages of 10% and 25%, respectively [3]. Sobolev et al. [71] mentioned that NS has been utilized in polymers as an additive to improve their strength and flexibility. They investigated the performance of hardened cement with NS for the same mechanical properties. Their experiments revealed that 50 -70 nm size NS could improve 1 day and 28 day compressive strength of mortar by 16% and 28 day flexural strength of mortar by 18%. To achieve this improvement, 0.25% NS had been used as an additive to cement along with a superplasticizer to facilitate NS dispersion.

Shakhmenko et al. [72] showed that the compressive strength of cement paste can be increased by 3 times or greater when 2% of cement (by weight) is replaced by NS synthesized by the sol-gel method. Figure 2.11 shows the influence of NS content on compressive strength of cement mortar during 90 days of curing [73]. With increasing the NS percentage, the compressive strength of mortar had increased during the observation period of 90 days. The maximum strength was obtained from a 5% NS, and this amount causes a significant strength improvement when compared with cement mortar without NS. However, 4 to 6% additions show similar results indicated a limit in the effectiveness of NS.

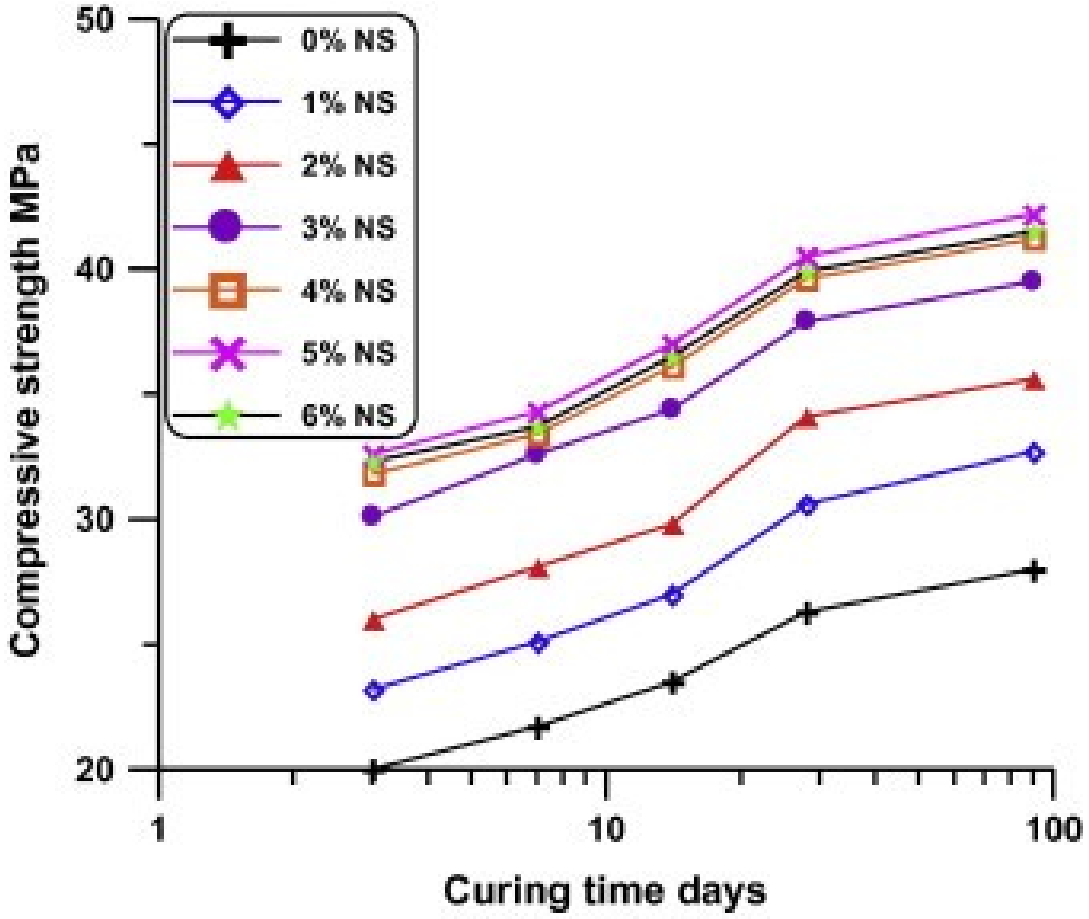


**Figure 2.11: Compressive strength of hardened cement mortars containing NS up to 90 days [73]**

In the reference [74], the authors added NS up to 6% NS by the total weight of the cementitious material and were able to improve the early age (3 day and 7 day) compressive strength of concrete by 18%. Li et al. have shown that increasing the replacement of cement by NS from 3% to 10% improves the effectiveness of improvement of compressive strength and flexural strength of the cement mortar [75]. They suggested that the aggregation of extensive nanoparticles may create weak zones in the form of voids which would lead to an inhomogeneous hydrate microstructure and low strength [75]. Conversely, other researchers have shown that having more than 2% NS by weight of cement resulted in the reduction of the compressive strength of the cement paste [1]. Therefore, the optimum cement percentage which can be replaced by NS has not yet been established.

### 2.14.4 Consumption of calcium hydroxide

The porosity of concrete can be reduced by the improved reaction rates and the nano filler effect of NS [1,76]. This reduces the water absorption and water permeability compared to normal concrete. In addition, NS consumes more calcium in concrete, which will reduce the calcium leaching rate [1,77]. Consequently, the pore structure of concrete is improved with NS. The ingress of water into the structure and chloride ion penetration will be lowered, providing a more durable concrete [1]. Singh et al. [78] analyzed the amount of CH formation in NS added cement paste compared with plain and silica fume (SF) added to cement paste with thermogravimetric analysis, XRD and SEM analysis. Their work revealed that the amount of calcium hydroxide formed in the

NS containing cement paste is less than for SF additions to cement (Table 2.2) indicating its high reactivity.

**Table 2.2: Calcium hydroxide content (%) in cement pastes [78]**

| | CH content % | | | |
|---|---|---|---|---|
| | **1 day** | **3 days** | **7 days** | **28 days** |
| Plain cement paste | 4·9 | 7·8 | 12·9 | 20·5 |
| Cement+SF (5%) | 3·1 | 5·8 | 9·6 | 16·4 |
| Cement+NS (5%) | 0·8 | 3·5 | 4·8 | 8·2 |

The durability of mortar when colloidal NS was associated was studied by Du et al. [79]. Their study included a comparison of mortar that had 0.5, 1.0, 1.5, and 2.0% colloidal NS addition by the cement weight with a reference mortar having a 0.3 water cement ratio. Their work revealed that the migration coefficient and the sorptivity decreased as the colloidal NS increased. Moreover, it was reported a 45% and a 30% decrease in the migration coefficient and the sorptivity, respectively, when 2% colloidal NS was added in the mortar. Besides, they mentioned that the drying shrinkage of cement mortar could be reduced by colloidal NS by densifying its microstructure.

## 2.15. Techniques to characterize the properties enhanced by NS

### 2.15.1 Hydration inhibition

As this research focuses on the analysis of the microstructural characteristics of the hardened cement, it is essential to study the hardened cement pastes at certain curing ages. Thus, the hydration inhibition at the specified point of time is necessary. The selection of the method of the inhibition is crucial to preserve the characteristics which will be studied. There are several techniques that researchers have used to inhibit the cement hydration, namely solvent exchange, freeze drying, microwave drying, oven drying, D-drying, supercritical drying and vacuum drying [80]. To preserve the pore structure of the cement pastes, the solvent method is better over the other methods which could damage the pore structure. In addition, the microstructures are not affected by this method and it is suitable for scanning electron microscopy [81].

The solvent exchange method involves replacing the water present in the hardened cement paste using a solvent such as an alcohol, acetone, etc. The suitable solvent should be small enough to penetrate into the pores in the hardened cement paste and be able to exchange the water molecules. The solvent should be miscible in water, have a lower boiling point to be able to evaporate without reaching a temperature that might affect the structure and the composition of the cement paste and has a lower surface tension not to damage pore structure [80].

### 2.15.2 Techniques to measure the hydration of cement

The research community has been employing many techniques to determine the hydration of cement. This includes calorimetric techniques, which measure the heat generated during the cement hydration reactions. Isothermal calorimetry is a convenient and commonly used technique.

The continuous monitoring of the heat of hydration is possible by this. Semi adiabatic colorimetry, solution calorimetry, conduction calorimetry are some of the other calorimetric techniques utilized by the researchers.

Various thermal analysis techniques have been utilized to quantify and analyze the products from the cement hydration. Differential Scanning Calorimetry (DSC), TG, and the measurement of non-evaporable water quantity are some of them. In these techniques, the chemically bound water, the formed CH, and the calcium carbonate quantity are the major focuses being analyzed. As the cement hydrates producing various phases in the hardened structure and these techniques could provide information of some the products, they cannot be used to directly determine the hydration. However, these techniques have been very useful in understanding the cement hydration reactions for the researchers.

In [40], the authors compared different methods of measuring degree of hydration of Portland cement. Quantitative XRD (QXRD), non-evaporable water as loss on ignition and by thermogravimetry, conduction calorimetry and measurement of chemical shrinkage were used by them to find a correlation among the methods. They were able to find a correlation between non-evaporable water and QXRD data, However, it was mentioned that the correlation was dependent on the chemical composition of the cement. Moreover, a close linear relationship was identified by them in the data of chemical shrinkage and QXRD and in the data of heat of hydration and QXRD data which was not much affected by cement type.

### 2.15.3 Techniques to evaluate the durability

In [68], the authors used SEM, mercury intrusion porosimetry (MIP), nanoindentation techniques to study about the NS incorporated cement paste. In addition to that, the resistance to calcium leaching and chloride penetration were investigated. They were able to obtain some useful information about macro pores which were above 5 μm, about micro pores, and about nano pores which were in the 20-100 nm range. A reduction in the volume of pores in each size has been reported when NS were added to the paste and it was more effective for the macro pores according to their findings [68].

# Experimental Programme

## Summary of the programme

In this research, nano-silica (NS) powder and NS suspensions were synthesized under varying conditions. The hydrolysis time for the precursor to achieve the gelation, the nitric acid to the precursor (tetraethyl orthosilicate) ratio, and the effectiveness of the stabilization on the composition were investigated in the synthesis of the NS powder. The stabilities of the NS suspension in water and calcium hydroxide solutions at different pH levels were tested by zeta potential analysis. The effectiveness of ultrasonication was investigated while the condensation reaction was taking place. Afterwards, the chemical composition and the particle sizes of NS were analyzed by EDS and Dynamic Light Scattering (DLS) respectively. The NS powder and the NS as suspensions in calcium hydroxide were included in cement pastes and their hydrations were investigated by the isothermal calorimetry. The best performing NS in terms of its composition and hydration by calorimetry was selected for further testing. Also investigated were ultrasonification and ethylene glycol as possible processing improvements. Subsequently, cement pastes were prepared having different amounts of the selected NS and commercial NS for comparative purposes. The pastes were cured for 2, 7, and 28 days. The hydration, microstructure, composition, and mechanical properties of the pastes were investigated by different methods. The three primary phases of the research are given in point form below, the experimental details follow in subsequent sections of this chapter.

- NS synthesis
    - Optimization of synthesis conditions
    - Optimization of the stability of NS

- Hydration studies with NS
    - Isothermal Calorimetry
    - Setting time by calorimetry
    - Non-evaporable water content

- Composition, microstructure and mechanical properties
    - Scanning Electron Microscopy
    - CH quantification by DSC
    - CH quantification by thermogravimetry/differential thermal analysis (TG/DTA)
    - CH quantification by XRD
    - Mercury Intrusion Porosimetry
    - Compressive Strength

Chapter 3.

3.1.

3.2.

## Materials, synthesis and characterization of NS

### 3.2.1 Materials for NS synthesis

Tetraethyl orthosilicate (TEOS; Aldrich, ≥99.0%), absolute ethanol (RICCA Chemical Company; ACS Reagent Grade, Anhydrous), ammonium hydroxide (Fisher; ACS plus Reagent Grade, 28.0 - 30.0 w/w %), and nitric acid (Anachemia, ACS Grade, 68 – 70 w/w %) were used to synthesize the silica via the sol-gel method. Calcium hydroxide powder (Fisher, certified) and distilled water were used to wash the as-synthesized silica.

As the precursor, TEOS was selected as it could produce mono dispersed nanoparticles. TEOS belongs to the family of silicon alkoxides and is hydrophobic and is immiscible in water. The molecular structure of TEOS is shown in Figure 3.1. The reaction rates are comparably greater in TEOS than long or bulk chain precursors due to the steric effect or the electronegativity [31,82].

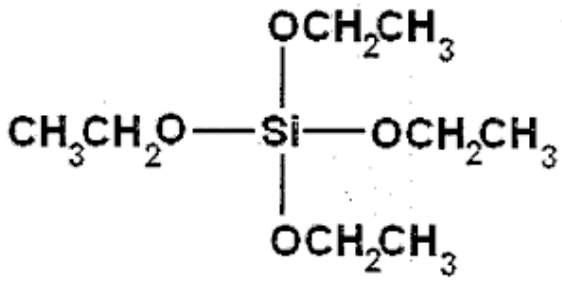


**Figure 3.1: Molecular structure of TEOS**

TEOS is immiscible in water, therefore a mutual solvent is required to dissolve TEOS in water and facilitate its reaction with water. As the solvent, ethanol was selected, it is the alcohol of the same alkoxy group. Moreover, in this research R is the $-CH_2CH_3$ group.

$$Si(OR)_4 + H_2O \rightarrow Si(OH)(OR)_3 + ROH$$

The reaction rates of TEOS in water and ethanol is slower than the transition metal alkoxides as Si is less electropositive [83]. In order to catalyze the hydrolysis reaction, nitric acid was required to be added drop-wise to bring the pH of the sol to be 1-2, as the rate of condensation is minimum at pH 2 [83].

Thereafter the condensation reactions take place as follows;

$$Si(OH)(OR)_3 + Si(OR)_4 \rightarrow (RO)_3Si\text{-}O\text{-}Si(OR)_3 + ROH$$

$$2Si(OH)(OR)_3 \rightarrow (RO)_3Si\text{-}O\text{-}Si(OR)_3 + H_2O$$

In order to catalyze the above reactions, ammonium hydroxide is selected as the catalyst which helps the formation of spherical particles.

3.2.1.1. In the next portion, some of the results are discussed; the synthesis of the three laboratory produced NS particles. As mentioned in the literature review the sol-gel process consists of several steps: hydrolysis, condensation, and stabilization. Additional steps were investigated to obtain particles of the required composition, size and reactivity

***Hydrolysis***

TEOS was dissolved in ethanol by stirring for about 20 minutes. The TEOS to ethanol ratio was taken as 0.65 vol/vol. Varying amounts of nitric acid and water (slightly more than the calculated amount required for a complete hydrolysis of TEOS) were added into the TEOS and ethanol solution to prepare the sol. The TEOS to ethanol ratio was selected from the ternary phase diagram of the TEOS – ethanol – water system at 25℃ so that all three are miscible [84–87]. The used nitric

acid had a concentration of 15.8 M (68 w/w %). Four amounts of nitric acid were investigated ranging from approximately 0.1% to slightly more than 50% by volume of the TEOS/Ethanol mixture. The volume quantities were added using disposable syringes that had 0.01 mL precision. The nitric acid quantity was set such that the pH of the sol is below 2 which favored the hydrolysis reaction. The gelation time of the sols were monitored by the visual observations of when the watery texture of the sol becomes a viscous gel texture. These mixtures were kept stirring for durations which were less than approximately half of their gelation times (Table 3.1) or 1-2 days for the trials that had longer gelation times in order to provide sufficient hydrolysis to form monomers for the condensation reaction. This procedure was performed to identify the suitable nitric acid to TEOS ratio to provide the optimum composition of NS. The suitable ratio of TEOS to nitric acid was used for the remaining processing steps and in the cement paste studies. For those studies, the sol was prepared by adding diluted nitric acid (as per the selected chemical ratio) to the TEOS and ethanol mixture instead of adding water and nitric acid separately. The sol stirring time was set to 2-4 days until the condensation reaction (described next) was initiated.

**Table 3.1: Samples for the gelation time**

| Sol ID | TEOS (mL) | Ethanol (mL) | Nitric acid (mL) | Water (mL) | pH of the sol |
|---|---|---|---|---|---|
| T-1 | 1.95 | 3.00 | 2.60 | 0 | 0 |
| T-2 | 1.95 | 3.00 | 0.20 | 0.40 | 1.0 |
| T-3 | 3.90 | 6.00 | 0.02 | 1.18 | 1.1 |
| T-4 | 3.90 | 6.00 | 0.01 | 1.19 | N/A |

### 3.2.2 Gelation time

Hydrolysis is the first step in transforming the precursor into a colloidal suspension. The gelation times obtained for the different sols prepared are given in Table 3.1. As mentioned earlier, it is difficult to measure the gelation time; the time is determined when the sol became more viscous from its initial watery texture under the visual observation. The gelation time was obtained from 2-3 samples. As mentioned in Chapter 3, the pH of the sols was maintained below 2 in order to facilitate the hydrolysis by minimizing the rate of condensation reactions [83]. The sols in Table 3.2 contain slightly more water than what was needed to completely hydrolyse TEOS stoichiometrically. The ratio of the total water quantity of sol to TEOS was kept a constant while changing the nitric acid amount in the sol to determine the most favourable nitric acid quantity for the reactions. As expected, the pH of the sols increased as the nitric acid amount decreased (Table 3.2). The nitric acid quantity influenced the gelation time of the sols; as the nitric acid quantity decreased, the gelation time increased. The lowest gelation time of 12 hours was obtained when allowing the hydrolysis to occur using 2.6 mL of the concentrated nitric acid as it is (15.8 M) for 1.95 mL of TEOS (T-1 sol in Table 3.2). The time of 12 hours was found to be fast in terms of controlling the hydrolysis reaction. The sol became very viscous and controlling the particle size was seemingly difficult. The highest gelation time was achieved for the sol T-4, where 0.01 mL of nitric acid was used for 3.9 mL of TEOS. The gelation time was very long which was more than five months. Given the length of time, it is doubtful whether hydrolysis is occurring in that sol rendering it impractical as waiting such a long time could create other significant ambient

environmental fluctuations. Therefore, for the compositional analysis this sample was omitted. The composition of T-2 was determined to be the best and this concentration was used for most of the research.

**Table 3.2: Gelation time of different sols**

| Sol ID | TEOS (mL) | Ethanol (mL) | Nitric acid (mL) | Water (mL) | pH of the sol | Gelation time |
|---|---|---|---|---|---|---|
| T-1 | 1.95 | 3.00 | 2.60 | 0 | 0 | 12 hours |
| T-2 | 1.95 | 3.00 | 0.20 | 0.40 | 1.0 | ~ 1 month |
| T-3 | 3.90 | 6.00 | 0.02 | 1.18 | 1.1 | Five months |
| T-4 | 3.90 | 6.00 | 0.01 | 1.19 | N/A | More than five months |

***Condensation***

3.2.2.1. Ammonia is a gelation catalyst used in the sol-gel industry to form spherical particles (Stöber method). As per the findings of Rahman et al. [88] and Park et al. [89] the feeding rate of ammonium hydroxide is crucial to determine the particle size of silica. Faster feeding rates lead to formation of larger particles due to higher rates of hydrolysis and polycondensation reaction occurrences [88]. Therefore, the resulting sols from the hydrolysis step were added dropwise (drops formed from 1 mL syringes) to ammonium hydroxide solutions. The addition of the ammonium hydroxide solution to the sol had shown a formation of visibly larger particles and was not successful practically due the high rate of evaporation of the sol. Thus, the addition of the sol to ammonium hydroxide was carried out. These solutions were prepared in a way that their pH became 10 – 11 after adding the sol. This pH is favorable for the condensation reaction. While this process was going on, vigorous stirring of the mixtures was maintained using magnetic stir bars. This stirring was maintained for one day. After identifying which mixture gave the best composition, the quantity of ammonium hydroxide was fixed for later cement paste studies. The ammonium hydroxide to water ratio to maintain the pH of the ammonium hydroxide solution in between 10 – 11 before and after addition of the sol (which reduces the pH of the ammonium hydroxide) was found by trial and error along with pH measurements. The fixed sol to ammonium hydroxide ratio is 1:9 (vol/vol) and the ammonium hydroxide solution had a 21:75 (vol/vol) commercial ammonium hydroxide to water ratio to maintain the previously mentioned pH range.

3.2.2.2. The effectiveness of utilizing ultrasonication while the condensation reaction was taking place was investigated for the fixed method of NS synthesis. The samples that were ultrasonicated and not ultrasonicated were analyzed for their composition and particle size. The ultrasonicated NS are identified NS_U and the not ultrasonicated are identified as NS_A. Moreover, its effectiveness was analyzed by cement paste studies which will be discussed later.

***Stabilization***

The stabilization is utilized to remove unreacted chemical species in the formed silica. A portion of the formed particles was dried at 70℃ under vacuum. Portions of these dried particles were heated at 600℃ in a tube furnace at ambient conditions to stabilize. This step can make highly reactive hydroxyl groups at the end of less active silica chains. If unreacted chemical species are

within the formed silica particles, they could subsequently affect the cement reactions when the cement pastes are prepared. Therefore, compositional analysis was performed to verify the effect of the stabilization.

### 3.2.3 Characterization of silica

During the phase of the research optimizing the step of NS synthesis, several techniques were used to characterize the chemical composition, particle size and tendency to agglomerate. This section outlines the methods used.

***Energy Dispersive X-ray spectroscopy***

Stabilized and non-stabilized samples as per section 3.2.2.2 were ground using an agate mortar and a pestle to remove the aggregation caused by the drying step. A double-sided carbon tape was pasted on a metal disc which was designated for SEM analysis. A minute amount of
3.2.3.1. powder from a sample was applied on the carbon tape as a very thin layer. The compositions of stabilized, non-stabilized, and ultrasonicated powders were analyzed by energy dispersive X-ray spectroscopy (EDS) under the vacuum mode, a probe current of 62 μA, and an accelerating voltage of 15.0 kV. The amount of carbon was disregarded for the nominal compositional calculations.

### 3.2.4 Compositional analysis

**Table 3.3: The compositions of silica for different nitric acid amounts and the effect of stabilization on the composition**

| Sample ID for Silica | Nitric acid (mL) /1.95 TEOS (mL) | Average Si wt.% | Average O wt.% |
|---|---|---|---|
| T-1-St | 2.60 | 38.61 | 61.39 |
| T-1-NSt | 2.60 | 37.26 | 62.74 |
| T-2-St | 0.20 | 38.18 | 61.82 |
| **T-2-NSt** | **0.20** | **46.64** | **53.36** |
| **T-2-NSt-U** | **0.20** | **46.61** | **53.39** |
| T-3-St | 0.01 | 39.47 | 60.53 |
| T-3-NSt | 0.01 | 32.89 | 67.11 |
| Nominal composition (wt. %) | | **46.74** | **53.26** |

Portions of synthesized particles were stabilized by drying followed by heating in a furnace. Table 3.3 shows the compositions as determined by EDS of synthesized NS with stabilization (samples designated St) and without stabilization (samples designated NSt). In addition, the composition of one NS sample which was obtained from the process of ultrasonication assisted gelation (designated NSt-U) is presented in Table 3.3. The closest

composition to the nominal silica composition was obtained for the silica samples synthesized from the non-stabilized sol having 0.2 mL nitric acid to 1.95 mL TEOS (sample T-2-NSt). The stabilization for the same sample caused less purity in the formed silica. The objective of stabilizing was to remove the unreacted chemical compounds and surface silanols and hydroxyls present, which is applicable mainly for silica films. However, the stabilization was found ineffective for the best ratio of nitric acid to TEOS. When the silica was formed with the same ratio and when the gelation was assisted with ultrasonication, the difference in composition change was insignificant, implying inconsequential effects from the ultrasonication on the composition.

***Zeta potential analysis***

3.2.4.1. The colloidal stability of a suspension depends on the attractive and repulsive forces among individual particles according to the DLVO theory. The attractive forces are attributed to the Van der Waals attractions and the repulsive forces are attributed to the surface charges of the particles and the thickness of the electrical double layer of the particles [90–92]. One of the methods to improve the dispersibility of the nanoparticles in a suspension is by increasing the surface charge of particles [90]. The pH value, or the balance between H+ and OH- ions, in a system is a factor that decides the electrostatic potential of the surface of the particles with respect to the surrounding suspension [92]. Therefore, it is possible to regulate the agglomeration of the colloidal suspension by varying the pH of the colloidal solution. The electrostatic potential at the boundary of the surface layer and the adjacent suspension is called the zeta potential. Figure 3.2 shows a schematic representation of the boundary where the zeta potential is measured in a negatively charged nanoparticle suspension. It also shows the ion layers settling around a charged particle, and what these layers are called.

Thus, zeta potential is related to the agglomeration of colloidal particles and the stability of the suspension can be optimized by measuring the zeta potential of particles in suspensions having different pH values. The zeta potential can be measured based on the electrophoresis. The particles in a dispersion having a zeta potential can migrate to an oppositely charged electrode when an electric field is applied to the dispersion. The particles flow at a velocity proportional to the zeta potential of the particles.

In this study, the silica suspensions washed with calcium hydroxide solutions with different pH (i.e. 5.9, 7.3, 8.4, 8.6, 9.6, and 11.0) were characterized by the zeta potential analysis. About 30 mL of each suspension having around 3 g/L of silica was prepared. About 5 mL of each suspension was placed in the cell. The zeta potential of these suspensions was measured using Zeta meter 3.0+ at 150 V full scale at ambient temperature. Twelve or more potential values were taken to obtain the average zeta potential of each suspension.

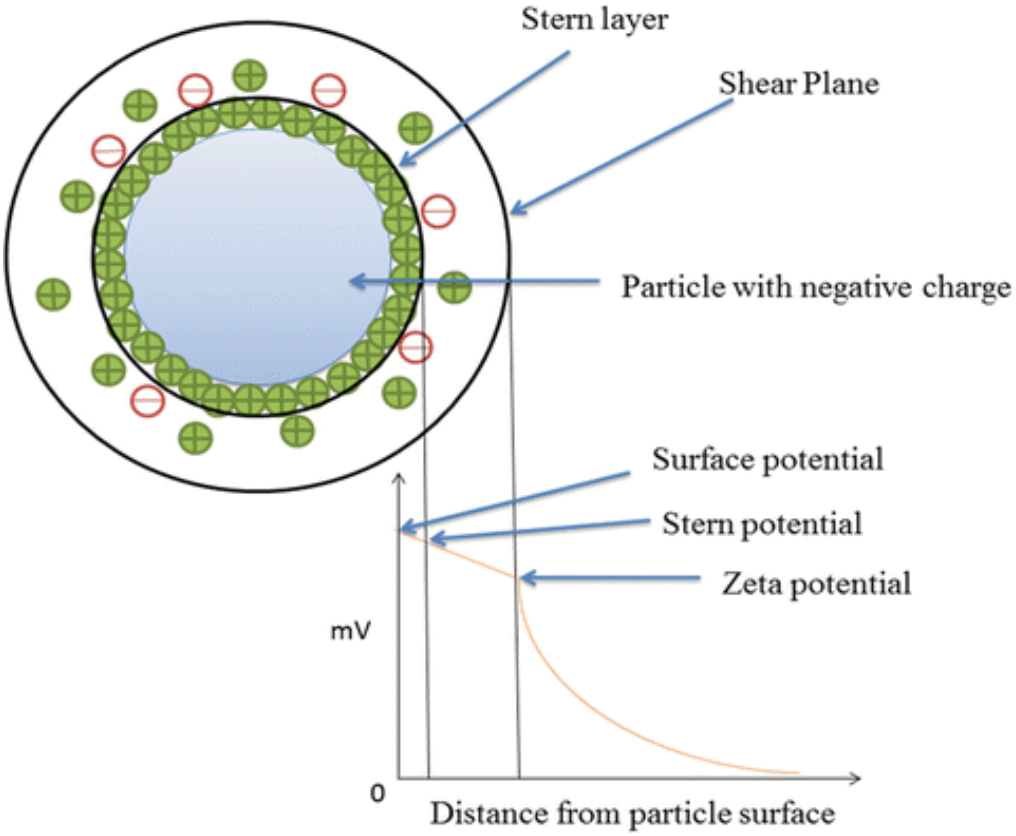


**Figure 3.2: Zeta potential of a particle [93]**

3.2.4.2.

***Removal of ammonium hydroxide***

The formed silica in ammonium hydroxide was centrifuged at 3500 rpm for approximately 20 minutes or more until the supernatant became clear. This step was to remove ammonium hydroxide as it delays the setting time of cement [94]. The supernatant was removed, and it was replaced with water or calcium hydroxide solutions having 5.9, 7.3, 8.4, 8.6, 9.6, and 11.0 pH values to analyze the zeta potential of the suspensions. This rinsing procedure was carried out at least five times or more until the odour of ammonium hydroxide was eliminated. The NS suspensions were ultrasonicated in a bath sonicator for 20 minutes. After determining the appropriate pH for the calcium hydroxide from the zeta potential analysis, NS for the cement paste studies were washed by calcium hydroxide solutions of pH 9-10 by centrifuging.

### 3.2.5 Zeta Potential of the suspension

Even though calcium hydroxide was utilized to replace ammonium hydroxide, the stability of NS as a suspension in calcium hydroxide was required before associating it in cement paste. Therefore, a zeta potential analysis was carried out for NS suspensions in calcium hydroxide having different pH values. The pH was controlled by varying the amounts of calcium hydroxide. The zeta potential values obtained for those suspensions are plotted against the pH values in Figure 3.3 **Error! Reference source not found.**. The zeta potential of all the suspensions were below -30 mV which was recommended by other researchers [95,96] as the threshold zeta potential for a

stable colloidal suspension. The -100 mV zeta potential indicates that the suspensions are well stabilized [96]. As such, the most stable suspensions could be obtained at pH above 9 levels. The maximum pH that the calcium hydroxide solution can reach is 12.4. However, the zeta potential was found to be stable above pH 9; this is easily achievable in calcium hydroxide solutions (0.015 g of calcium hydroxide/1 L of water). Also, it was necessary to centrifuge the suspensions five or more times with this calcium hydroxide solutions in order to completely remove ammonium hydroxide.

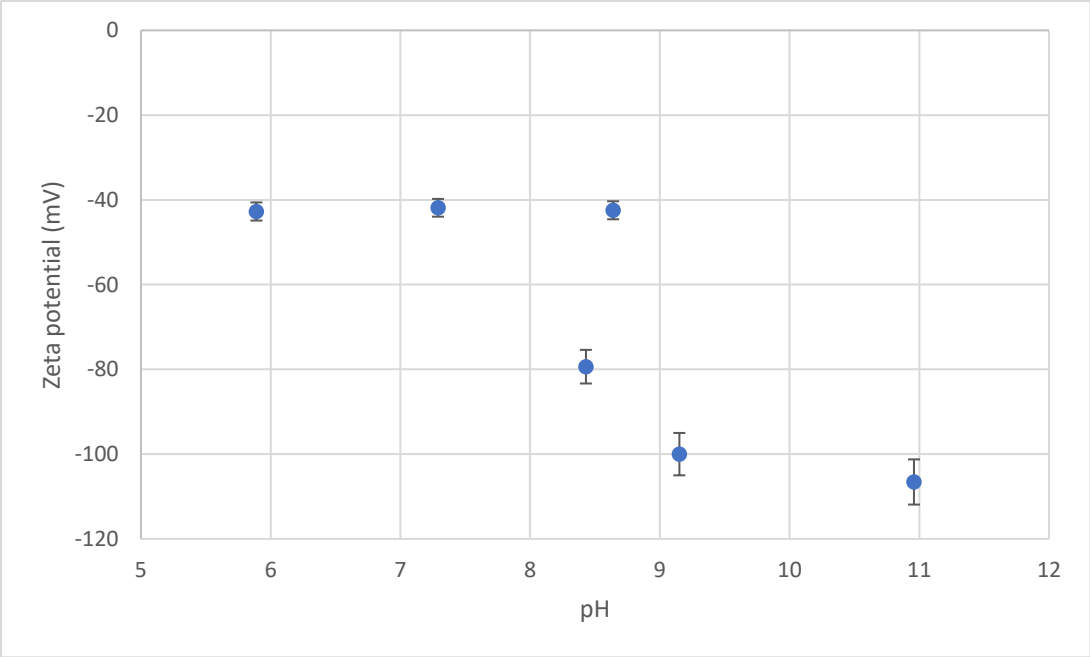


**Figure 3.3: Zeta potential vs. pH plot for the synthesized silica as a suspension in $Ca(OH)_2$**

3.2.5.1.

***Improvements for dispersing NS in the suspensions***

In order to improve the stability of the particles in the suspensions, the effect of ethylene glycol as a dispersant for NS was investigated. Ethylene glycol was first dissolved in a part of the calcium hydroxide solutions of pH 9-10. Then NS (washed with calcium hydroxide) was mixed with the ethylene glycol and calcium hydroxide mixture. A number of NS concentrations and ethylene glycol to NS ratios were investigated (Table 3.4). The particle size analysis for the suspensions were measured by dynamic light scattering. The NS mixed with ethylene glycol are identified as NS_EG. The NS concentrations were selected to prepare suspensions that can be directly added to the cement paste having 0.48 water/cementitious material ratio and the NS percentages (1% and 4%). The ethylene glycol/NS ratio were selected to provide enough ethylene glycol molecules to coat on the surface of the silica molecules. Limited studies were undertaken using this synthesized NS in cement pastes.

**Table 3.4: Concentration and ratios of ingredients in NS_EG**

| Ethylene glycol/NS (mol/mol) / NS concentration | 13.9 | 21.08 | 28.07 |
|---|---|---|---|
| 77 g/L | 4-50 | 4-75 | 4-100 |
| 2 g/L | - | 1-75 | 1-100 |

***Particle size analysis***

3.2.5.2 The Malvern, Zetasizer Nano S90 instrument was used and the technique behind the instrument was Dynamic Light Scattering (DLS). Where necessary, the refractive index was considered to be 1.54 for silica and 1.331 for the dispersant when ammonium hydroxide was used as the suspension for the particle size calculation. Approximately 30 mL of each suspension was taken and ultrasonicated prior to the examination.

***Viscosity***

3.2.5.3. The viscosity values are necessary to calculate the particle size by the Malvern, Zetasizer Nano S90. Therefore, the viscosity of the NS suspensions was measured using a vibrating viscometer (model: A & D, VC-10) and Ostwald viscosimeter; 40 mL of each NS suspension was taken and ultrasonicated for 3 min at 60 % amplitude. The commercial silicas were taken as they were.

### 3.2.6 Nano-silica (NS) synthesis

A significant amount of time was dedicated to optimizing synthesis steps for generation of NS particles. Figure 3.4 shows a flow chart of the steps that were followed to optimize the silica synthesis process. At each step, the resulting properties (e.g. composition) were measured varying the conditions (e.g. ratios of chemicals). Each step is described in the next sections.

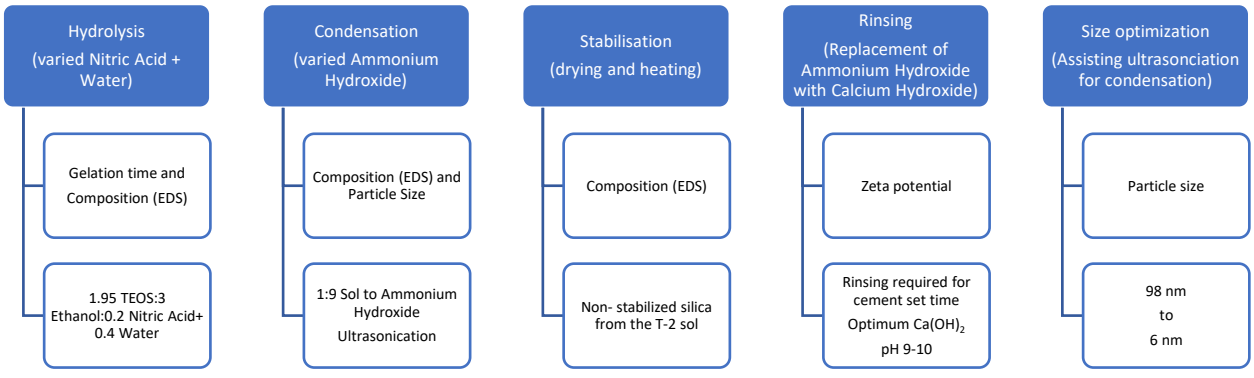


**Figure 3.4: The steps of silica synthesis, variables investigated, test methods used and optimum result**

## Materials and Methods for NS in Cement paste

As the major influence of adding nanoparticles to cement pastes is increased hydration, the objective of this research was to investigate early ages after casting. The samples prepared for the hardened cement pastes and were cured for 2, 7, and 28 days. Methodology largely focussed on the measurement of hydration by various techniques as well as the development of pore structure and mechanical properties. The next several sections outline the incorporation of NS into cement pastes and the methods used.

### 3.3.1 Materials for cement pastes

General-use Portland cement from the Lafarge St. Constant plant, distilled water, and as-synthesized silica were used for the preparation of cement pastes. Normal Portland cement was selected for this study as it is the most common type of cement currently used in the industry and also due to the high percentage of tricalcium silicate content in this cement. The chemical composition and the physical characteristics of the cement given by the manufacturer are given in Table 3.5.

**Table 3.5: Chemical and physical characteristics of cement**

| **Chemical Composition** | **Percentage (%)** |
|---|---|
| $SiO_2$ | 19.0 |
| $Al_2O_3$ | 4.7 |
| $Fe_2O_3$ | 2.9 |
| CaO | 60.9 |
| MgO | 2.7 |
| $SO_3$ | 4.0 |
| Loss on ignition | 4.3 |
| **Potential Phase** | **Percentage (%)** |
| $C_3S$ | 55 |
| $C_2S$ | 15 |
| $C_3A$ | 8 |
| $C_4AF$ | 9 |
| **Physical Characteristics** | |
| Fineness (Blaine) ($cm^2/g$) | 468 |
| Retained on 45 μm (%) | 5.5 |

***NS suspensions for the preparation of cement pastes***

The NS suspensions were concentrated to have 15% or more of NS in the calcium hydroxide solution. The concentrated suspension was ultrasonicated and about 15 – 20 mL of the suspension was taken to crucibles. The crucibles containing the NS suspensions were dried at 105℃. After the dried NS achieved a stable weight, the NS content per liquid weight was assessed. Then the concentrated suspension was diluted with calcium hydroxide solutions (pH 9 - 10) to obtain the NS suspensions given in Table 3.6. (For example, to prepare a cement paste with 4% NS of which the cementitious material content is 100 g and water/cementitious material ratio is 0.48, 96 g of cement is taken and mixed with 52 g (4 g of NS + 48 g of water) of the suspension, no additional water was added).

3.3.1.1.

**Table 3.6: Concentrations of NS suspensions (0.48 water/cementitious material ratio)**

| Cement replacement percentage (%) | NS percentage of the suspension (weight%/ water weight) required to obtain the corresponding cement replacement | If the cementitious materials weight is 100 g, the required suspension weight (g) |
|---|---|---|
| 0 | 0 | - |
| 1 | 2.04 | 49 |
| 2 | 4.00 | 50 |
| 4 | 7.69 | 52 |
| 6 | 11.11 | 54 |
| 7.2 | 13.04 | 55.2 |
| 8 | 14.29 | 56 |

3.3.1.2.

***Cement paste preparation***

For Vicat set time and isothermal calorimetry tests, cement pastes were mixed as detailed in the section describing each method. For non-evaporable water content, differential scanning calorimetry, thermogravimetry, scanning electron microscopy, compressive strength and mercury intrusion porosimetry, small paste prisms were cast and cured until testing. The NS suspensions were prepared in a way that it can be directly added to the cement having the water and the NS amounts as per the ratios given in Table 3.7. First, the NS suspensions with relevant NS concentrations or distilled water was added into a beaker. Cement was then added to the beaker while recording the time. It was mixed using a spoon for 2-3 minutes. The paste was then poured to the molds which had 1 cm x 1 cm x 7 cm cavities (for non-evaporable water content, thermogravimetry, differential scanning calorimetry, scanning electron microscopy, and mercury intrusion porosimetry) and 2.5 cm x 2.5 cm x 2.5 cm (for compressive strength). Each cavity was tamped using a 1 cm x 1 cm x 7cm PVC rod for 25 times. Then, the molds were jolted by lifting by roughly 10 cm and releasing it on to the table 60 times to remove air bubbles. The material quantities were taken so that they satisfy the cementitious material ratio (Cement/NS) and the water to cementitious material ratio given in Table 3.7. The total weight of each cement paste mixed was 150 g.

The molds were then placed inside a sealed box (~75cm x 7.5 cm x 25 cm) which contained a water level of 25 mm. Afterwards, the molds were placed on a surface in a way that they could not contact the water and were leveled flat. Finally, the specimens were demolded after a day and placed inside open jars in the same sealed box for curing until the required age was reached.

**Table 3.7: Mixture proportions**

| Sample Name | Cementitious material (cm) ratios | | w/cm |
|---|---|---|---|
| | Cement | NS | |
| Control | 1.000 | 0 | 0.48 |
| 1%_NS_A | 0.990 | 0.010 | 0.48 |
| 2%_NS_A | 0.980 | 0.020 | 0.48 |
| 4%_NS_A | 0.960 | 0.040 | 0.48 |
| 6%_NS_A | 0.940 | 0.060 | 0.48 |
| 8%_NS_A | 0.920 | 0.080 | 0.48 |
| 1%_NS_U | 0.990 | 0.010 | 0.48 |
| 2%_NS_U | 0.980 | 0.020 | 0.48 |
| 4%_NS_U | 0.960 | 0.040 | 0.48 |
| 6%_NS_U | 0.940 | 0.060 | 0.48 |
| 7.2%_NS_U | 0.928 | 0.072 | 0.48 |
| 4% NS_EG | 0.960 | 0.040 | 0.48 |
| 1%_HS 40 | 0.990 | 0.010 | 0.48 |
| 2%_HS 40 | 0.980 | 0.020 | 0.48 |
| 4%_HS 40 | 0.960 | 0.040 | 0.48 |
| 6%_HS 40 | 0.940 | 0.060 | 0.48 |
| 1% CB8 | 0.990 | 0.010 | 0.48 |
| 4% CB8 | 0.960 | 0.040 | 0.48 |
| 1% CB9 | 0.990 | 0.010 | 0.48 |
| 4% CB9 | 0.960 | 0.040 | 0.48 |

3.3.1.3.

***Hydration inhibition***

Except for the compressive strength tests, the hardened cement pastes which achieved their required age were immersed in acetone for about one hour. Afterwards, acetone was replaced with fresh acetone. This acetone replacement was carried out for a total of 3 times or more on an hourly basis. Then, they were kept immersed in acetone for at least a day. Hardened solid cement paste specimens for SEM, MIP, TGA, and the Non-evaporable water content test along with ground cement paste powders for XRD and DSC were then dried in a vacuum oven at 40℃ for a day. The dried samples were stored in a desiccator for an hour or until the test was performed.

### 3.3.2 Setting time

Setting time was measured by two techniques in this research. The Vicat test is a very common test often used for quality controls purposes for cement manufacture as well as comparative behaviour when investigating the influence of material selection on the early stages of cement hydration. This test was used for a few mixtures at the beginning of the test program; isothermal calorimetry was used for the remainder of the research.

The Vicat test was performed as per ASTM C 191 with a few modifications to the standard method [97]. The water/cementitious material ratio (w/cm) was fixed at 0.35 for all the samples

instead of preparing a paste with the standard consistency. The mixing was carried out by using a 5 L mixer (Hobart). The test was carried out at room temperature in an environment with uncontrolled humidity. This test was carried out early in the program to quantify the influence of ammonium hydroxide on set time. Four mixtures were cast: a control sample (cement and water), a sample using aqueous $NH_4OH$, a sample using aqueous $Ca(OH)_2$ and a sample containing NS.

For the isothermal calorimetry, the time corresponding to the 25% of the acceleration peak on the rate of heat evolution versus time was measured as the initial setting time [98]. Figure 3.5 shows the point of time that is designated as the initial setting time from a temperature vs time curve which is equivalent to the rate of heat flow vs time.

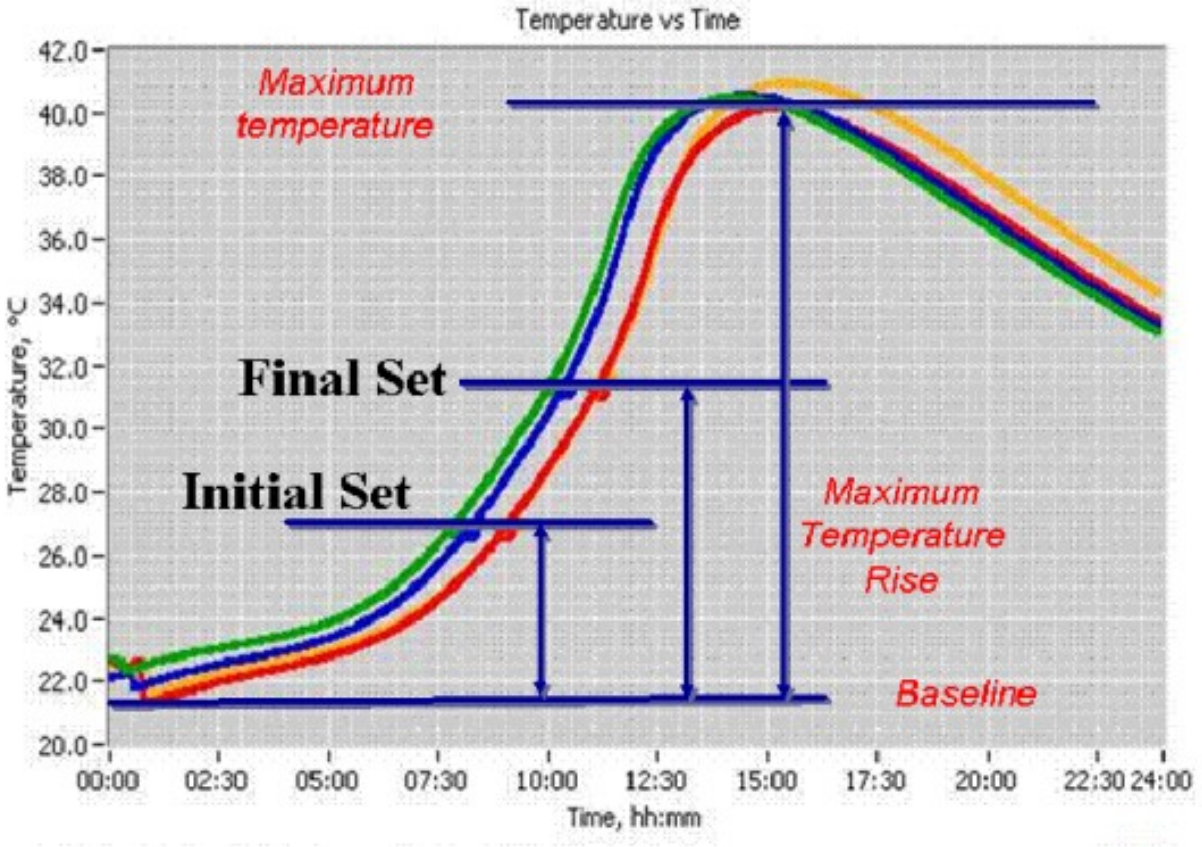


**Figure 3.5: Determining the setting time by the fractional method [98]**

Initially, this test was carried out to study the effect of the washing process. The setting times were obtained from the rate of heat evolution versus time graph which was itself obtained from the isothermal calorimeter (model- I-CAL 4000). This presumed setting time was measured for the cement pastes with NS as a suspension in distilled water, NS as a suspension in $Ca(OH)_2$, as-synthesized NS in powder form, and without any NS. The setting time from this method was also determined for higher percentages using the isothermal calorimeter model I-CAL 2000.

### 3.3.3 Hydration

Several methods were used to measure the influence of NS on hydration behaviour. Isothermal calorimetry and non-evaporable water were direct measurement techniques and are

detailed in this section. Other techniques, such as determination of the consumption of calcium hydroxide, are detailed in the next section.

***Isothermal calorimetry***

Isothermal calorimetry was used to estimate setting time as previously mentioned. However, the main purpose of isothermal calorimetry was to investigate the influence of NS on the early hydration period, mainly the acceleration phase. The preliminary tests were carried out using the isothermal calorimeter, model I-CAL 4000 where 0.1 NS percentages were tested. The other tests were carried out by the isothermal calorimeter model- I-CAL 2000. Water or the NS suspension mixed with water was measured to a plastic cup (Figure 3.6) designated for the isothermal calorimeter. Immediately after adding the water, the data logging was started. The cement and the liquid were mixed using a wooden stick for 90-150 s. Then, the cups were placed in the calorimeter, while the temperature was set at 23℃. The heat flow was measured for 72 hours with reference to a metal cylinder (Figure 3.7) recommended by the manual of the calorimeter. The thermal mass of the reference can be considered as similar to 20 g – 100 g of cement paste. For all the tests the average of energy or the power of the two channels were taken, except for the preliminary analysis where only one sample from one channel was used. The weights of the pastes were 22 g for the pastes with NS_A and 44.4 g for the pastes with other NS types. The ratios of the materials mixed are given in Table 3.7.

3.3.3.

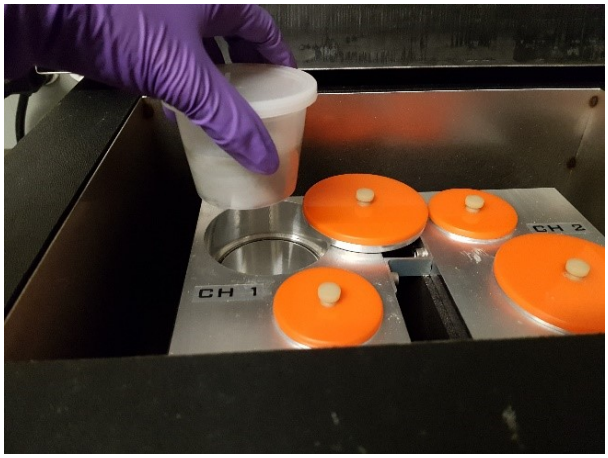


3.3.3.2. **Figure 3.6: The container used for the calorimetry**

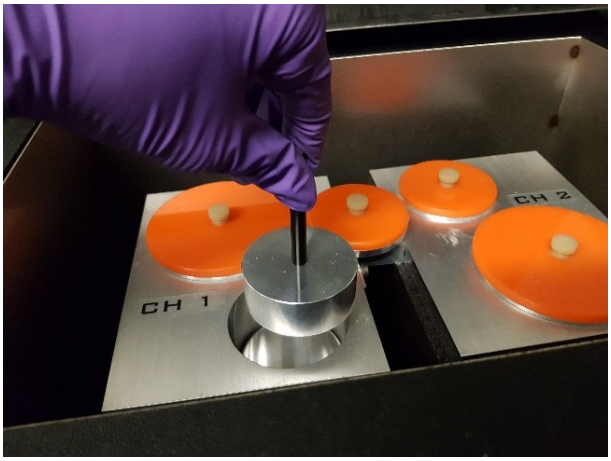


**Figure 3.7: The reference mass for the calorimetry**

***Non-evaporable water content***

Non-evaporable water was determined by heating hardened cement paste samples in a furnace. To ensure the crucible did not affect the results, alumina crucibles were heated in a muffle furnace at 950℃ for 3 hours. Then, they were cooled in the furnace and placed in a desiccator for at least 2 hours. Afterwards, the weights of the crucibles were taken, then 1-3 g of dried samples were cut from the prisms (prepared as per the section 3.3.1.2) and were placed in crucibles, and the specimens were heated at 950℃ for 3 hours. The samples were then cooled in the furnace., and the cooled samples were placed in a desiccator for at least 2 hours. The samples were subsequently weighed.

The cement that was taken to prepare the pastes was heated to 950℃ and cooled in the same way. The weight loss of cement on ignition was calculated. The mass loss due to the

chemically bound water content was calculated by the weight loss and it was corrected for the loss on ignition of the cement.

### 3.3.4 Composition, microstructure and mechanical properties

#### *Differential scanning calorimetry*

Differential scanning calorimetry was used to quantify the calcium hydroxide as a further measure of hydration and reactivity. For differential scanning calorimetry, specimens immersed in acetone were ground using a mortar and a pestle. The ground specimens were sieved using 75 µm and 45 µm sieves. The powder passing through the 75 µm sieve and retained on the 45 µm sieve
3.3.4.1. was taken and dried as per section 3.3.1.3. A portion of roughly 25 mg – 35 mg of ground paste was measured into an aluminium pan. The aluminium pan was closed with an aluminum lid. As the reference, a closed aluminium pan and lid were taken. The reference and the sample were subjected to heating at a rate of 5℃/min from 23℃ to 600℃ using the TA Instruments-2010 DSC apparatus.

A calibration curve was created to quantify the energy corresponding to CH decomposition. Mixtures of 10%, 20%, 80%, 90%, and 100% CH in aluminum oxide powder were prepared. The mixtures were subjected to heating using the same parameter as the cement paste. The energy corresponding to CH for each mixture was plotted with the CH percentage to find the relationship of the energy variation with the CH quantity as per the method used by Moukwa et al. [99] and Kim et al. [100]. Using the gradient of the curve, the CH content of the hardened cement paste was quantified by the following equation.

$$The\ CH\ content = The\ energy\ corresponding\ to\ CH\ decomposition \times the\ gradient$$

The energy was determined by the endothermic peak area of the CH composition calculated using the TA Universal Analysis software.

3.3.4.2.

#### *Thermogravimetry*

For thermogravimetry, portions of about 20 – 40 mg were cut from the cement paste prisms. The initial mass of the pieces was taken. The samples were heated from 23℃ to 900℃ at a rate of 5℃/min using the TA Q50 analyzer under an $N_2$ atmosphere. The weight loss during the CH decomposition reaction was determined by the Universal analysis software. Finally, the equivalent
3.3.4.3. CH amount was calculated. Only, preliminary batches of cement paste with NS_A were tested using this technique.

#### *X-ray diffraction spectroscopy*

For XRD, the samples were ground using a mortar and pestle. The powder passing through a 45 µm sieve was taken for the analysis. Nine parts of this powder were mixed with one part of crystalline silicon. The samples were then analyzed for XRD from 10- 90 degrees (2θ) using Cu
3.3.4.4. Kα radiation. The voltage and the anode current used were 40 kV and 45 mA respectively. The cement pastes were analyzed by using Bruker, D8 Advance X-ray diffractometer and the silica samples were analyzed by Philips X-ray Diffractometer. For the Rietveld refinement the intensity values were scaled-down and analyzed by X'pert Highscore software.

#### *Scanning electron microscopy*

For the scanning electron microscopy tests, the samples were cut using a diamond saw cutter. Then the samples were epoxy impregnated inside a vacuum chamber at 0.12 Bar. Then, they were ground using 400 grit sandpaper until the surfaces of the specimens were revealed. The

samples were ground again with 800 grit paper. They were polished with alcohol based 6 µm and 0.5 µm diamond paste. In each step, absolute ethanol was used as the lubricant. After each step of grinding and polishing, the specimens were ultrasonicated in absolute ethanol to remove the residue created. The polished specimens were dried at 40℃ in the vacuum oven for 24 hours. Finally, they were sputtered gold palladium for three cycles prior to carrying out the SEM. They were analyzed using Scanning Electron Microscope, Hitachi, S-3400 N.

Some of the cement paste samples (Figure 5.13) and NS samples were analyzed by using FEI Quanta 450 Environmental Scanning Electron Microscope. Carbon coating was applied instead of gold sputtering on the cement paste samples in Figure 5.13.

***Mercury intrusion porosimetry***

For MIP, between 1-3 g of the hardened and dried cement paste specimens were taken and tested by a Micrometrics, Pore sizer 9320. The mercury intrusion was carried out by the low
3.3.4 pressurization (0 psi - 20 psi) followed by the high pressurization (15 psi – 30000 psi). The surface tension of Mercury, and the advancing and receding angles were taken as 0.485 N/m and 135° respectively.

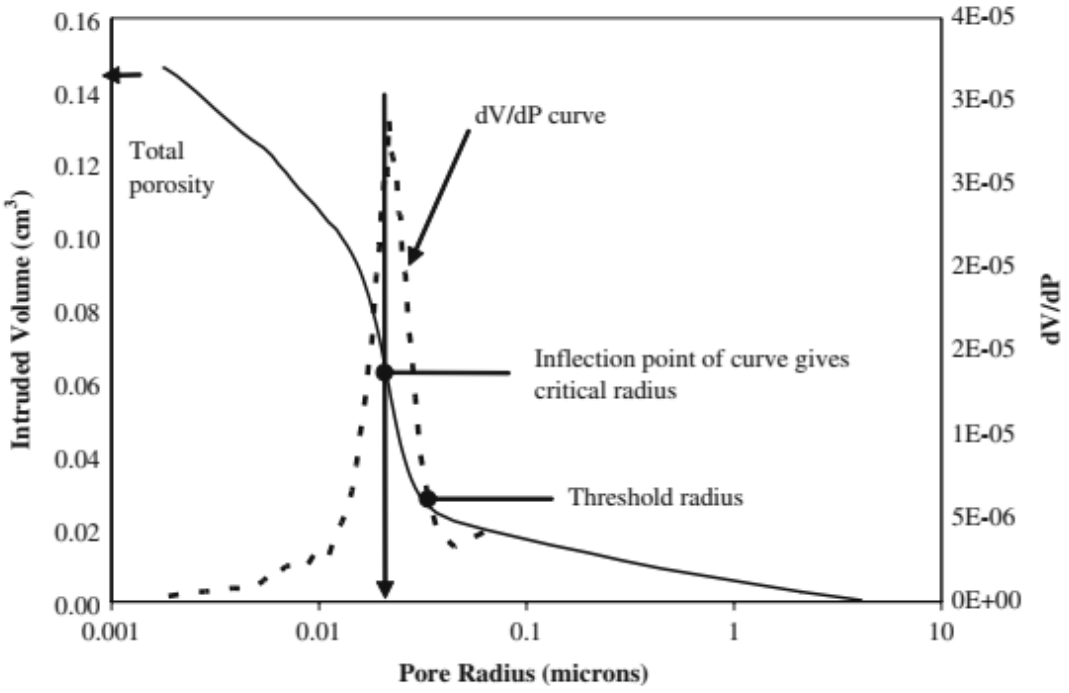


**Figure 3.8: Determination of the critical pore size [101]**

Several pore size parameters can be obtained by the MIP. One is threshold pore size at which the mercury starts to enter and percolate into the pore structure in significant amount [101]. However, it is difficult to determine the exact point of the threshold pore diameter. Another parameter is the critical pore diameter at which the mercury is intruded into the pore system at its maximum rate per pressure change [102]. The critical pore diameter can be determined from the maximum point of the derivative curve of the cumulative intruded volume vs. pore radius curve as

shown in Figure 3.8 [101,103]. It is also equivalent to the inflection point of the cumulative volume vs. pore size cure [101]. This is the pore size that which allows "the maximum percolation of chemical species" into the cement paste due to its frequent occurrence [103].

***Compressive strength***

The cement paste was mixed as per the section 3.3.1.2. The paste was poured into a mold which had 25 mm cubic cavities. The curing was carried out the same way. The samples were tested for the compressive strength at a loading rate of 0.5 N/s. Three samples were tested and the average value was taken as the compressive strength except that two samples were tested for the pastes with NS_A.

3.3.4.6

## Testing program

3.4.

Three laboratory synthesized NS types with a small variation of the synthesis method were used to prepare cement pastes as well as three commercially available NS types for the comparison of the results. Their names, particle sizes, pH and other details are given in Table 3.8.

**Table 3.8: Details of NS used in this research**

| Name of NS | Particle size | pH of the suspension | Counter ions or other ions in the suspension | Manufacturer/company |
|---|---|---|---|---|
| NS_A | 91 nm, 98 nm, 109 nm | 9 - 10 | $Ca^{+}$ | Laboratory synthesized (not ultrasonicated) |
| NS_U | 5.2 nm, 6.4 nm, 6.5 nm | 9 - 10 | $Ca^{+}$ | Laboratory synthesized (ultrasonicated) |
| NS_EG | 5.9 nm, 5.7 nm, 6.1 nm | 9 | $Ca^{+}$ | Laboratory synthesized (ethylene glycol) |
| HS-40 | 12 nm | N/A | $Na^{+}$ (not specified whether they act as counter ions) | Fisher |
| CB-8 | 3 – 100 nm | 9.5 | $Na^{+}$ | Levasil |
| CB-9 | 45 – 47 nm | 9.5 | $Na^{+}$ | Levasil |

### 3.4.1 Sample identification

The cement paste samples are labelled in a way that the NS percentage and the type of silica incorporated were included in their labels. Additionally, all the hardened pastes contained their curing time. The identification started with its percentage, then the silica type and its curing time were separated by an underscore "_". For example, if a hardened cement paste has a label 4%_NS_U_7d, it represents that the paste has 4% NS from the NS_U type, and that it was cured for 7 days. The samples prepared for the tests are given in Table 3.9.

**Table 3.9: Samples prepared for the tests**

| Mixture | Calorimetry | SEM | DSC | TGA | Non evaporable water content | MIP | Compressive strength |
|---|---|---|---|---|---|---|---|
| Control | X | X | X | X | X | X | X |
| 1%_NS_A | X | X | | X | X | X | X |
| 2%_NS_A | X | X | | X | X | X | X |
| 4%_NS_A | X | X | | X | X | X | X |
| 6%_NS_A | X | | | X | X | X | X |
| 8%_NS_A | | X | | X | | | |
| 1%_NS_U | X | X | X | | X | X | X |
| 2%_NS_U | X | X | X | | X | X | X |
| 4%_NS_U | X | X | X | | X | X | X |
| 6%_NS_U | X | | X | | | | X |
| 7.2%_NS_U | X | | | | | | |
| 4% NS_EG | X | | | | | | |
| Commercial NS | | | | | | | |
| 1%_HS 40 | X | | | | | | X |
| 2%_HS 40 | X | | | | | | X |
| 4%_HS 40 | X | | | | | | X |
| 6%_HS 40 | X | | | | | | X |
| 1% CB8 | X | | X | | | | |
| 4% CB8 | X | | X | | | | |
| 1% CB9 | X | | X | | | | |
| 4% CB9 | X | | X | | | | |

# Chapter 4

# Results

In this chapter, the results obtained by the methods as described in Chapter 3 are presented. Some of the results obtained in the process of optimizing the NS synthesis were presented in Chapter 3 for the ease of understanding. The rest of the results and the characterization of NS are presented in this chapter. Then, the results from associating the synthesized NS in cement paste are provided. After that, a comparison of the results with commercial NS is given. In this chapter, the results will only be discussed individually rather than comparing with each other unless necessary. The individual conclusions obtained by each trial and test will also be presented separately. The Discussion chapter will compare results from all tests.

## NS synthesis

### 4.1.1 Selection of the suspension media for silica based on the setting time

### 4.1.

**Table 4.1: Mixture proportions, mixing method, and the setting times obtained by Vicat test**

| Sample | Water/ cement ratio (w/c) | Cement (g) | Distilled water (g) | $NH_4OH$ (g) | As-synthesized Silica (g) | Setting time (min) |
|---|---|---|---|---|---|---|
| Control sample (cement+water) | 0.35 | 450 | 158 | - | - | 277 |
| Cement+ Aqueous $NH_4OH$ | 0.35 | 450 | 158 | 9.41 | - | 365 |
| Cement + Aqueous $Ca(OH)_2$ | 0.35 | 450 | 158 | - | - | 285 |
| Suspension (cement+ as-synthesized silica as a suspension in $NH_4OH$) | 0.35 | 450 | 158 | 9.41 | 0.89 | 339 |

According to the findings in Chapter 3, the ratios of silica synthesis ingredients were fixed with respect to inclusion of NS in cement pastes. Before associating NS in cement, it was important to investigate how the chemical compounds in the silica suspensions affect the cement hydration reactions.

Table 4.1 shows the effect of the chemical compounds in NS suspensions on the setting time of the cement as determined by the Vicat test. Three cement pastes without NS (control, with ammonium hydroxide and with calcium hydroxide) as well as NS with ammonium hydroxide. The

water to cement ratio was maintained at 0.35. The control sample (only containing distilled water) resulted in an initial setting time of 277 min. The sample containing ammonium hydroxide took 365 min for the initial set, indicating a significant delay on the order of 90 min. This behavior was visible for the NS suspension containing cement paste as well. However, the delaying effect was minimized by more than 25 min due to the presence of NS. This implied that even with 0.2% NS (by weight) addition, the setting time of the cement could be reduced. This work revealed the necessity of the elimination of ammonium hydroxide from NS suspensions. Calcium hydroxide was an alternative to replace ammonium hydroxide as it could maintain the pH of the hardened cement paste, provide the basic condition that is required for the formed NS suspensions, and not be harmful for the cement hydration reactions and the hardened cement paste. Thus, the initial setting time of the cement was tested for the calcium hydroxide solution and was found out that it could result in almost the same setting time of the control sample. This was confirmed by the setting time obtained by the fractional method which will be discussed in the next section. Thus, the ammonium hydroxide was replaced in the NS suspensions with calcium hydroxide for the remaining cement paste studies.

As discussed previously, assessing the compatibility of the silica with the potential suspension media was performed by the setting time test. In addition, isothermal calorimetry was used to investigate the setting of the cement with water which was used as the control sample, the setting of cement with aqueous ammonium hydroxide to assess the effect of ammonium hydroxide, and the setting of cement with aqueous calcium hydroxide to assess its effect.

Table 4.2 gives the comparison of the setting time assessed for the samples mentioned. The time corresponding to 25 % of the peak height of the rate of heat evolution curve was determined as the setting time by the fractional method (section 3.3.2). This method overestimates the setting time. However, the trend is comparable with the Vicat method. The control sample gave an initial setting time of 375 min by the fractional method, while the sample with the ammonium hydroxide gave a longer setting time of 540 min confirming the previous results that the ammonium hydroxide delays the setting time of cement. Moreover, associating calcium hydroxide did not show much variation in the setting time, again verifying no adverse effect on the setting of cement by calcium hydroxide at its pH which was the same as that of the stabilized silica suspension.

**Table 4.2: Comparison of setting time by Vicat and fraction method**

| Sample | Setting time by Vicat Apparatus (min) ( Table 4.1) | Setting time measured by fraction method (min) | Remarks |
|---|---|---|---|
| Cement + water | 277 | 375 | |
| Cement + Aqueous $NH_4OH$ | 365 | 540 | pH of the $NH_4OH$ solution: ~11. 5 |
| Cement + Aqueous $Ca(OH)_2$ | 285 | 375 | pH of the $Ca(OH)_2$ solution: ~10. 5 |

### 4.1.2 Particle size analysis

Figure 4.1 shows the particle size distribution measurement for the silica suspensions in ammonium hydroxide for NS_A type silica without rinsing with CH. For this sample, the technique used to measure the particle size was DLS. There are two size distribution peaks for both curves for this sample. Ninety percent (90%) of the particles (by number) belong to the visibly significant peak and 10% of particles (by number) are in 500 nm range which is barely visible comparatively. The modes of these particle size distributions of the most significant peaks lie at 91 nm and the mean sizes are 109 nm and 98 nm. The span of the curve ranges from 68 nm – 255 nm and 50% of the particles are below 100 nm for both curves.

Figure 4.2 shows three particle size distribution curves for NS_U type silica. Two of the three curves overlap completely. The particle size distributions give 5.2 nm, 6.4 nm and 6.5 nm average sizes for the silica. The particle sizes range from 3 nm – 20 nm giving a narrow size range. Fifty percent (50%) of the particles (by number) are below 5 nm for two curves and for the other curve, it's below 6 nm. There was only one peak for each particle size distribution. This indicated that there were no agglomeration present in the NS_U type silica. As well the ultrasonication resulted in substantially smaller particles. During the ultrasonication, a high number of bubbles created in the liquid media. Subsequently, these bubbles implosively collapse by acoustic cavitation [102–104]. As a result of that, extreme pressure and hot spots are created in liquid which are supplemented by rapid heating and cooling [103]. Occurrence of this procedure reduces the gelation time and creates milder conditions for the condensation reaction [102,103]. This could be the reason for the size reduction in NS_U silica.

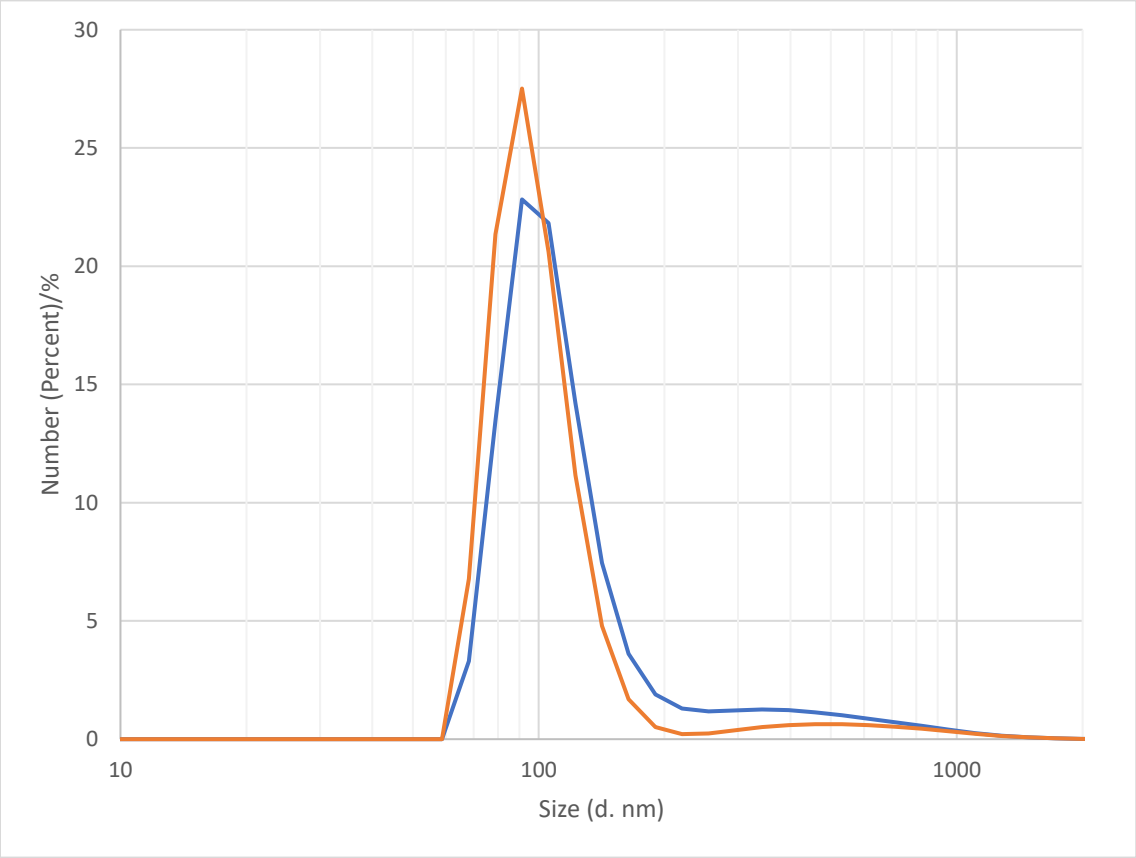


**Figure 4.1: Particle size analysis of NS_A**

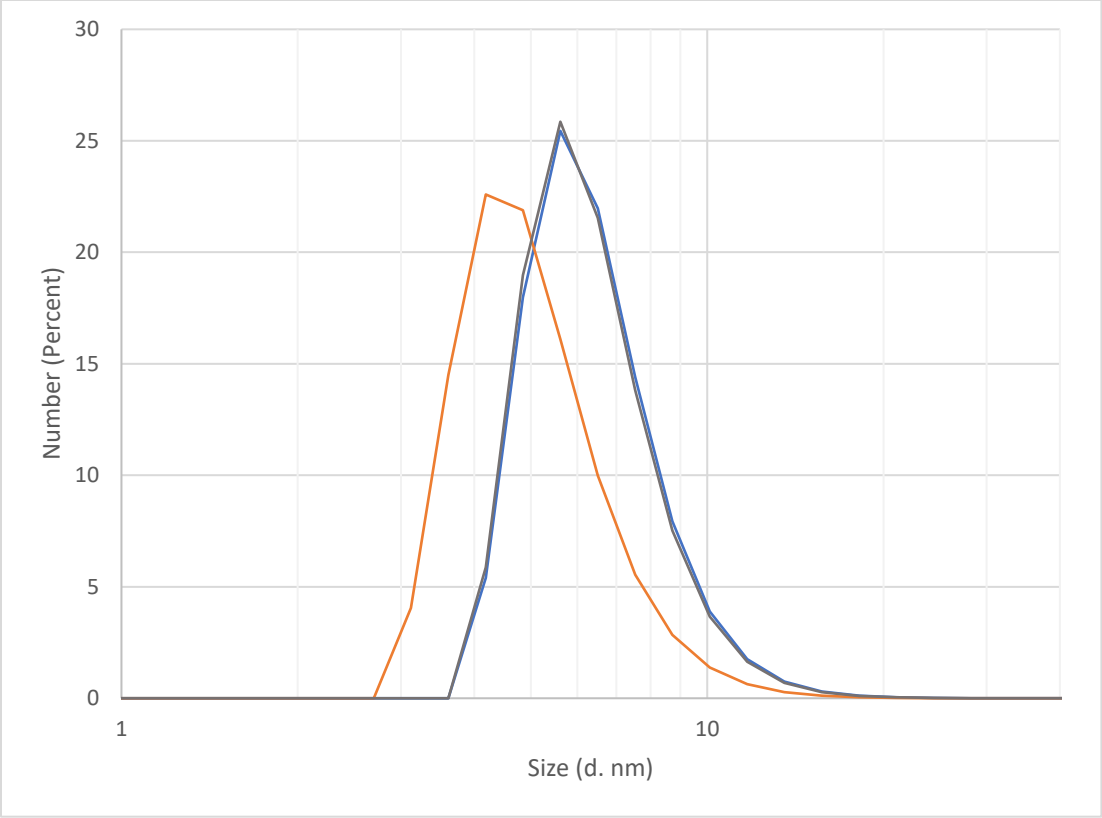


**Figure 4.2: Particle size analysis of NS_U**

For this sample, the technique used to measure the particle size was DLS. There are two size distribution peaks for both curves for this sample. Ninety percent (90%) of the particles (by number) belong to the visibly significant peak and 10% of particles (by number) are in 500 nm range which is barely visible comparatively. The modes of these particle size distributions of the most significant peaks lie at 91 nm and the mean sizes are 109 nm and 98 nm. The span of the curve ranges from 68 nm – 255 nm and 50% of the particles are below 100 nm for both curves.

**Table 4.3: Particle size of NS_EG**

| Sample ID (NS_EG) | NS concentration (g/L) | EG/NS (mol/mol) | Average particle size (nm) | Viscosity (mPa.s) |
|---|---|---|---|---|
| 1-75 | 2 | 21.08 | 191 | 2.48 |
| 1-100 | 2 | 28.07 | 311 | 2.91 |
| 4-50 | 77 | 13.9 | 4 | 2.52 |
| 4-75 | 77 | 21.08 | 6 | 3.07 |
| 4-100 | 77 | 28.07 | 7 | 3.78 |

Table 4.3 presents the particle average particle size obtained by the DLS and the viscosity measured for the NS suspensions containing ethylene glycol. The first digit of the sample ID gives information about the total NS concentration of the suspension (Table 3.4), 1 represents that the NS concentration is 2 g/L and 4 represents that it is 77 g/L. The number followed by "-" provides details about the ethylene glycol/NS ratio; 50, 75, and 100 are for 13.9 mol/mol, 21.08 mol/mol, and 28.07 mol/mol respectively (Table 3.4). The results suggest that the particle size increases with the ethylene glycol/NS ratio increase for the tested range of the ratio. Also, it shows a particle size reduction as the NS concentration increases. This can be due to that it could be favorable to coat ethylene glycol on to the surface silanols at these concentrations which reduces the particle size or at lower NS concentrations, ethylene glycol crosslinks silica particles to form larger particles.

### 4.1.3 XRD analysis of silica

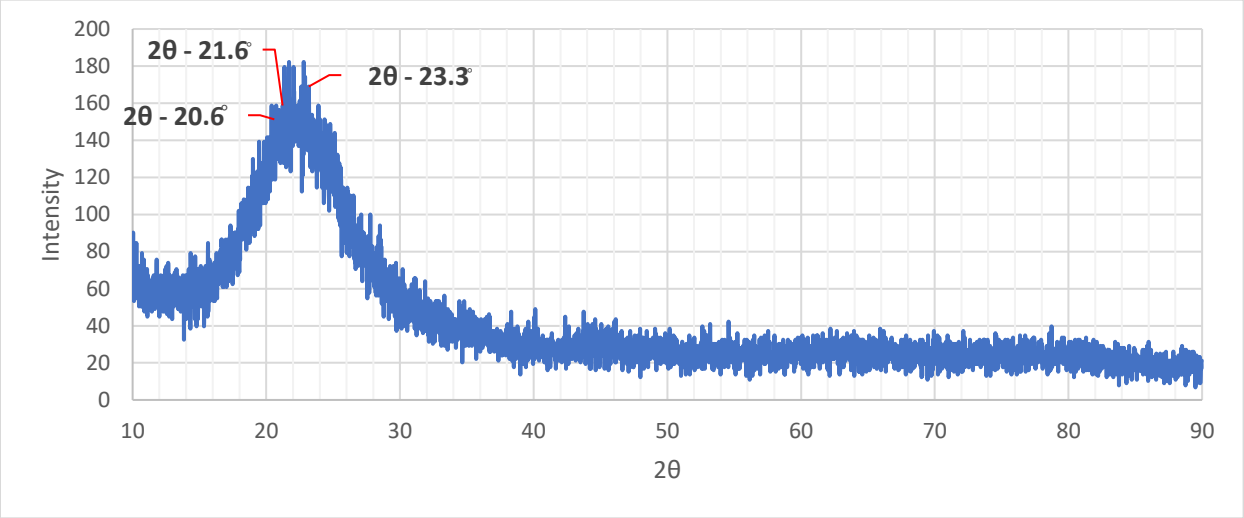


**Figure 4.3: XRD pattern of NS_U**

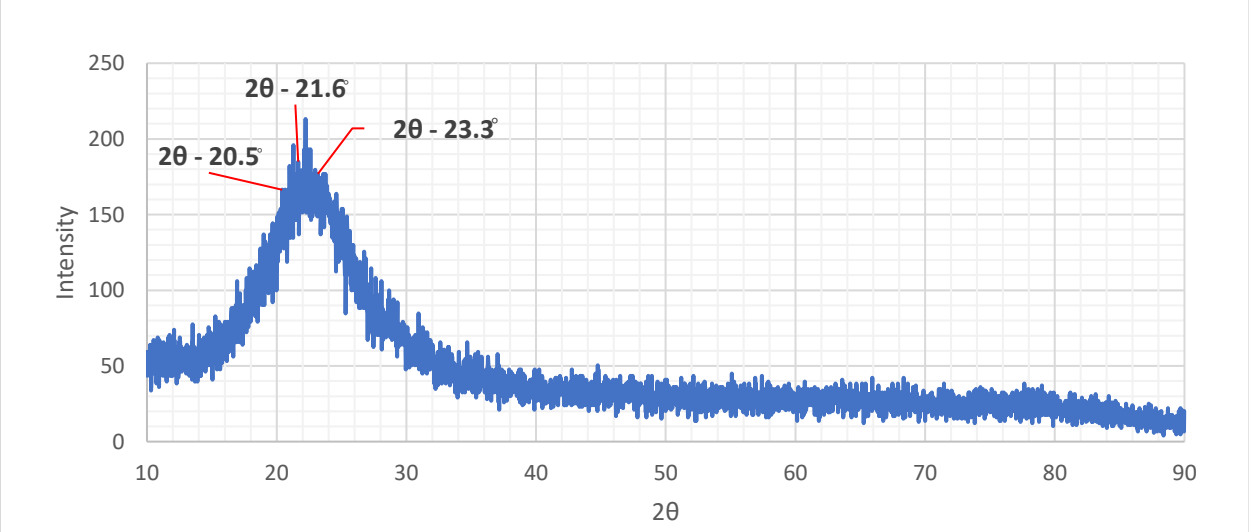


**Figure 4.4: XRD pattern of NS_A**

Figure 4.3 shows the XRD pattern of the NS_U type silica and this pattern matched to the tridymite phase of silica (the primary peak at the 2θ value of 20.5°) [107]. The main three XRD peaks for this phase of silica are at the 2θ values of 20.5°, 21.6°, and 23.3°. Also, it is possible that the metastable α phase of this structure exists below 117℃ temperature, which after transits to its β phase [107]. This was confirmed by the DSC results of 6%_NS_U paste cured for 2 and 7 days, which provided the evidence that the pastes contained unreacted silica and its transition around 120℃. However, the pattern indicates that the silica is amorphous to a considerable degree by having its characteristic broad amorphous band and by having peaks which are less sharp for the matched phase.

Figure 4.4 shows the XRD pattern of the NS_A type silica. This NS type also matched to the tridymite phase of silica. As mentioned before about the previous sample, this sample also has amorphousness to a certain degree by having the characteristic broad band for vitreous silica. However, DSC data is not available to confirm that the crystallinity is from the tridymite phase.

### 4.1.4 SEM on nano-silica (NS) particles

Figure 4.5 - Figure 4.8 show the SEM images of NS dried from the NS_A, and NS_U suspensions. The silica particles in the images reveal xerogel agglomerates caused by the drying step performed on them for SEM analysis. Even though they seem coalesced, they provide good indications about their size. Figure 4.5 and Figure 4.6 are the images of silica from the suspension NS_A. The rough particle size measurements obtained for the images give values around 90 nm which validate the DLS results obtained for the same suspensions. The dimensions given on Figures 4.7 – 4.9 are a random sampling of particle diameters. Figure 4.7 and Figure 4.8 are images of silica from the suspension NS_U. The particle size measurements indicate that the particle sizes are around 65 nm to120 nm. However, the dashed yellow circles on the images show that there are clusters of even smaller particles in the sample. Drying the samples was necessary to perform SEM analysis and that could have resulted in xerogels which can be seen as connected particles instead of separate particles. During drying in an oven by slow heating, the gel structure of the particles shrank by becoming closer to each other. These results also show the non-desirable effect of the formation of xerogel agglomerates by having the drying step in particle synthesis, which was eliminated by using the particle suspensions.

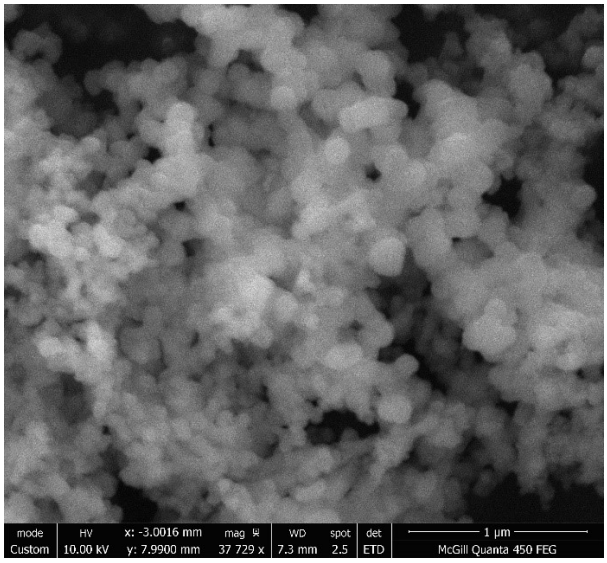


**Figure 4.5: SEM image of NS_A**

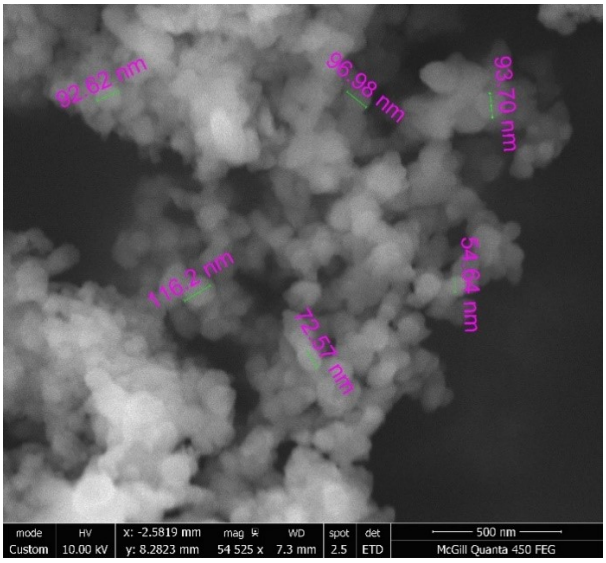


**Figure 4.6: SEM image of NS_A**

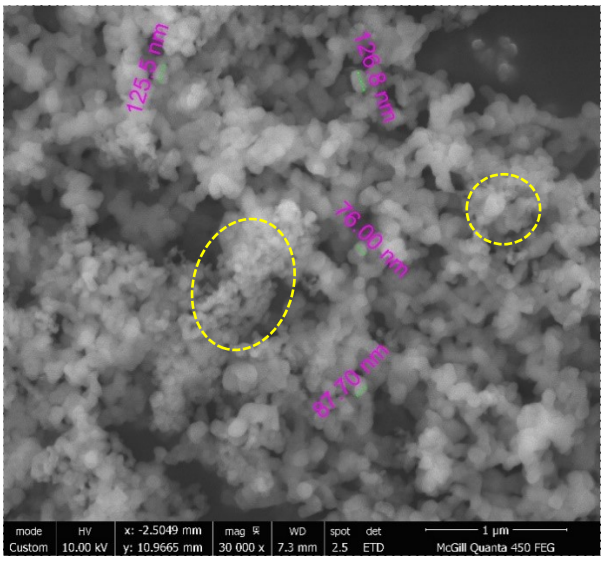


**Figure 4.7: SEM image of NS_U**

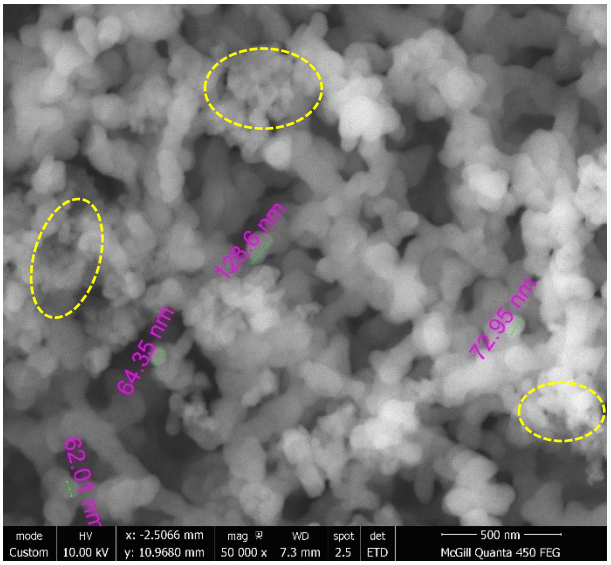


**Figure 4.8: SEM image of NS_U**

**4.2.**

## Association of synthesized silica in the cement paste

### 4.2.1 Utilization of silica as powders and suspensions

To achieve one of the objectives of this research, which is to minimize agglomeration, the effect of using NS in liquid state or powder form was necessary as many previous researchers have used NS in a powdered form. Therefore, the hydration of cement was examined when silica was utilized in a powder form (i.e. silica mixed with cement), as a suspension in calcium hydroxide, as a suspension in water and control cement paste without NS. The energy release as measured by isothermal calorimetry is commonly used to assess cement hydration. The cumulative energy of the samples is shown in Figure 4.9. It can be seen that the lowest cumulative energy was obtained for the sample in which silica had been mixed in powdered form. The highest cumulative energy

was obtained for the sample containing silica as a suspension in water which can be seen in the magnified image of the graph (151000 s – 251000 s). Nevertheless, the cumulative energy of the samples containing silica as a suspension in calcium hydroxide are very similar. The amount of cement replaced in the trial was 0.2 % by weight. This amount does not seem sufficient to produce a significant improvement in cement hydration. Yet, slight hydration improvements are visible in samples that contain silica as a suspension in water (sample 1) and as a suspension in calcium hydroxide (sample 2) when compared to the control sample (sample 4). The less desirable effect of including silica as a dry powder is disclosed by this trial.

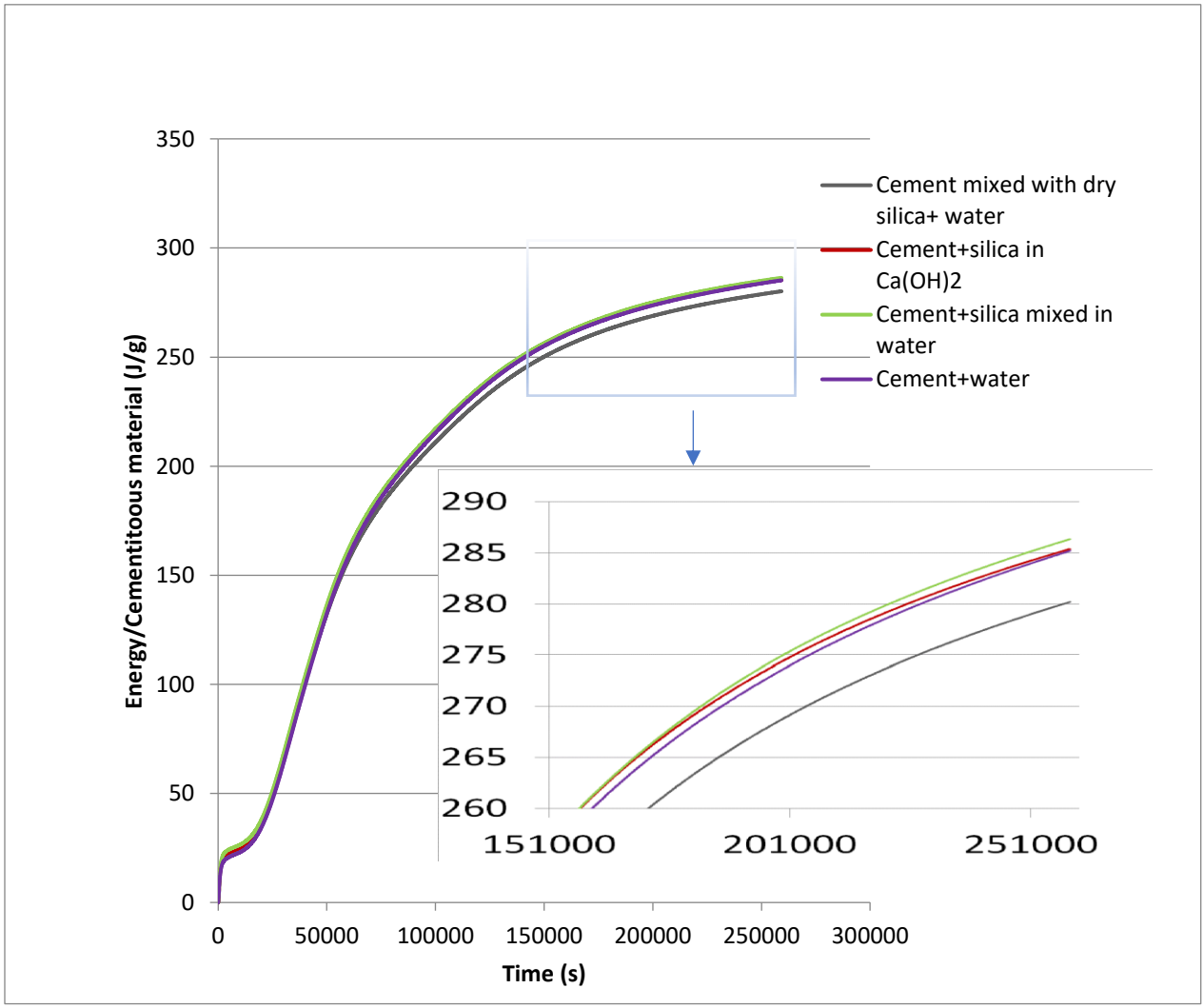


**Figure 4.9: Cumulative energy of cement pastes for to assess the silica association method (solid/liquid)**

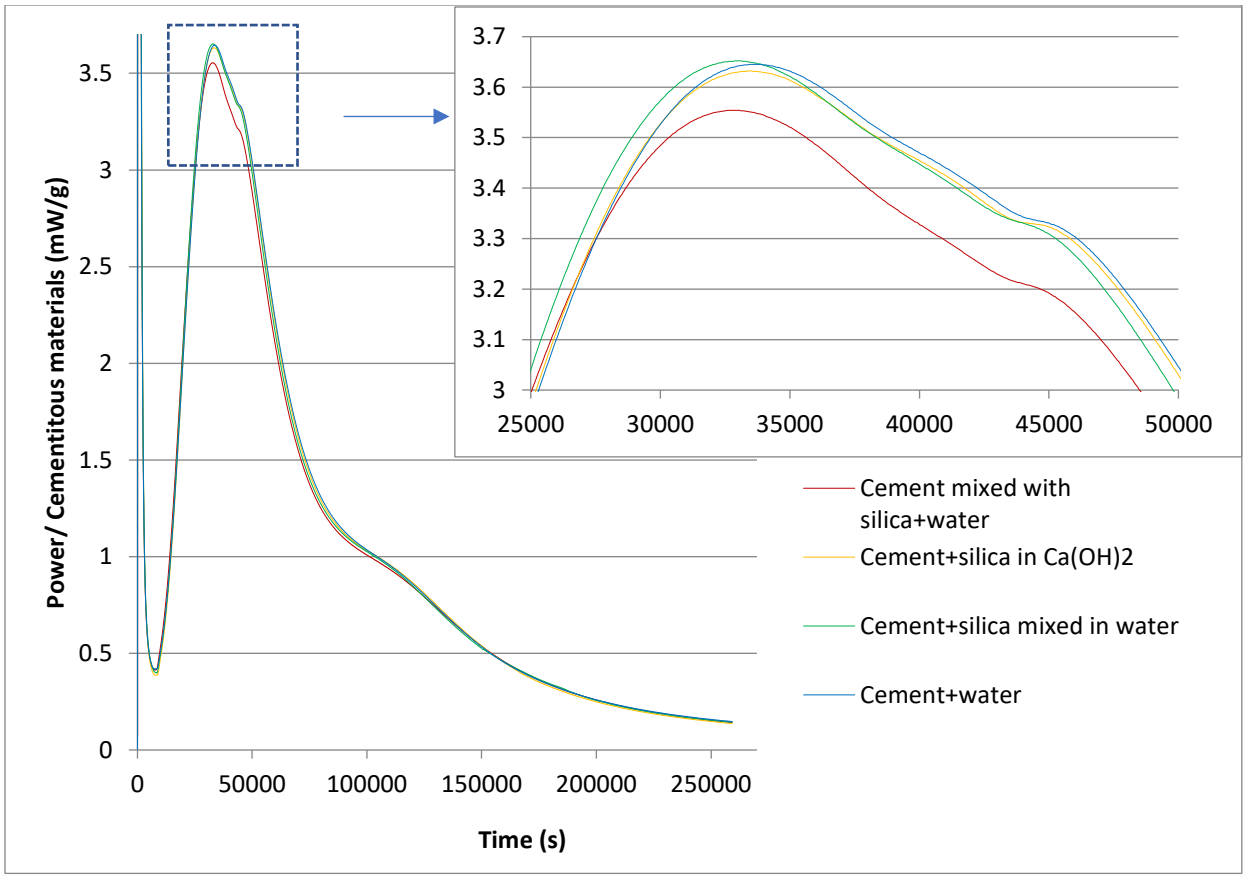


**Figure 4.10: Heat Evolution of cement pastes for to assess the silica association method (solid/liquid)**

The heat evolution curves for the same samples are shown in Figure 4.10. The peak representing the hydration of $C_3S$ (tricalcium silicate) almost overlap each other except the peak that relates to the sample which had been mixed with silica in powdered form. The maximum rate of heat flow from that sample is lower than the other samples which also confirms the hypothesis that the utilization of silica in liquid form is better than in powdered form. The magnified image of the maxima of the curve exacerbates this fact. The reason for the small hydration improvements is that the amount of silica utilized in this trial is 0.2% by weight of cement.

### 4.2.2 Hydration of NS_A type silica included cement pastes

Figure 4.11 shows the rates of heat evolution of 1%, 2, %, 4%, 6% NS_A type NS cement pastes with time compared with the control cement paste. All the pastes containing NS exhibit a higher heat flow than the paste without NS. The acceleration period of all pastes has occurred earlier than that of the paste with no NS. In between 2-6 hours, the hydration takes place faster as the amount of NS replacement increases. However, the 4% NS curve surpasses the 6% NS curve after 6 hours. This implies that the 4%_NS paste has more heat evolution and more hydration than the 6%_NS paste after 6 hours. The highest heat evolution is attributed to 4% NS inclusion for this NS type and indicates the highest hydration for the same percent and the type of NS. Also, this percentage aligns with the work of the researchers [10–13].

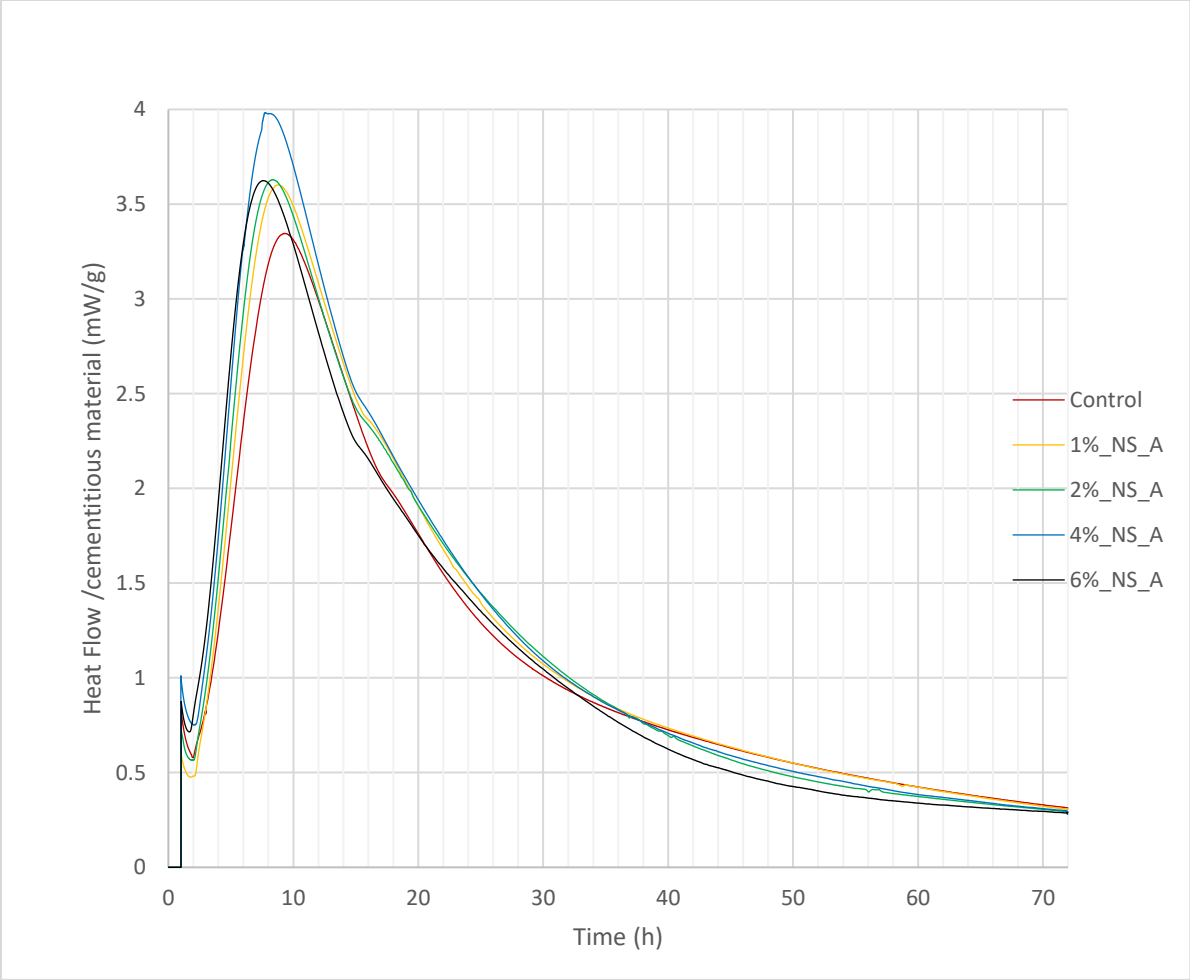


**Figure 4.11: Heat Evolution of NS_A type silica included cement pastes**

Figure 4.12 shows the cumulative heat evolved for the cement pastes mentioned in the above paragraph. The highest heat evolved, or the highest cumulative energy corresponds to the curve of the paste containing 4% NS. The control cement paste showed the lowest cumulative energy during the first 72 hours of the test. Similar to Figure 4.11, the total heat evolved has an increasing trend with the increasing NS percentage during the early stage up to the first 9.5 hours. This period is attributed to the acceleration period of Figure 4.11 and it is pertaining to the hydration of $C_3S$. As such, the rate of $C_3S$ reaction has increased with the increasing percentage of NS. However, the curve attributable to the 6% NS paste deviates from this trend after around 6 h. This implies that a higher heat has been generated by the 6% NS paste during the first 6 h which can compensate and match the trend of the cumulative energy before its downfall at around 9.5 h. The total hydration of 6% NS paste is still higher than the other curves before this point. At around 20 h and 30 h, the 2% NS and the 1% NS curves surpass the 6% NS curve. At 72 h, the 6% NS curve still lies above the curve of the paste without NS while having close values. This implies that most of the 6% NS paste's hydration due to the presence of NS occurred initially. Due to the higher concentration of NS in the suspension, it is possible that there may be agglomerates present in the suspension which was used for the preparation of 6% NS cement paste and the segregated NS particles in the suspension could have accelerated the hydration reactions at the earlier stage.

Table 4.4 presents the percentage increase of hydration for the pastes at two days considering that the energy of the control sample at two days is 100%. The cumulative energies of hydration at 48 hours (for example, see Figure 4.12) and they were compared with that of the control sample. As described earlier, the table shows that the hydration increases with the NS percentage in the cement paste up to 4% replacement. The increase in hydration by using 1% and 2% NS are 6.12 and 6.97%, respectively. While the values are close, when the NS percentage becomes 4%, the increase in hydration at two days almost doubled. This value decreased to just over its half when the NS percentage was 6%.

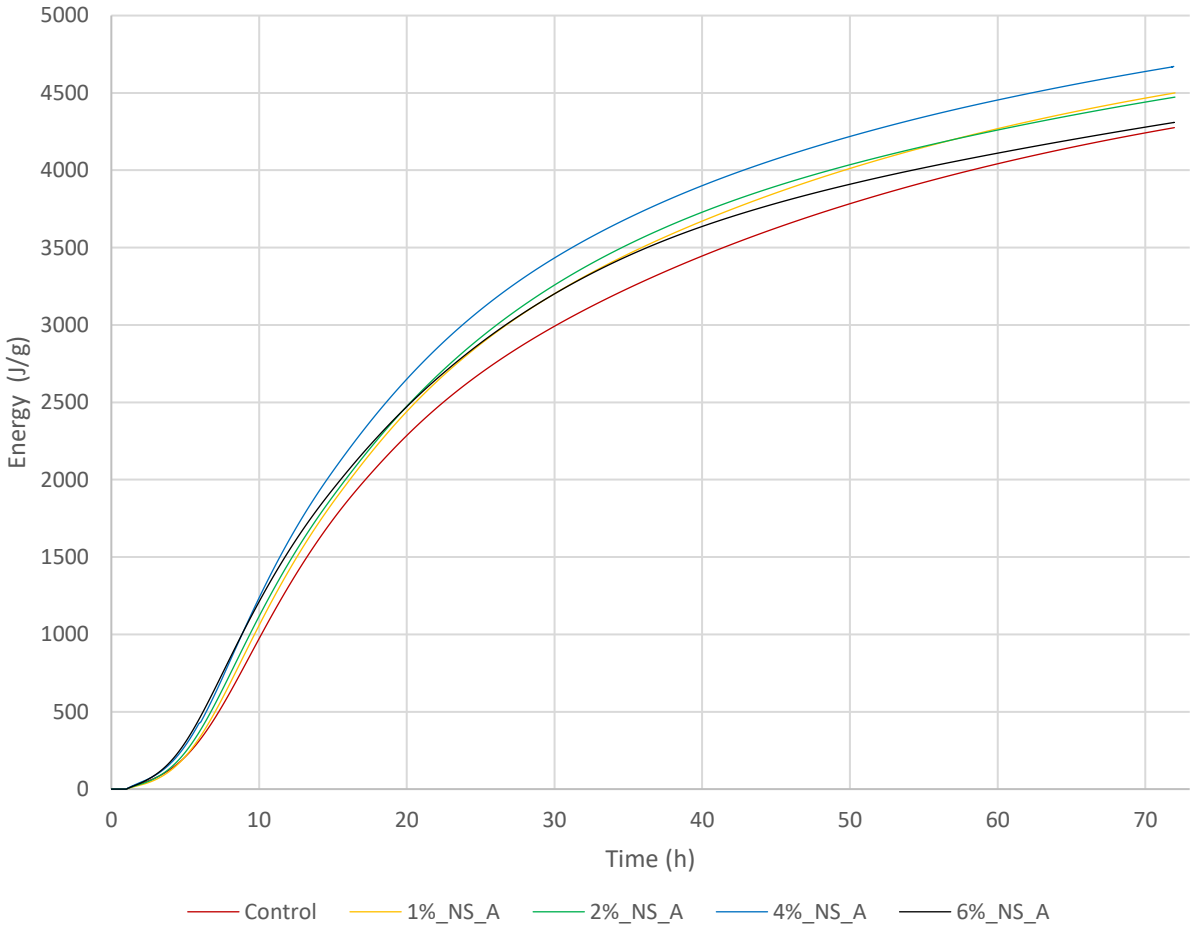


**Figure 4.12: Cumulative energy of NS_A type silica included cement pastes**

**Table 4.4: Percentage increase of hydration at two days for the NS_A type silica included cement pastes**

| NS_A paste designation | Percentage increase of hydration at two days (%) |
|---|---|
| 1%_NS_A_2d | 6.12 |
| 2% _NS_A_2d | 6.97 |
| 4%_NS_A_2d | 11.80 |
| 6%_NS_A_2d | 3.76 |

### 4.2.3 Hydration of NS_U type silica included cement paste

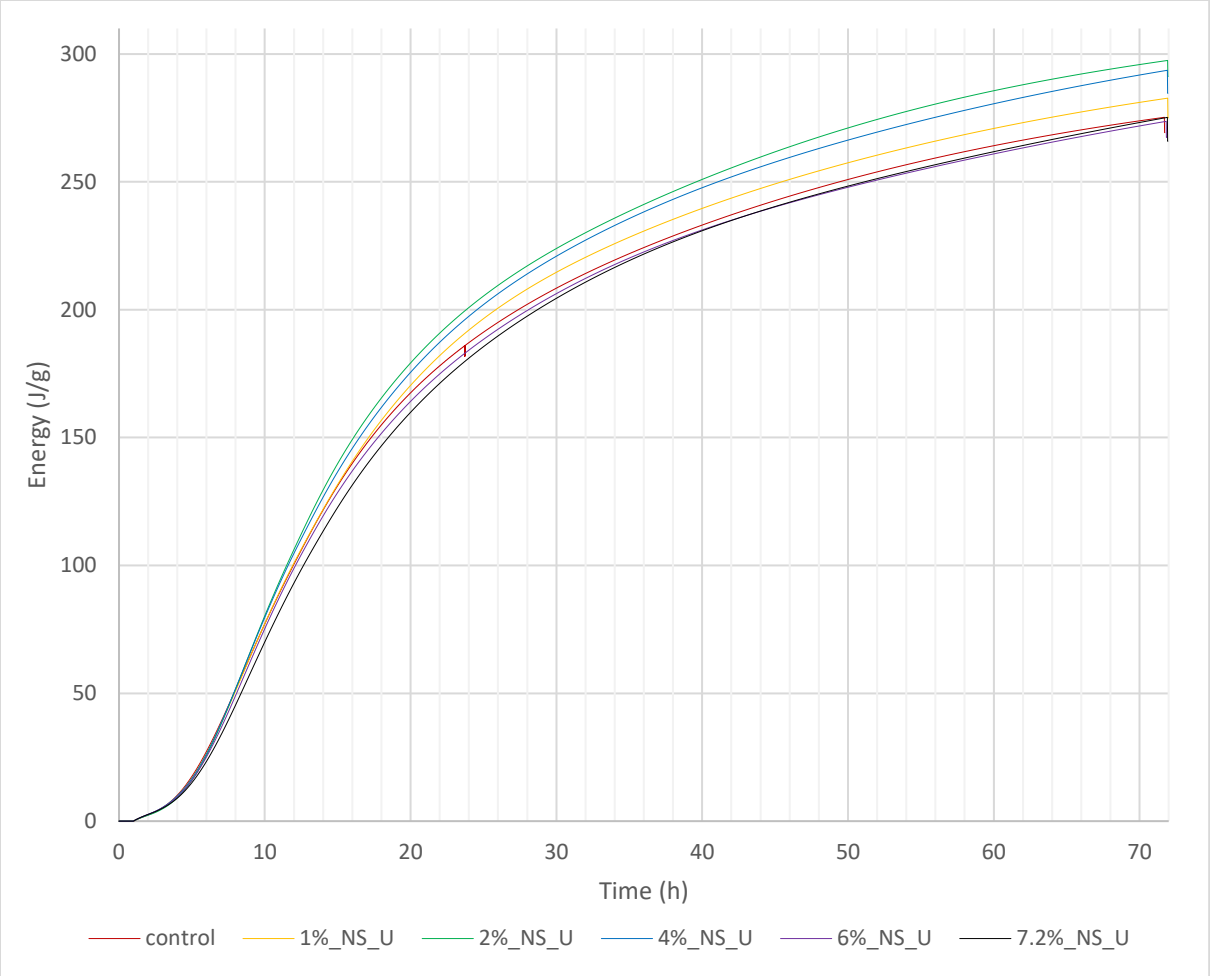


**Figure 4.13: Cumulative energy of NS_U type silica included cement pastes**

Figure 4.13 shows the heat of hydration for the cement pastes that have NS_U type NS. The total energy generated for all the pastes seem to be nearly the same during the first 1.5 hours. Then, it is apparent that the paste having 7.2% NS deviates from the trend exhibiting lower hydration than the other pastes. This could be due to a presence of agglomerated NS particles in the 7.2 % NS paste. The other curves keep showing similar behavior to each other until around 9 hours of the test. After 9 hours, the other pastes also deviate showing the highest hydration for 2% NS and 4% NS pastes, a less similar hydration from the control and 1% NS pastes, and a much less hydration than the 6% NS paste. Still, the 7.2% NS paste's hydration is lower than the others. At around 16 hours, all the curves show different hydration trends. After that, the pastes for 7.2% NS, 6 % NS, control, 1% NS, 4% NS, and 2% NS show incremental hydration increases. This trend is valid throughout the whole period of the test for the pastes with 1% NS, 2% NS, and 4% NS. The curves for the other pastes converge to a same hydration which is lower than the hydration of the 1% NS paste after around 35 hours. However, the control sample shows slightly more hydration than the 6% NS and 7.2 % NS samples, but at the end of 72 hours these three samples show almost the same hydration. This could be due the presence of agglomerated NS particles in the concentrated NS suspensions used to make the pastes. Nevertheless, replacing 7.2% of the

cement by this type of NS showed almost the same hydration of the control sample within three days. Considering the association of NS_A type NS in cement paste, this NS type does not show a trend where the hydration improves as the NS additions increase. This could be due to the fineness in NS_U type silica than the NS_A type silica which could have led to some agglomeration resulting from the highly concentrated suspensions. Ultimately, in terms of hydration and association of NS_U type NS, 2% cement replacement gives the best hydration within the three days. The reason for not testing 8% NS addition was the tendency of settling of particles increased as the NS content in the suspension increased. Also, the cumulative energy of hydration at three days did not show significant improvements beyond 4% NS addition.

Figure 4.14 presents the heat flow variation of NS_U type NS included cement paste. Approximately during the first 6 hours of the tests, the curves for all the pastes, except the pastes that have 6% NS and 7.2 % NS, aligned together showing similar hydration during that period. The 6% NS and 7.2% NS samples show a slower rate of hydration than that of the other pastes having their curves shifted rightward. This period is attributable to the setting of the cement. Before this period, the cement hydrolysis happens. The energy released from the $C_3S$ hydration occurs after the hydrolysis has taken place and the system has been saturated by the hydroxyl ions, calcium ions, etc. After that period the curves diverge showing incremental high heat flow in the order; control, 1% NS, 4% NS, and 2% NS. The 7.2% NS, control, 6% NS, 1% NS, 4% NS and 2% NS show their maximums in an order such that the 7.2 % NS paste has the lowest maximum heat flow and the 2% NS paste has the highest maximum heat flow. It implies that the pastes have hydration improvements due the $C_3S$ hydration in the same order. Having the least hydration in 7.2 % NS paste suggests that there could be less reaction in that paste. This could be due to the presence of agglomeration. Considering the 20 hours – 30 hours period in the deceleration stage of the graph where pozzolanic reactions from excess NS particles could possibly occur [108] consuming the CH formed during the acceleration period, the control sample shows the least heat flow suggesting its lower hydration than the NS included pastes. It could be due to a dissolution or a breaking up of NS particles at the deceleration period where the hydration is controlled by diffusion [109,110]. Also, it should be noted that at the point where the curves reached their steady stage at which hydrations reactions occur at a very slow rate to show a significant heat output, the control sample still has the lowest heat flow indicating more pozzolanic reactions could be taking place over the time.

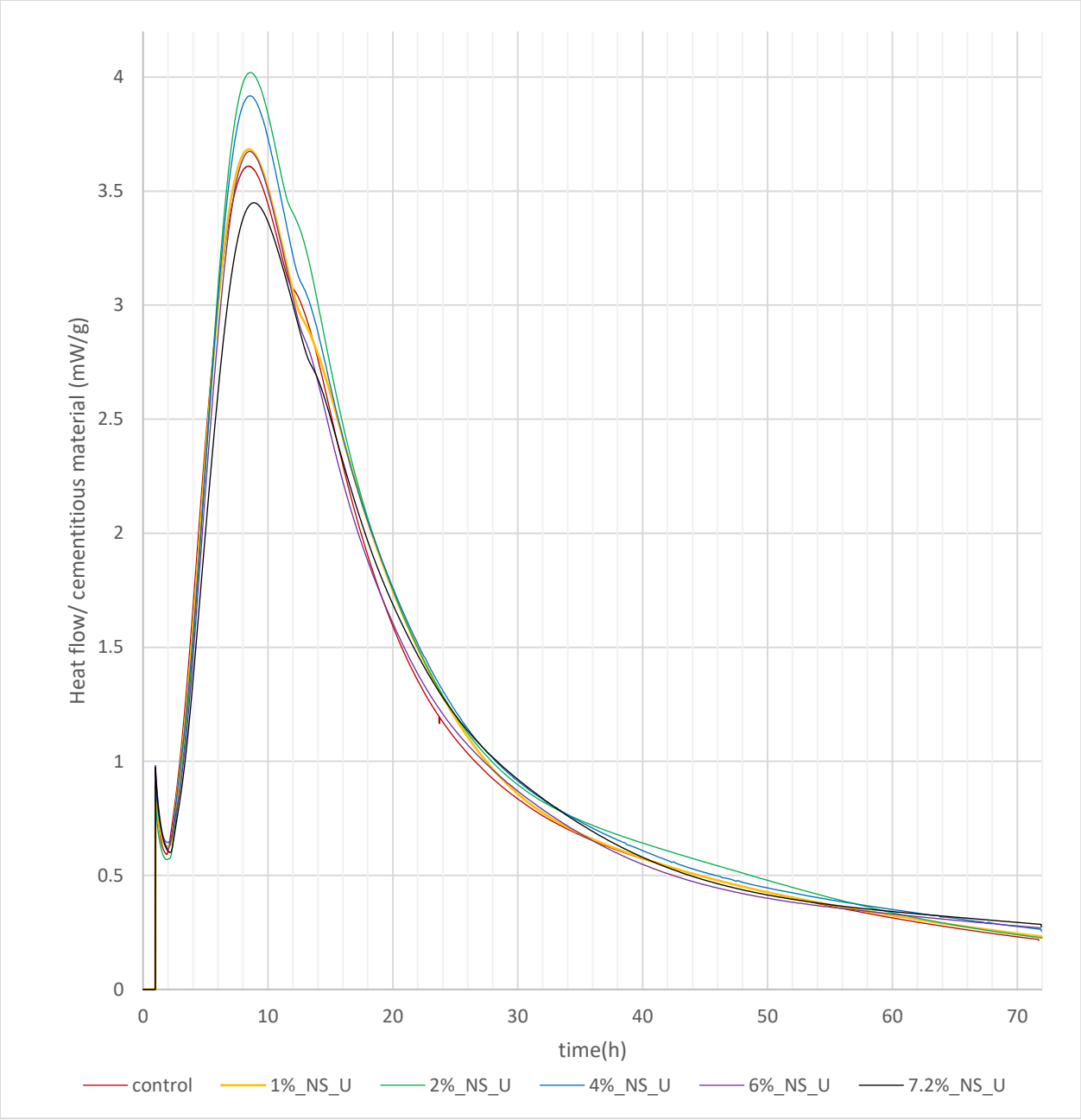


**Figure 4.14: Heat Evolution of NS_U type silica included cement pastes**

**Table 4.5: Percentage increase of hydration at two days for the NS_U type silica included cement pastes**

| NS_U paste designation | Percentage increase of hydration at two days (%) |
|---|---|
| 1%_NS_U_2d | 2.65 |
| 2% _NS_U_2d | 7.98 |
| 4%_NS_U_2d | 6.17 |
| 6%_NS_U_2d | -1.13 |
| 7.2%_NS_U_2d | -1.00 |

Table 4.5 shows the percentage of hydration increase in the cement pastes with NS_U compared to the control sample's hydration. The cumulative energies of hydration at 48 hours were obtained from Figure 4.13. The results indicate that the hydration of the pastes increases up to 4% NS_U inclusion, and then the hydration decreases when the NS_U percentage increases beyond 6%. When considering the hydration improvements, the maximum hydration is attributable to the paste with 2% NS_U.

### 4.2.4 Hydration of NS_EG type silica included cement paste

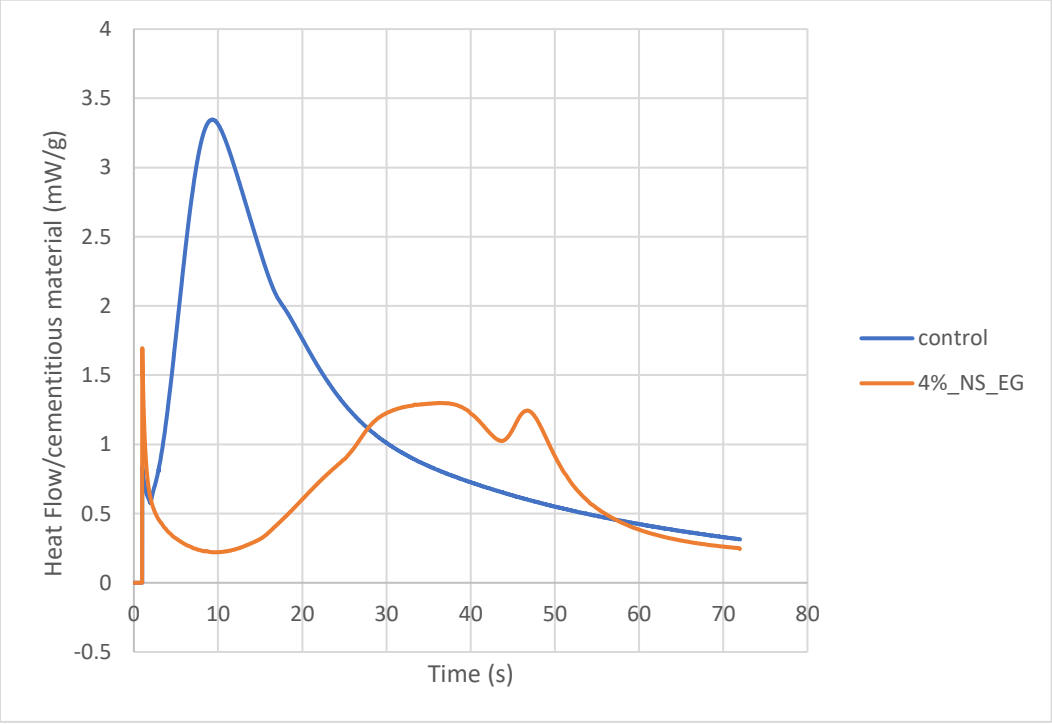


**Figure 4.15: Heat flow variation of NS_EG included cement paste**

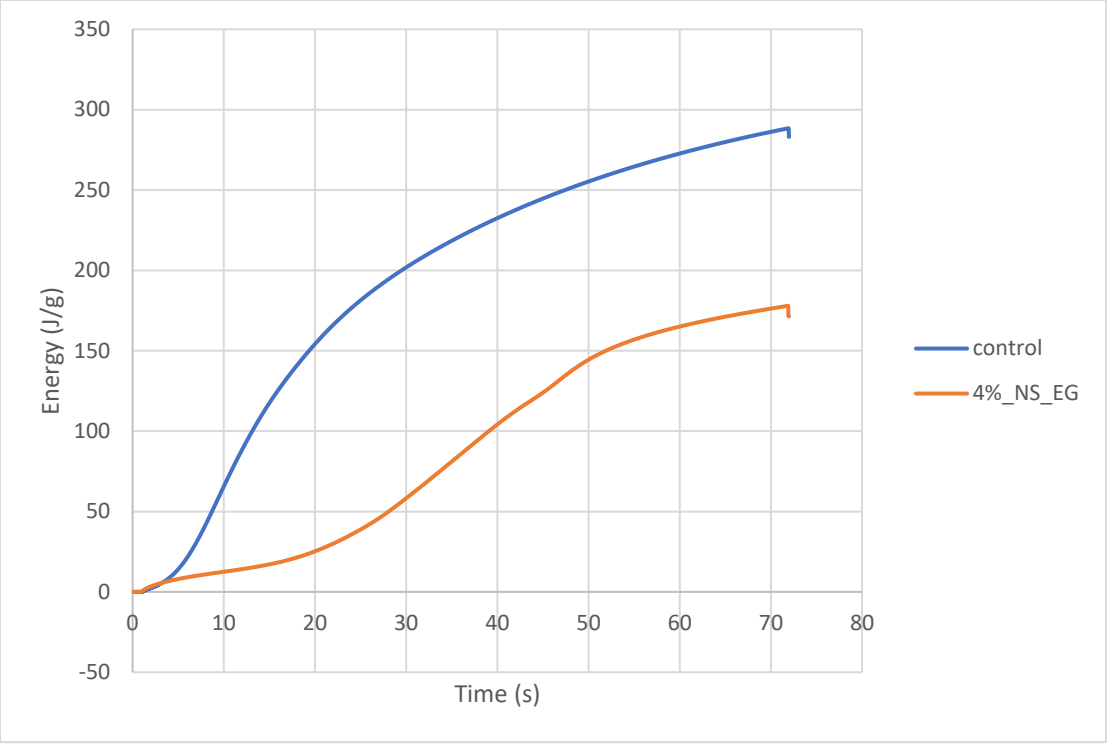


**Figure 4.16: Cumulative energy vs. time for NS_EG included cement paste**

Figure 4.15 and Figure 4.16 show the heat flow variation and the cumulative energy curves for the cement paste with NS_EG. The paste contained 4% NS_EG from the 4-50 suspension mentioned in Table 3.4. It is apparent that NS_EG is not effective in improving the rate of hydration. The occurrence of the $C_3S$ hydration peak shows a significant delay and the peak shows a significant height reduction. The delay and the peak height reduction must be due to the ethylene glycol in the suspension. The cumulative energy vs time graph also shows a large reduction in the cumulative heat released from the paste with NS_EG compared to the control paste. This indicates that the ethylene glycol in the suspension affected the hydration of the cement adversely.

### 4.2.5 Non-evaporable water content of NS included cement pastes

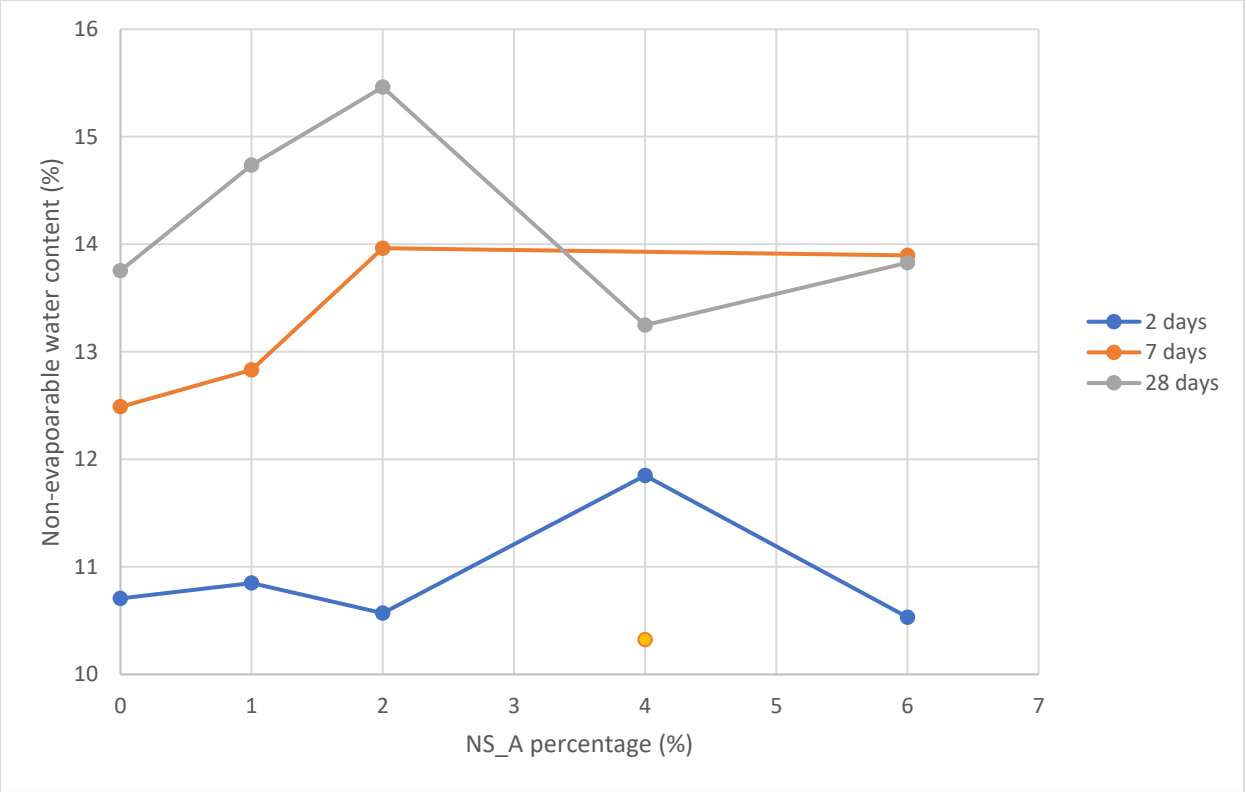


**Figure 4.17: Non-evaporable water content of NS_A type silica included cement paste**

Figure 4.17 presents the variation of the non-evaporable water content measured for the 2, 7, and 28 days cured cement pastes with the NS_A type. Non- evaporable water content is the water consumed in the hydration reactions and it is chemically bound to the hydrated cement. The curve for the 2 days non-evaporable water content does not show much variation in their contents as the NS percentage in the pastes increases except for the paste that contain 4% NS_A. the paste with NS_A depicts an increase in the non-evaporable water content which can be deduced as an increase in hydration. The trend of this curve however does not agree with calorimetric studies which could be due to the human errors during this test. The curves of the 2 days and the 7 days pastes show a similar behavior up to 4% NS_A addition depicting a hydration increase with the NS_A content. Within 2 – 7 days, the paste with 6% NS_A show more hydration similar to the paste with 4% NS_A. As the effectiveness of the NS_A shows later in this paste, it could be due an activation of the pozzolanic reaction in this sample. It can be noted that the 7 days cured paste with 4% NS_A show an unusual drop which could be a human error. However, after 28 days of hydration, the non- evaporable water contents of the cement pastes that contain NS_A more than 4% are slightly equal or slightly lower than that of the control sample. This fact and the 7 days curve indicate that these pastes achieved similar hydration compared to the control sample within 7 days. Overall, an improvement of hydration can be seen in cement pastes with NS_A even though this test does not show much effectiveness of NS_A within first two days.

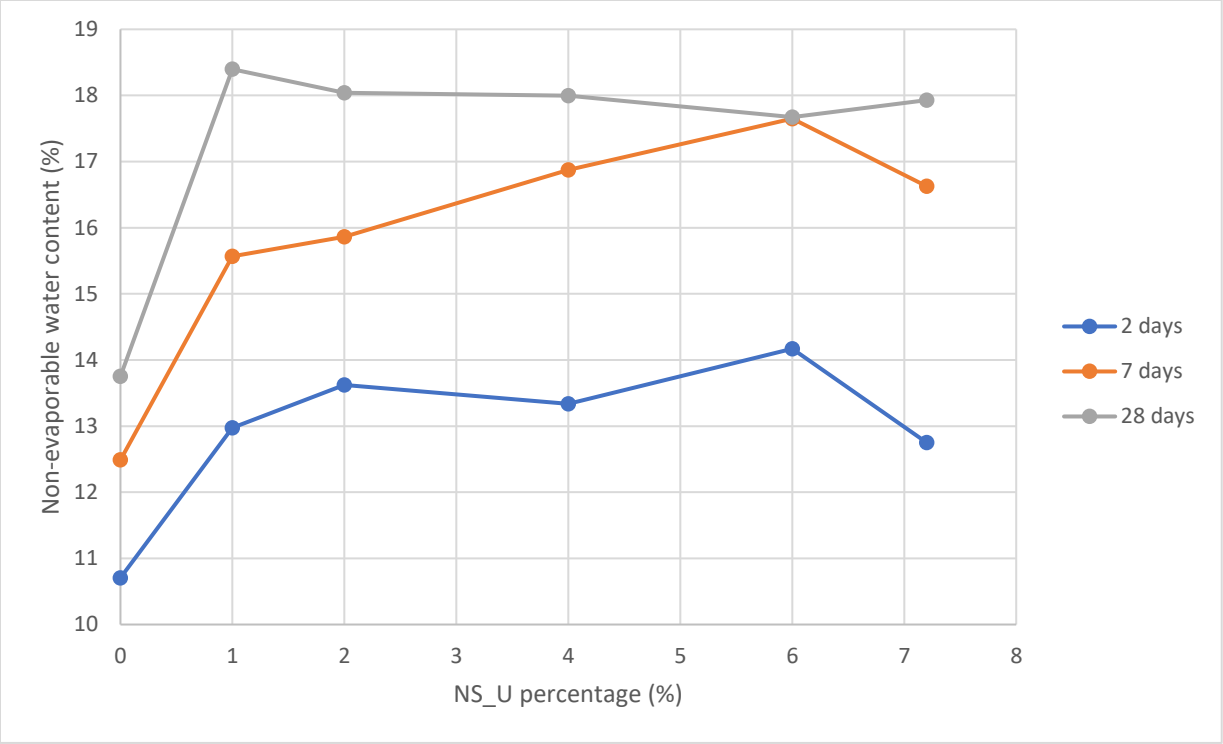


**Figure 4.18: Non-evaporable water content of NS_U type silica included cement pastes**

Figure 4.18 shows the variation of the non-evaporable water content measured for the 2, 7, and 28 days cured cement pastes with the NS_U type. As mentioned before, non-evaporable water content is a measurement of the chemically combined water to the hydrated products in the hardened cement paste. The 2 days and the 7 days curves show similar behaviors having increasing trend of the non-evaporable water content or the hydration up to 6% NS_U addition and a drop of the hydration compared to the 6% afterwards. When the curve for the 2 days results are considered, 2% and 4% show a similar hydration which is more than the hydration of the cement paste with control. The 7.2% NS_U addition does not show much hydration improvements within two days and value is close to that of the control sample. These results agree with the calorimetric studies except the pastes with 6% and 7.2% NS_U. After 7 days, all the pastes show improvements in hydration and the paste with 7.2% NS_U also show hydration improvements similar to that of the paste with 4% NS_U unlike that it did not show effects of NS_A (Figure 4.17) during 2 days. When the curve of the 28 days pastes is considered, all the pastes show more hydration than the control paste. However, the hydration achieved by all the NS_U addition seems similar at this curing stage. Considering the curves for 7 days and the 28 days, an early achievement (within 7 days) of the 28 days hydration can be seen in the pastes that contain 4% or more NS_U. This can be due to the pozzolanic activity of the unreacted NS_U which did not participate the nucleation seeding effect. Also, nucleation action is visible in all the cement pastes except the paste contain 7.2% NS_U has a lower nucleation seeding than the other by having lower non-evaporable water content. This can be due to that it does not have similar amounts of cement to show its improvements by nucleation seeding.

### 4.2.6 Thermal analysis of cement pastes and CH quantification

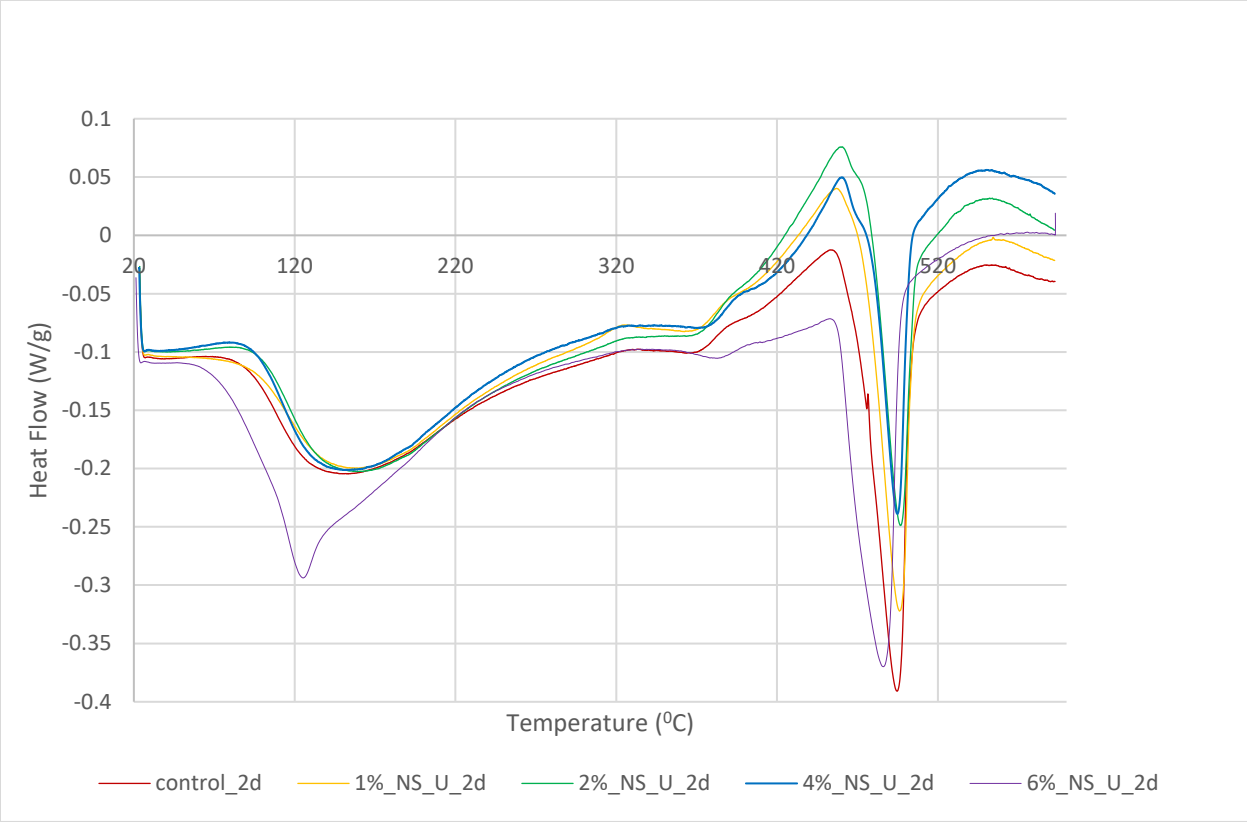


**Figure 4.19: DSC thermograms for two days cured NS_U type silica included cement pastes**

Figure 4.19 shows the DSC curves for the heat flow variation of 2 days cured NS_U type cement pastes. The endothermic peaks in the range of 120℃ – 150℃ indicate the dehydroxylation of ettringite in the paste. The endothermic peaks around 480℃ indicate the dehydroxylation of CH in the pastes. Under heating, CH decomposes losing its water forming CaO. As this is an endothermic reaction, it absorbs the heat which can be identified from the heat profile as a trough. The area above these troughs decreases as the amount of NS included in the pastes increases except for the 6% NS cement paste. The area above the trough is related to the amount of CH in the paste; the amounts of CH for 2, 7 and 28 days for the various NS additions in given later in this section. Therefore, it can be deduced that the quantity of formed CH decreases as the NS is included in the cement up to 4%. This decrease is attributed to the occurrence of pozzolanic reactions and the consumption of CH by the NS. The area above the trough of the 6% NS included paste is almost the same as that of the paste without any NS. However, the area related to the ettringite amount is significantly higher than that of the other samples. The troughs in the range of 100 - 200℃ are attributed to CSH, calcium aluminate hydrate (CAH), $CaSO_4 \cdot 2H_2O$, $Ca_3Al_2O_6 \cdot 3CaSO_4 \cdot 26H_20$, and some other hydrates of cement minerals [111]. Also, the sharp trough that is at around 120℃ indicates the transition of α tridymite to β tridymite. Jones and Segnit [112] and Dollase [113] mentioned that the this transmission could occur in between 107℃ – 180℃. Other researchers [107,114] mentioned the conversion temperature is at 117 ℃. This provides evidence that there

are unreacted NS particles in the 6% NS containing sample, which could be agglomerated NS particles as this sharp trough is not apparent in other samples.

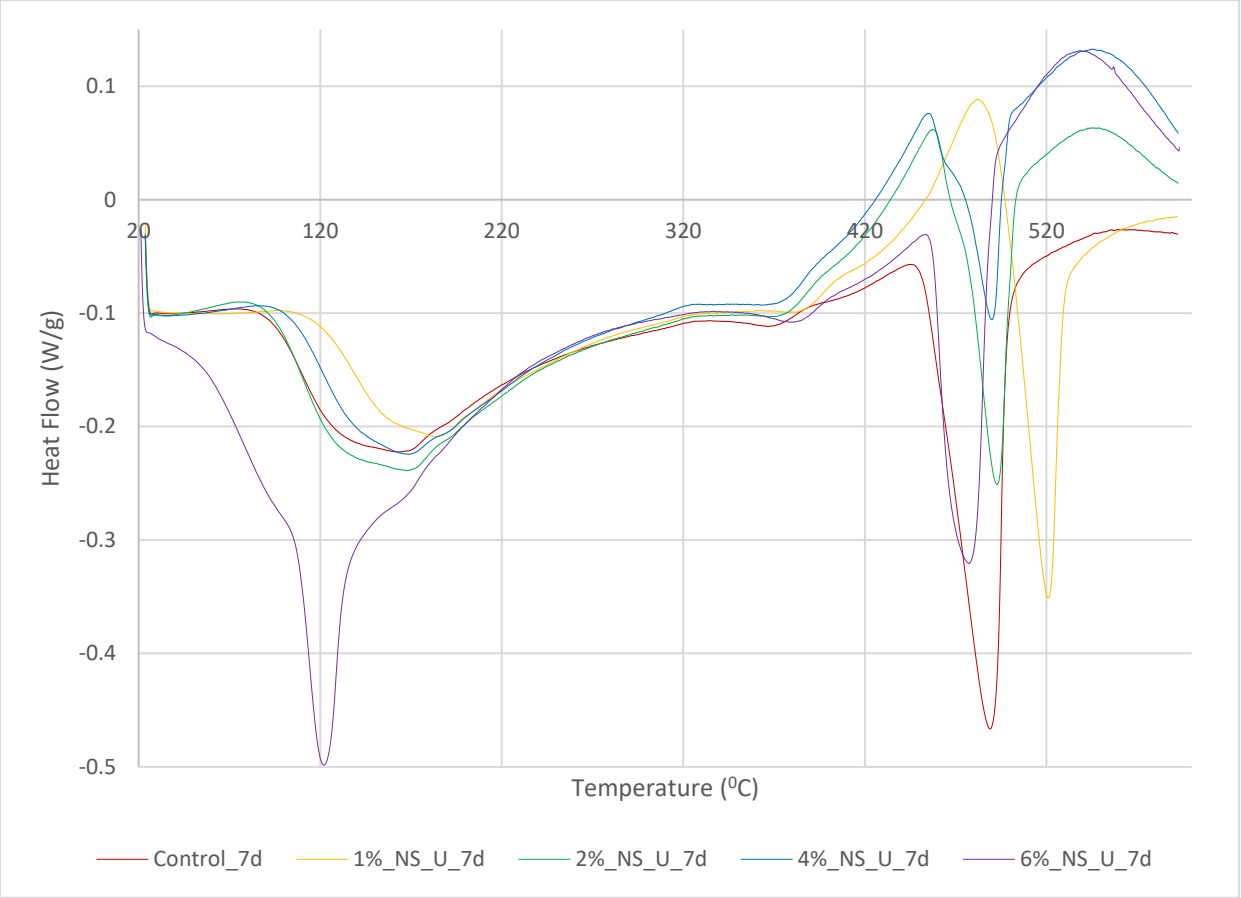


**Figure 4.20: DSC thermograms for seven days cured NS_U type silica included cement pastes**

Figure 4.20 shows the heat flow curves for 7 days cured NS_U type NS cement pastes. They contain 1%, 2%, 4%, 6% and no NS. For each curve, there are two major troughs visible similar to the curves of 2 days cured pastes. The troughs attributable to the CH decomposition show that the CH content of the pastes decreases as the NS percentage in the paste decreases except for the 6% NS containing cement paste. The area above the trough of the 6% NS paste is roughly between the areas of the troughs which relate to 1% NS and control pastes. Moreover, the shape of the first trough belonging to the 6% NS paste is different from the others. This indicates that there could be other hydration products that are not present in the control, 1% NS, 2% NS, and 4% NS pastes and that there are unreacted silica particles of which transitions occur at around 120℃.

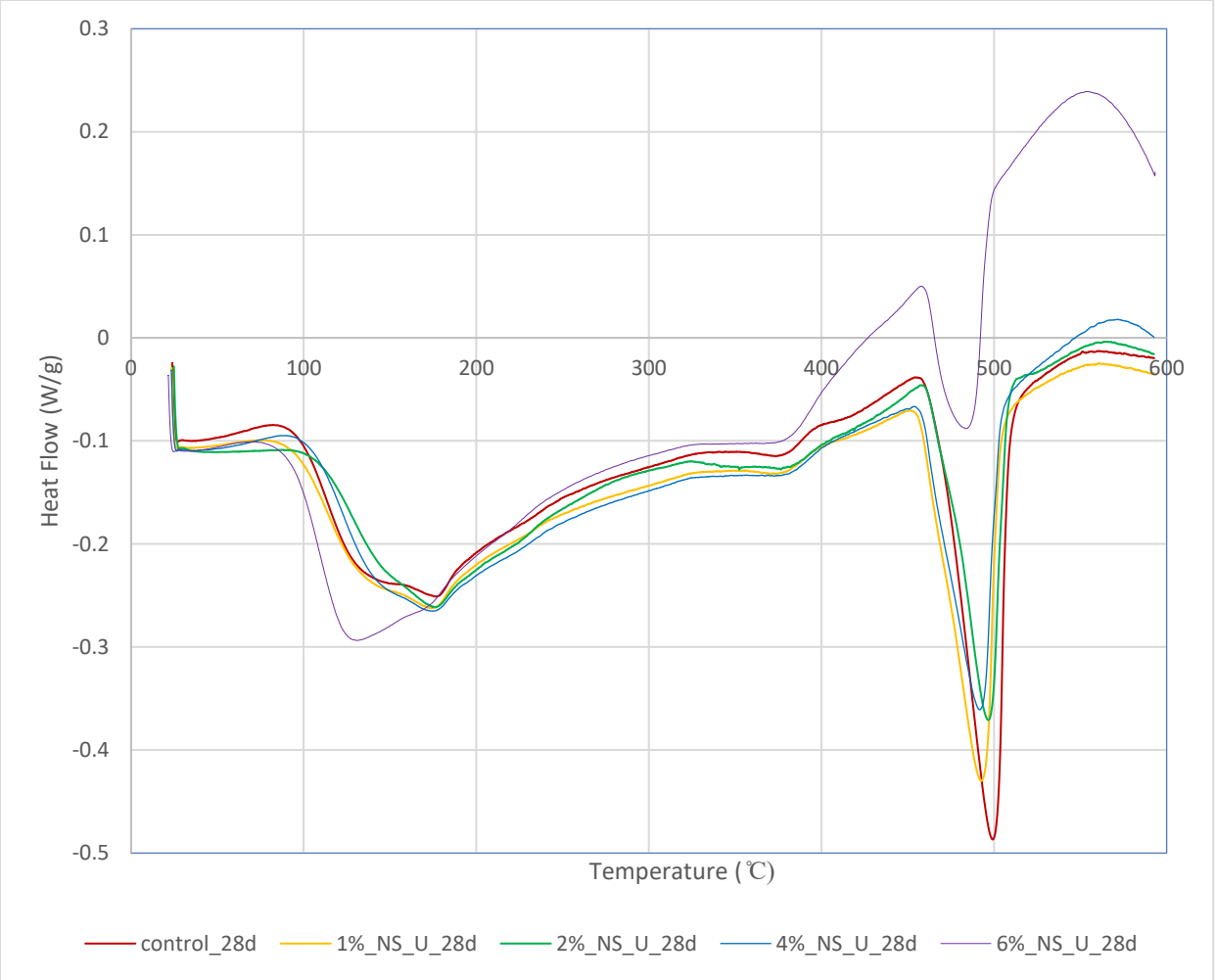


**Figure 4.21: DSC thermograms for 28 days cured NS_U type silica included cement pastes**

Figure 4.21 shows the heat flow variation of cement pastes including NS_U type silica that have been cured for 28 days, measured by the differential scanning calorimetry. Similar to the descriptions for Figure 4.19 and Figure 4.20, the first trough which is related to CSH is almost the same for all the pastes except for the paste that had 6% NS. Nonetheless, the difference is not as significant to those for the 2 days and 7 days cured pastes. Also, the sharp trough is absent here unlike in the curves of 2 days and 7 days. This reveals that the added silica has reacted by the time of 28 days. The areas of endothermic troughs related to the CH decomposition becomes smaller as the NS percentage in the pastes increases. This reveals that the added NS consumed CH in the pastes.

Figure 4.22 presents the quantified CH amount variation with the NS percentage. As discussed earlier, this figure summarizes the CH quantity of all the pastes based on their curing ages separately. As the NS percentage increases up to 4%, the CH quantity decreases for all the pastes regardless of the age. The quantity of CH of two days cured 2% NS and 4% NS pastes is almost the same, but the difference increases with time. It is obvious that the CH quantity of the pastes increases with the time for all NS additions as more reactions occur. However, the 6% NS

paste shows the opposite while reducing the CH content by 28 days. This shows that NS has consumed the CH in the pastes at the beginning in the pastes that have 4% NS or less, while the paste having 6% NS consumed the formed CH later. This again indicates that there could be agglomerated NS in the 6% NS paste which did not allow the early CH consumption by the time they had reacted.

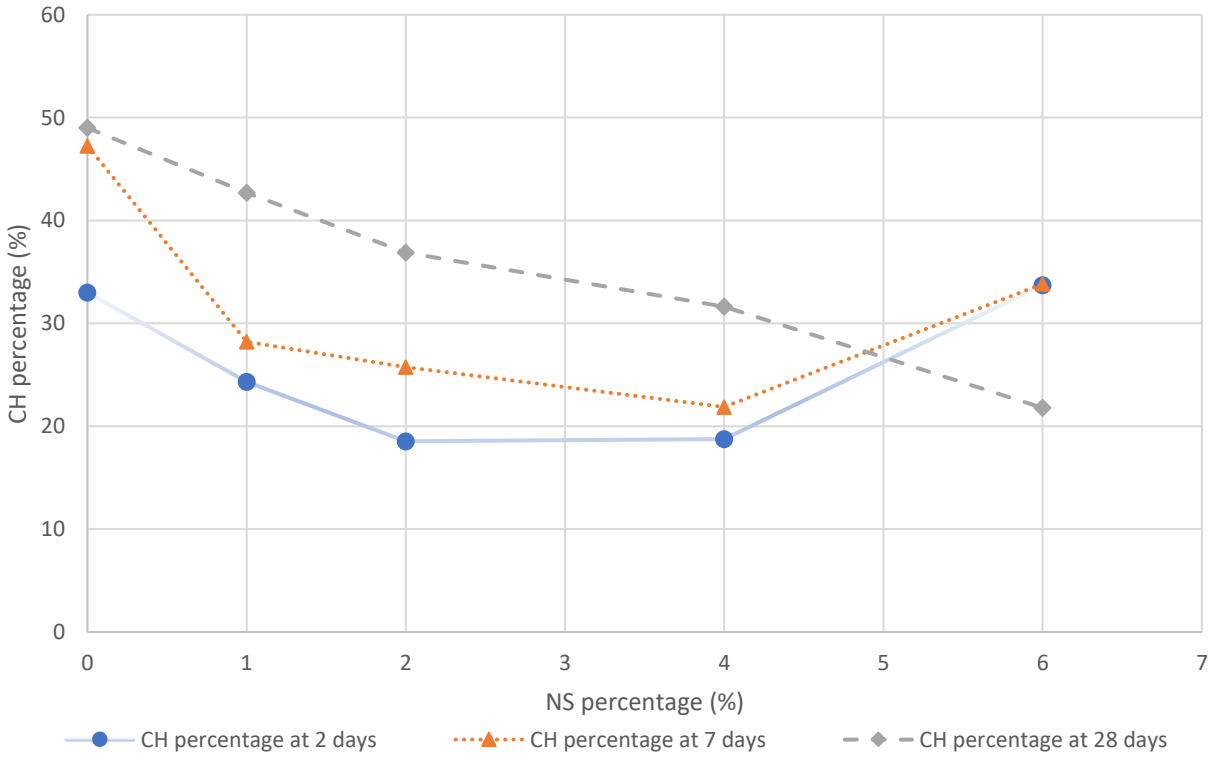


**Figure 4.22: CH quantity variation of NS amount for NS_U type silica included cement pastes**

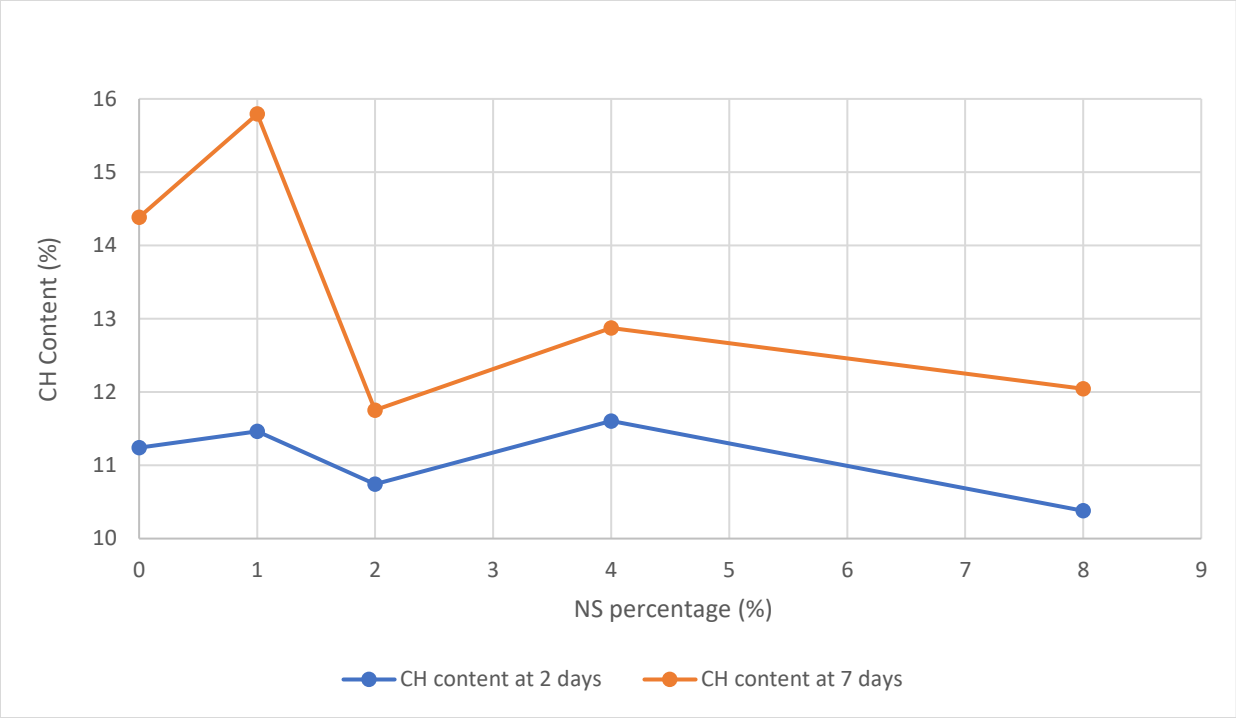


**Figure 4.23: The CH content by TG for NS_A type silica included cement pastes**

Figure 4.23 shows the CH content of NS_A type cement pastes including NS_A type measured by the thermogravimetric analysis (TGA). The CH content of the curve for two days does not show much difference other than a slight overall decrease with the NS percentage. The maximum decrease is about one percent of the total weight of the cement pastes. However, the CH content of the 7 days cured CH pastes show about a 4 % CH content decrease as the NS percentage increases from 1% to 8%. The 2%, 4%, and 8% NS inclusions have dropped the CH content of the cement pastes to a similar amount of around 12% from the 14%. However, the 1% NS included paste shows about a 2% increase in the CH content. It should be noted that the average particle size of the NS utilized for these pastes was 190 nm and are from the same NS batch used for preliminary analysis.

### 4.2.7 The pore structure of the NS included cement pastes

**Figure 4.24 presents cumulative volume of mercury intruded vs pore size graphs for the two day cured cement pastes with NS_A. As the percentage of NS_A increases, the curves have generally shifted to the left signifying an overall pore size reduction by associating NS_A silica. Also, it can be seen that the total mercury intruded volume has reduced as NS_A percentage increases except for 2%_NS_A_2d paste (Table 4.6). This suggests a reduction in porosity by including NS_A in the cement paste. The threshold pore diameter of the pastes also reduced as the NS_A included in the pastes increased (**

Table 4.6). This suggests that the NS_A included cement pastes would be more resistant to chemical attacks. When considering the intrusion curve of the paste, 2%_NS_A_2d, its intruded volume increase starts after around 0.06 µm pore sizes. This reveals that its porosity composes from the pores of 0.06 µm or less. Moreover, this sample has a significant portion of pores in the

0.005 µm – 0.01 µm size range. So, it can be deduced that a significant pore structure refinement can be achieved in two days by associating NS_A in the cement paste.

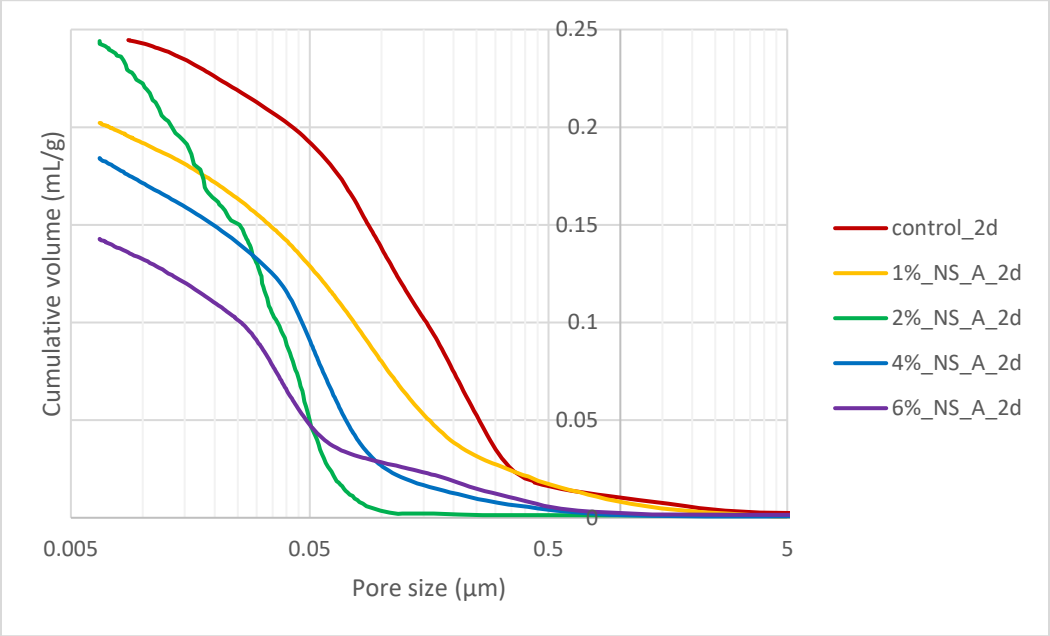


**Figure 4.24: Cumulative volume vs. Pore size of 2 days cured cement pastes with NS_A**

Figure 4.25 shows the cumulative volume of mercury intruded vs pore size graphs for the seven day cured cement pastes with NS_A. Similar to Figure 4.24, the curves have shifted to the left showing a pore size refinement compared to the control cement paste. Also, the pastes having NS_A show less intruded pore volumes compared to the control paste indicating a porosity reduction achieved by the NS_A inclusion (Table 4.6). The curves however do not imply an increasing trend of pore refinement with increasing NS_A percentage. Also, the curves of the cement pastes with NS_A are considered, the porosity of these pastes mainly consist of the pores below 0.06 µm whereas the control paste has a significant portion of porosity from the pores above 0.06 µm. A reduction in the threshold pore diameter with increasing NS_A is visible in the seven days cured cement pastes as well except in the 2%_NS_A_7d paste which shows a threshold pore diameter almost similar to that of the 6%_NS_7d paste.

Figure 4.26 is the cumulative volume of mercury intruded vs pore size graphs for the twenty-eight days cured cement pastes with NS_A. As the curing time increased, the pore structures of the pastes composed of mainly the pores below 0.05 µm. At this curing time, a slight pore size reduction can be seen in NS_A included cement pastes. Also, it can be inferred that NS_A is effective in filling effect attributable to the nanoparticles and earlier achievement of the 28 days hydrated pore structure by considering all three figures.

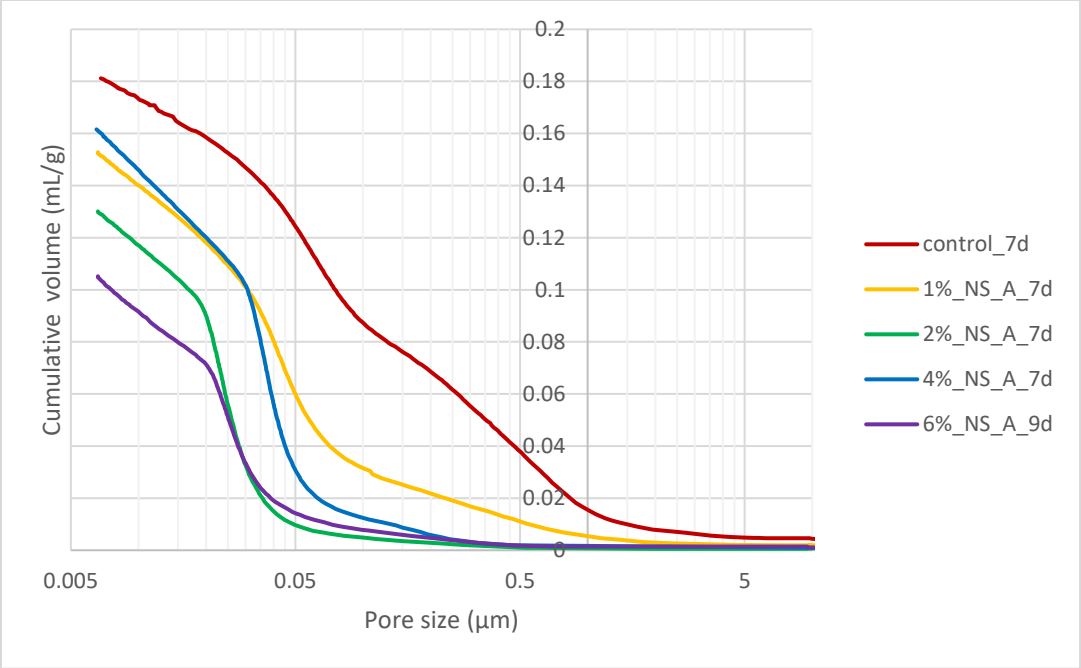


**Figure 4.25: Cumulative volume vs. Pore size of 7 days cured cement pastes with NS_A**

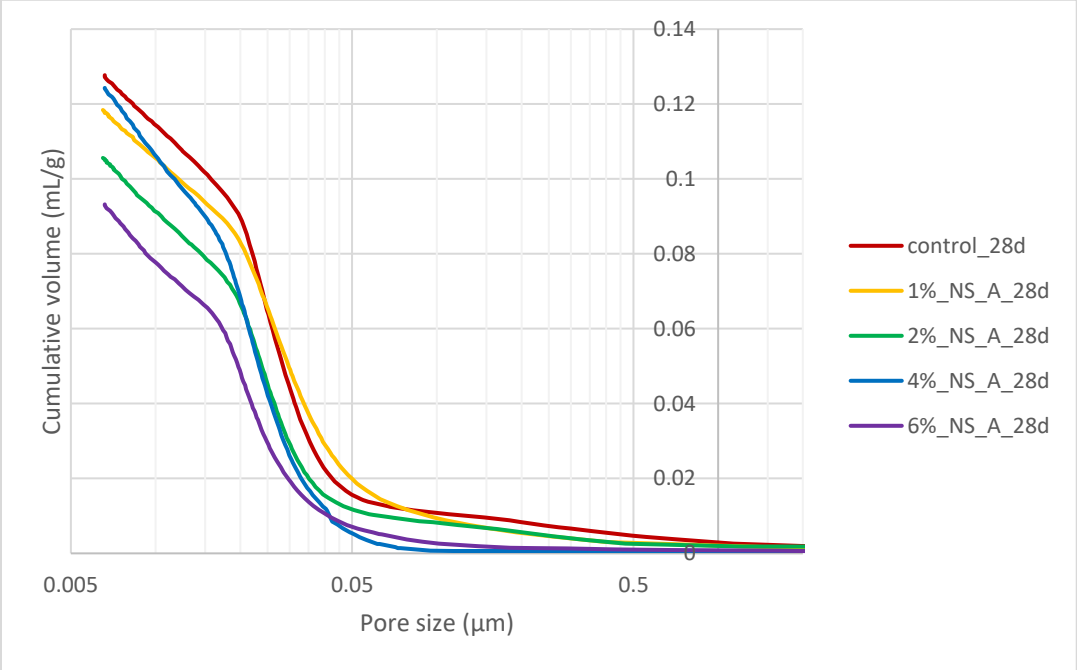


**Figure 4.26: Cumulative volume vs. Pore size of 28 days cured cement pastes with NS_A**

**Table 4.6: Critical pore diameters of cement pastes including NS_A**

| Sample ID | Critical pore diameter (μm) | | | Total Porosity (%) | | |
|---|---|---|---|---|---|---|
| | *At 2 days* | *At 7 days* | *At 28 days* | *At 2 days* | *At 7 days* | *At 28 days* |
| Control | 0.234 | 0.054 | 0.037 | 31.65 | 26.40 | 19.80 |
| 1%_NS_A | 0.102 | 0.039 | 0.029 | 30.28 | 24.32 | 19.91 |
| 2%_NS_A | 0.040 | 0.023 | 0.024 | 26.32 | 21.31 | 17.83 |
| 4%_NS_A | 0.056 | 0.035 | 0.022 | 28.54 | 25.53 | 20.14 |
| 6%_NS_A | 0.035 | 0.023[i] | 0.021 | 23.38 | 17.29[ii] | 15.98 |

[i] The critical pore diameter of the 6%_NS_A sample were measured in 9 days
[ii] The porosity of the 6%_NS_A sample were measured in 9 days.

Table 4.6 shows the critical pore diameter and the total porosity obtained for the 1, 2, 4, and 6% NS_A included cement pastes cured for 2, 7, and 28 days. The critical pore diameter of the cement paste shows an overall decreasing behavior for 2 and 7 days. The 28 day critical pore diameter does not show a significant difference indicating the effect of the NS on the pore structure is significant only during early ages. When comparing the critical pore diameter of the NS included cement with control_2d, a 7-fold reduction can be seen; a reduction is from 0.234 μm to 0.035 μm. After curing for 7 days, the critical pore diameter of the control sample reduced to 0.054 μm. Nevertheless, the samples which had 2% or more NS achieved the critical pore sizes close to that value in two days indicating rapid filling up of capillary pores from more hydration products.

Figure 4.27 shows the cumulative volume of mercury intruded vs pore size for the two day cured cement pastes with NS_U. As the curves show similar intruded volumes, the total porosity of the cement pastes seemed unaffected by including NS_U in the cement paste. However, a considerable amount of mercury intrusion into the NS_U cement pastes started at a smaller pore size as the NS_U percentage increases resulting a reduction of the threshold pore size by NS_U. Also, the curves of NS_U pastes became steeper and shifted to the left as the NS_U content increased. This implies that NS_U would make narrow pore size distributions and reduce the mean pore size of the cement pastes, as its content increases in the cement paste.

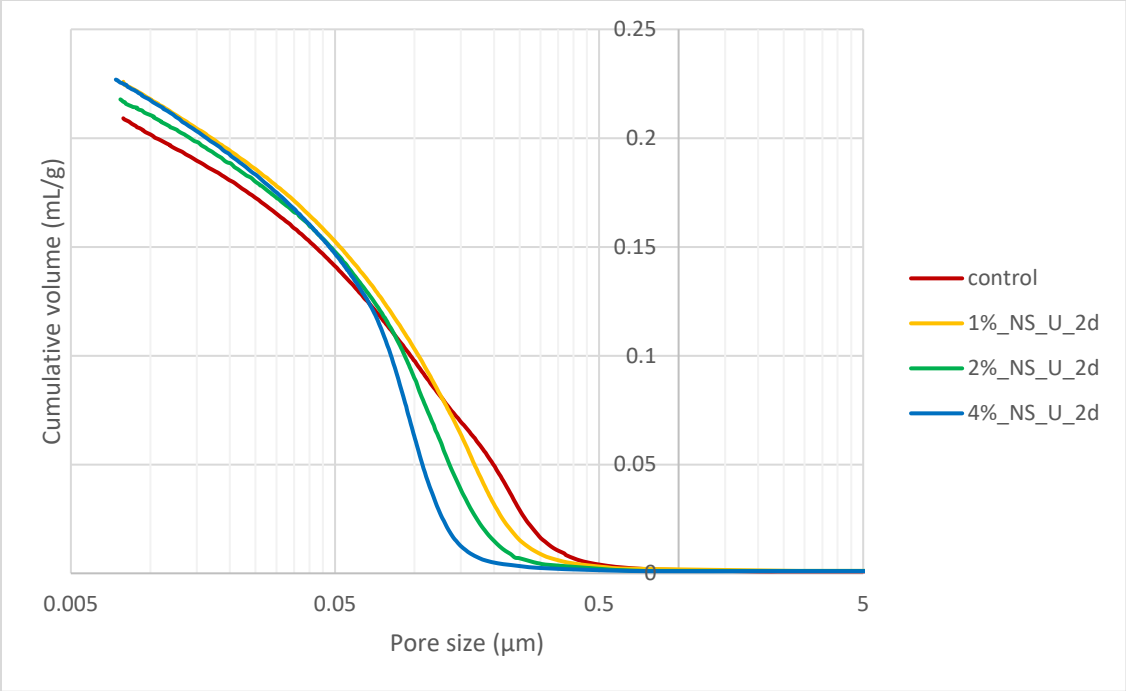


**Figure 4.27: Cumulative volume vs. Pore size of 2 days cured cement pastes with NS_U**

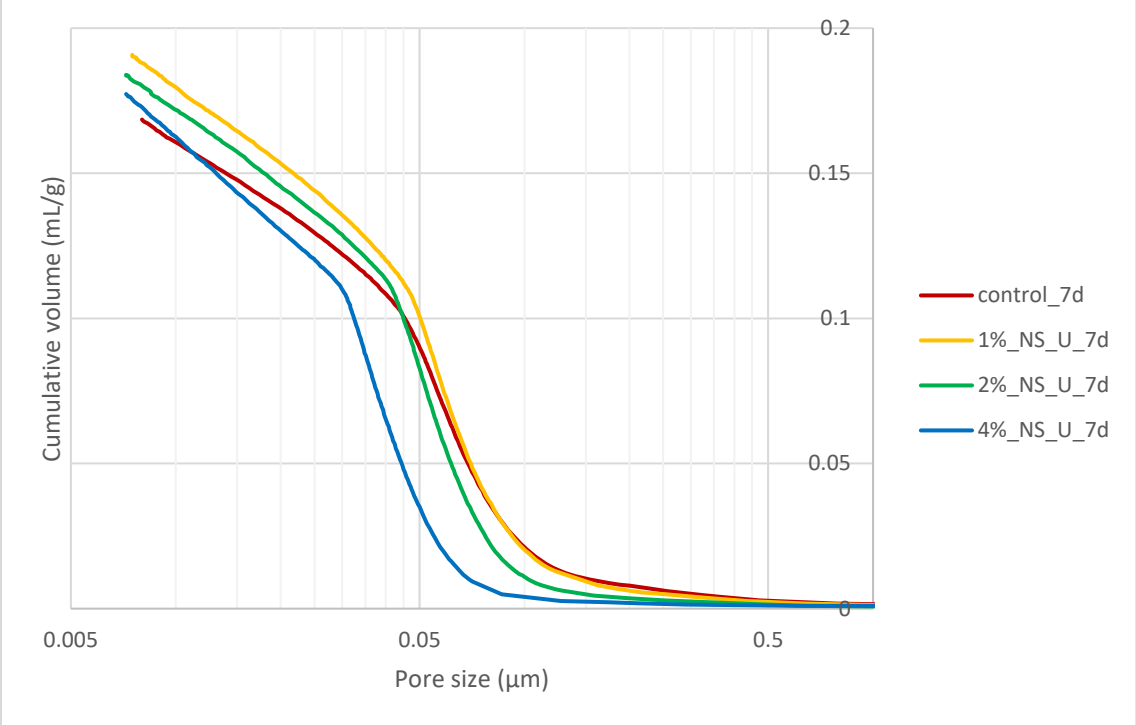


**Figure 4.28: Cumulative volume vs. Pore size of 7 days cured cement pastes with NS_U**

Figure 4.28 shows cumulative volume of mercury intruded vs pore size graphs for the seven day cured cement pastes with NS_U. For this NS, the pore structure refinement seemed to be

slower than NS_A type. Even though the NS_U included pastes show pore structure improvements within 2 days, the effectiveness of the NS_U for 1% and 2% contents appears diminishing. Only a slight improvement of the pore size is visible in the paste that contain 2% NS_U. However, the paste that contain 4% NS_U shows its effectiveness at 7 days by shifting its curve to the left compared to the others. This could be due to the pozzolanic activity of the unreacted NS particles in the cement paste. Also, the threshold pore diameter has been reduced in the pastes with 2% and 4% NS_U.

Figure 4.29 shows the cumulative volume of mercury intruded vs pore size for the twenty-eight day cured cement pastes with NS_U. The curves of the control and 1% NS_U containing pastes show similar behaviors while the curves of 2% and 4% NS_U containing pastes show similar pore size improvements compared the curves of the control and 1%_NS_U_28d. Even though the paste containing 2% NS_U did not show much effect within 2 -7 days, it has achieved an improved pore structure similar to the paste containing 4% NS_U. This indicates that 4% NS containing cement achieved this improvement within 7 days while the other took 28 days.

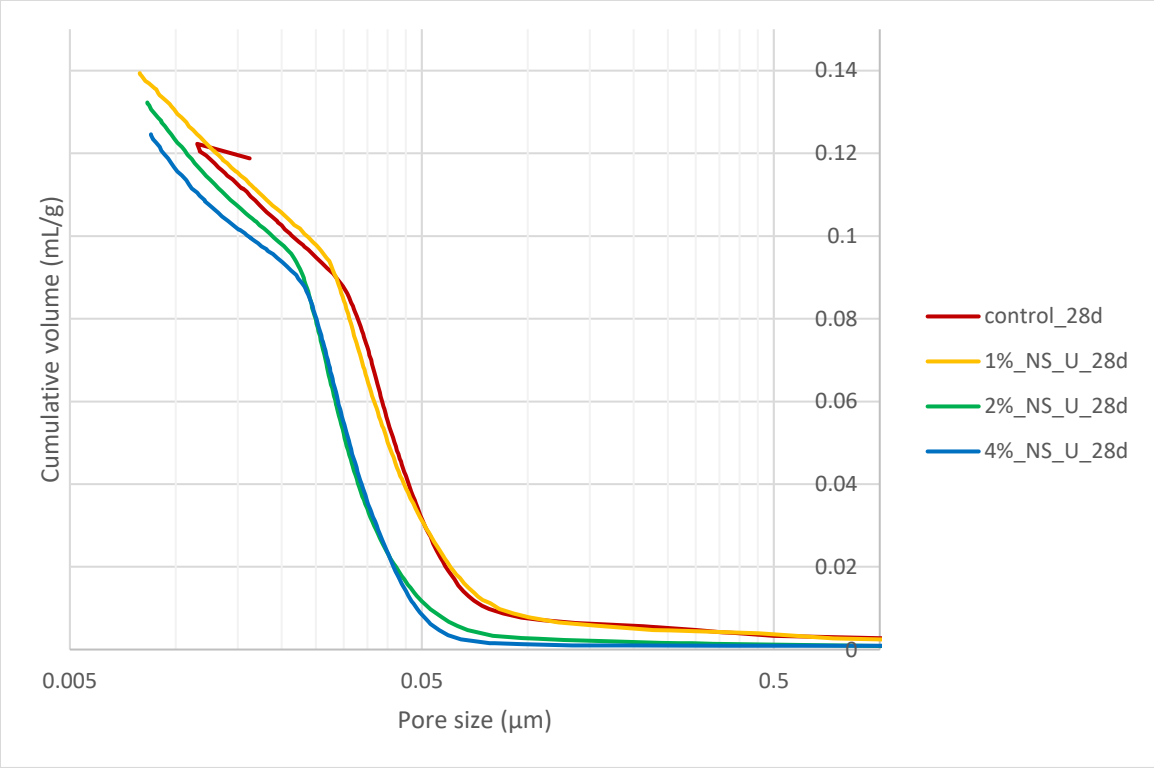


**Figure 4.29: Cumulative volume vs. Pore size of 28 days cured cement pastes with NS_U**

Table 4.7 shows the critical pore diameter and porosity obtained from MIP for cement pastes associated with NS_U type silica. The decreasing trend of the critical pore diameter with the increasing NS percentage is more visible in the cement pastes having NS_A type silica than that of NS_U type silica. The possible noticed difference between these pastes is the particle size and particle size distribution differences which could affect the reactivity of the cement minerals.

**Table 4.7: Critical pore diameters of cement pastes including NS_U**

| Sample ID | Critical pore diameter (μm) | | | Porosity (%) | | |
|---|---|---|---|---|---|---|
| | *At 2 days* | *At 7 days* | *At 28 days* | *At 2 days* | *At 7 days* | *At 28 days* |
| Control | 0.234 | 0.054 | 0.037 | 31.65 | 26.40 | 19.80 |
| 1%_NS_U | 0.168 | 0.054 | 0.032 | 33.11 | 28.08 | 22.02 |
| 2%_NS_U | 0.092 | 0.048 | 0.026 | 32.05 | 27.98 | 21.14 |
| 4%_NS_U | 0.088 | 0.035 | 0.027 | 33.16 | 26.88 | 19.55 |

### 4.2.8 SEM on NS included cement pastes

Figure 4.30 shows the EDS mapping obtained for the cement pastes after 2 days of age. Figure 4.30 (a) and (b) are respectively the BSE microstructures of cement pastes without NS and with 4% NS at x1000 magnification. Figure 4.30 (c) and (d) display the Si mapping, while Figure 4.30 (e) and (f) are the O mapping of the control and 4% NS samples, respectively. These images do not show any $SiO_2$ agglomerates of 5 μm or larger when the NS was included in the paste. Kong et al. [68] observed NS agglomerates around 100 μm which were larger than the cement particles. However, in this research associating NS as suspensions, such larger agglomerates were not visible. This indicates the agglomeration problem can be minimized by using NS as suspensions in calcium hydroxide.

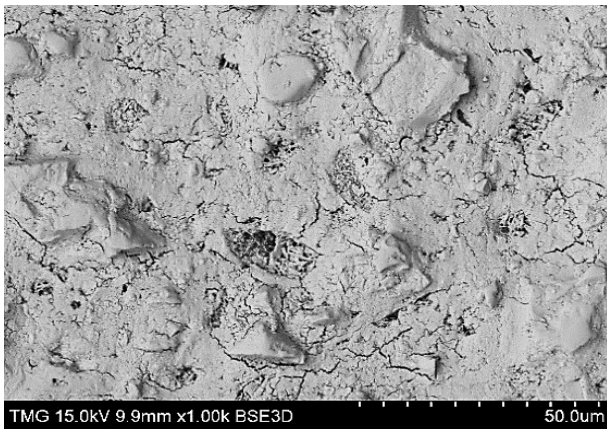


(a) Control BSE

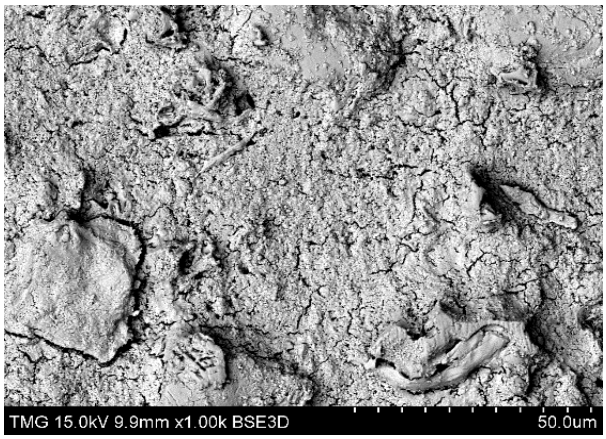


(b) 4% NS BSE

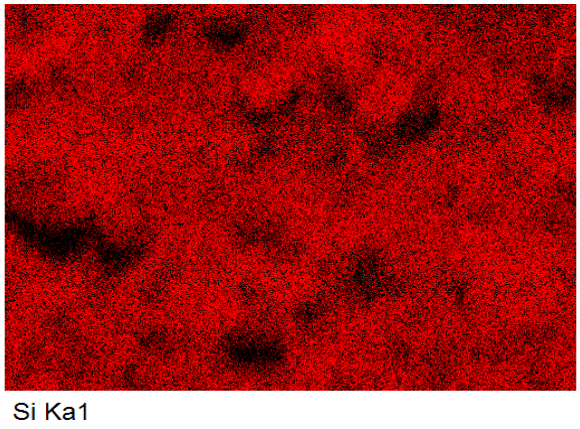


(c) Control Si mapping

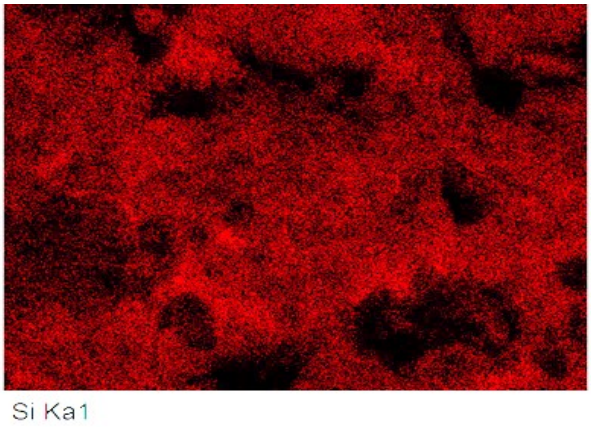


(d) 4% NS Si mapping

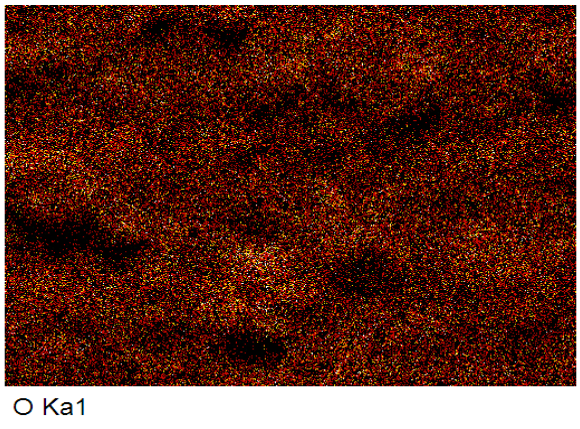


(e) Control O mapping

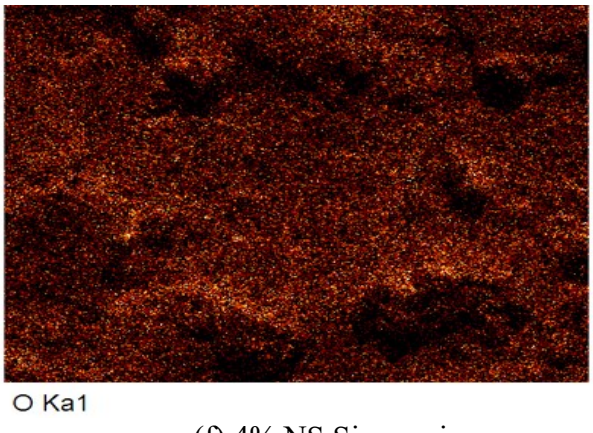


(f) 4% NS Si mapping

**Figure 4.30: BSE images and the Si and O mapping of the control sample and 4% NS_A type silica included cement pastes**

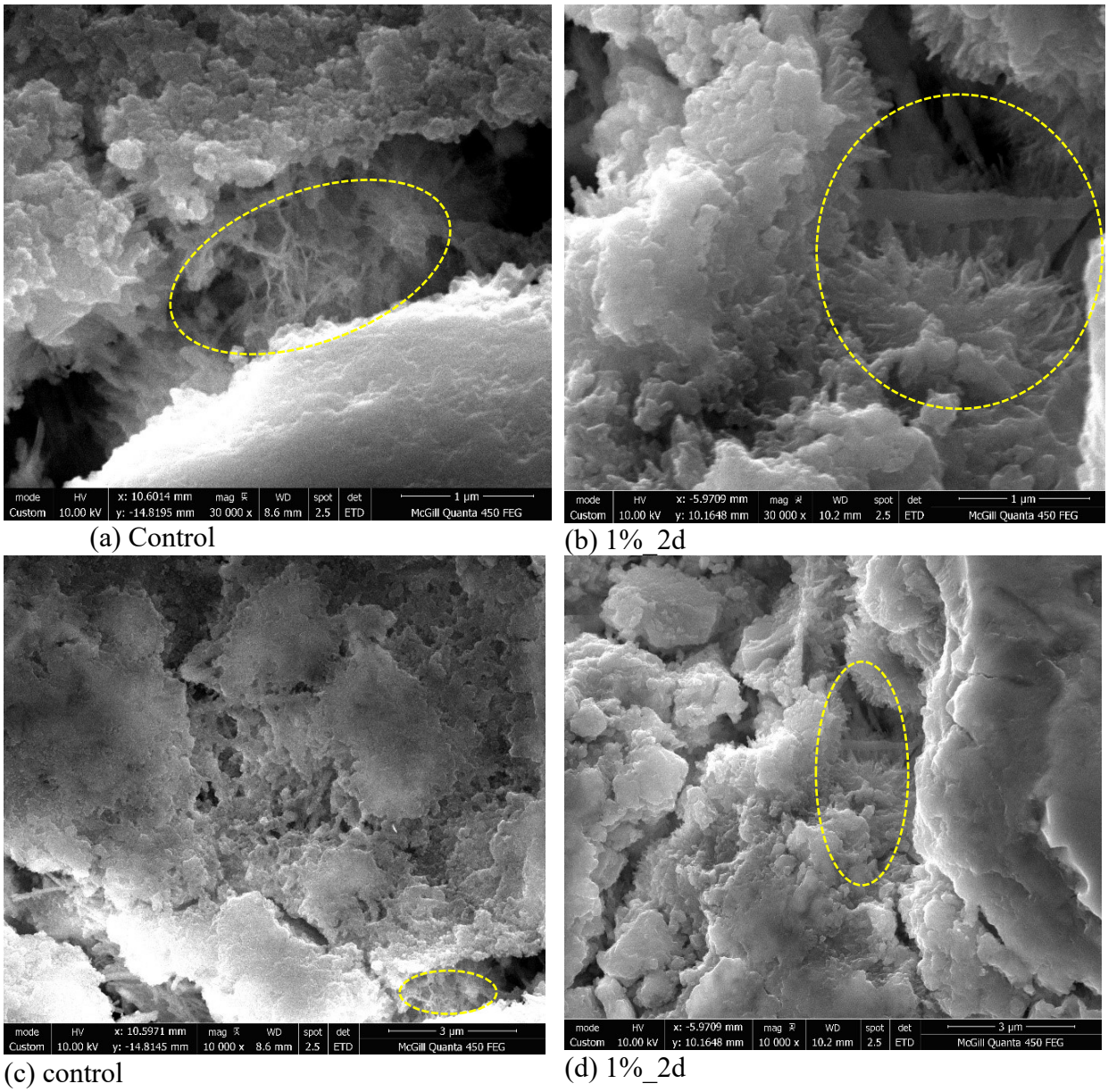


(a) Control (b) 1%_2d

(c) control (d) 1%_2d

**Figure 4.31: BSE images of cement pastes including NS_U type NS**

Figure 4.31 shows the SEM images of the hardened cement pastes of the control sample and the 1% NS_U sample. When comparing (a), (b), (c), and (d) of Figure 4.31, the images (b) and (d) have larger bridge-like CSH formations than those of in image (a) and (c) which are circled in the images. Also, no NS agglomeration was visible in the NS_U included cement pastes [image (b) and image (d)].

### 4.2.9 Compressive strength of NS_A type NS included cement paste

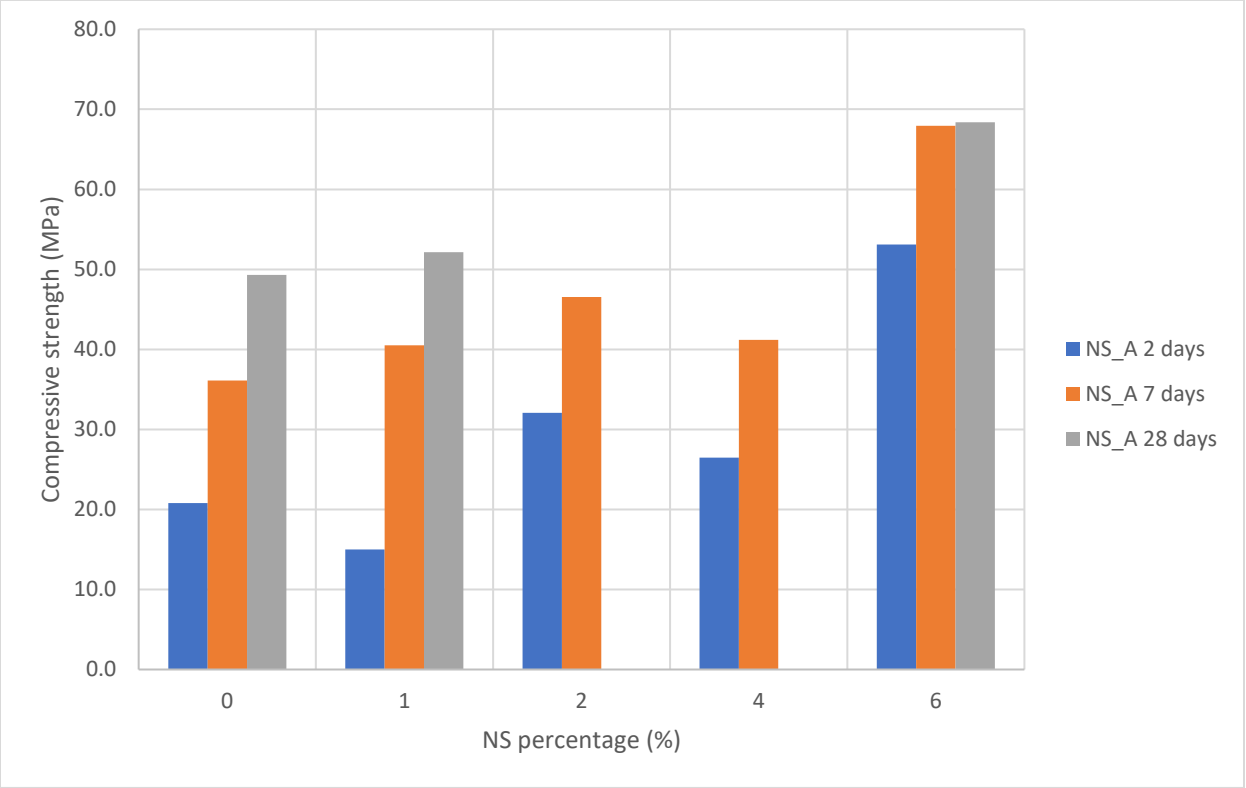


**Figure 4.32: Compressive strength of NS_A type silica included cement pastes**

Figure 4.32 illustrates the compressive strength of cement pastes with NS_A. At two days, the strength of the cement pastes with NS_A has increased with NS_A inclusion except for the paste with 1%_NS_A. However, it does not show a significant trend for the increase. At 7 days, the strength of the cement paste except that of the 4%_NS_A paste increased with a trend as the NS_A percentage increased. As the non-evaporable water content of 4%_NS_A (Figure 4.17) also show a significant reduction compared to the others, it can be assumed that this paste has not hydrated like this others. It could be a problem in preparation of the paste. However, it still has more strength than the control sample. Considering the 7 days cured pastes with 2% NS_A and 6% NS_A, the paste with 2% NS_A show a strength closer to that of the 28 days cured control paste and the paste with 6% NS_A show a strength (36%) more than the 28 days cured control paste. The strength of the cement pastes at 28 days also show strength improvements with NS_A inclusion. Considering the paste with 6% NS_A, its strength at 7 days and 28 days are very close indicating that the paste a faster hydration in the paste. These evidence reveal that NS_A improves the strength of the cement paste and that improvements occur earlier compared to the normal cement paste.

### 4.2.10 Compressive strength of cement pastes including NS_U type NS

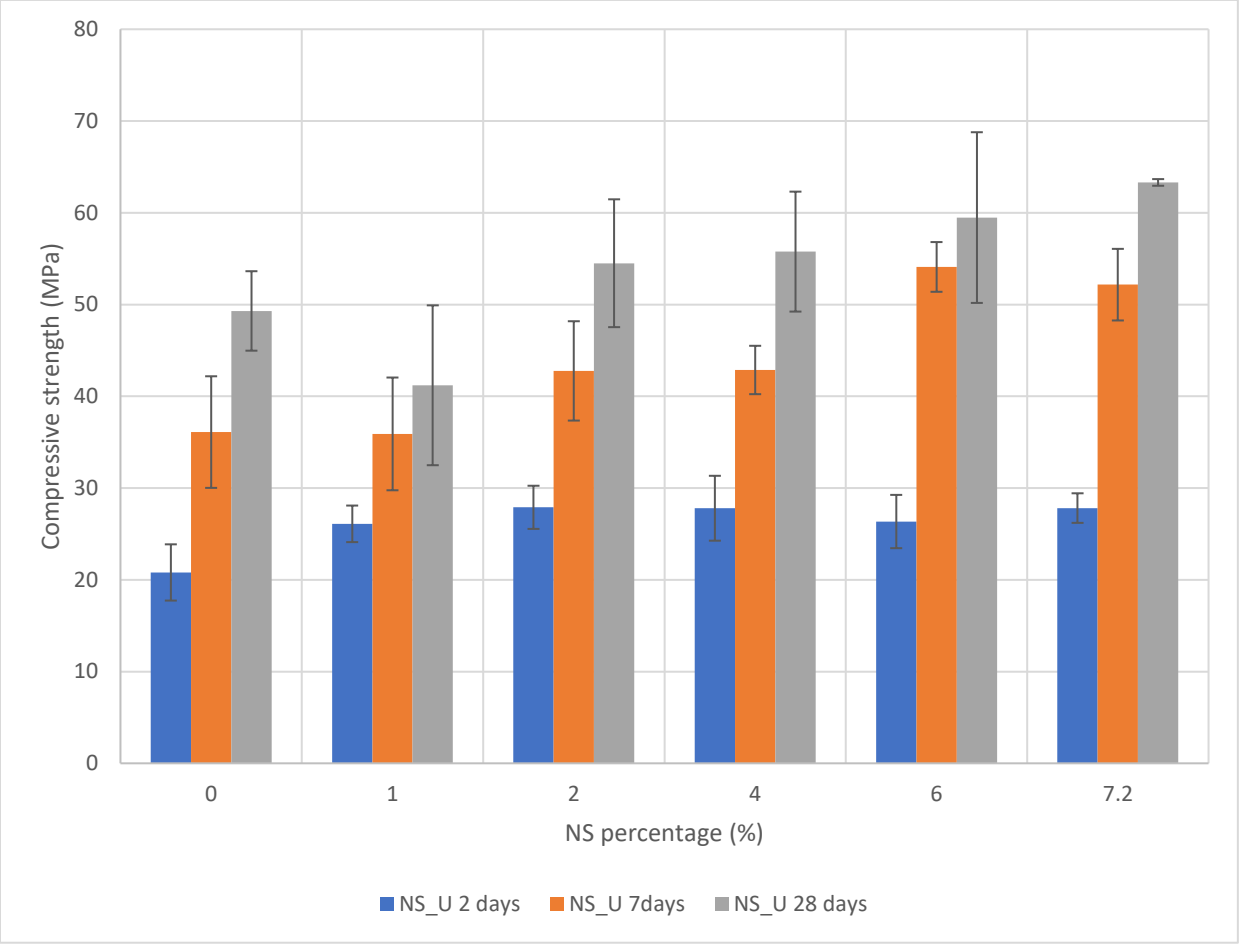


**Figure 4.33: Compressive strength of NS_U type silica included cement pastes**

Figure 4.33 shows the compressive strength of NS_U type cement paste for 2, 7, and 28 days. Considering the three series for different curing days, all the pastes that contain NS_U type silica shows an increase in the compressive strength except for the paste that contains 1% NS_U type silica at 7 and 28 days. All the pastes that have been cured for two days exhibit 27-34% compressive strength improvements. While the pastes which include 1% NS and 6% NS show 27% compressive strength increases, the other pastes show compressive strength increases of around 34%. Even though there's no trend in compressive strength improvement for two days cured specimens with respect to the NS addition, there is a definite compressive strength improvement with NS addition.

When comparing the 7 days cured specimens, a trend in compressive strength improvement is visible as the NS percentage increases. The pastes that have no NS and 1% NS have almost the same compressive strength at 7 days; the pastes that have 2% NS and 4% NS reveal about 19% compressive strength improvements; and the pastes that have 6% and 7.2% NS show 50% and 45% compressive strength improvements, respectively. The 28 day cured cement pastes also

exhibit compressive strength improvements as the NS percentage increases except the 1% NS included cement paste. The increase in the compressive strength is in the range of 11% - 28%.

## Results of commercial silica in the cement paste

### 4.3.1 Hydration of CB8 and CB9 silica included cement pastes

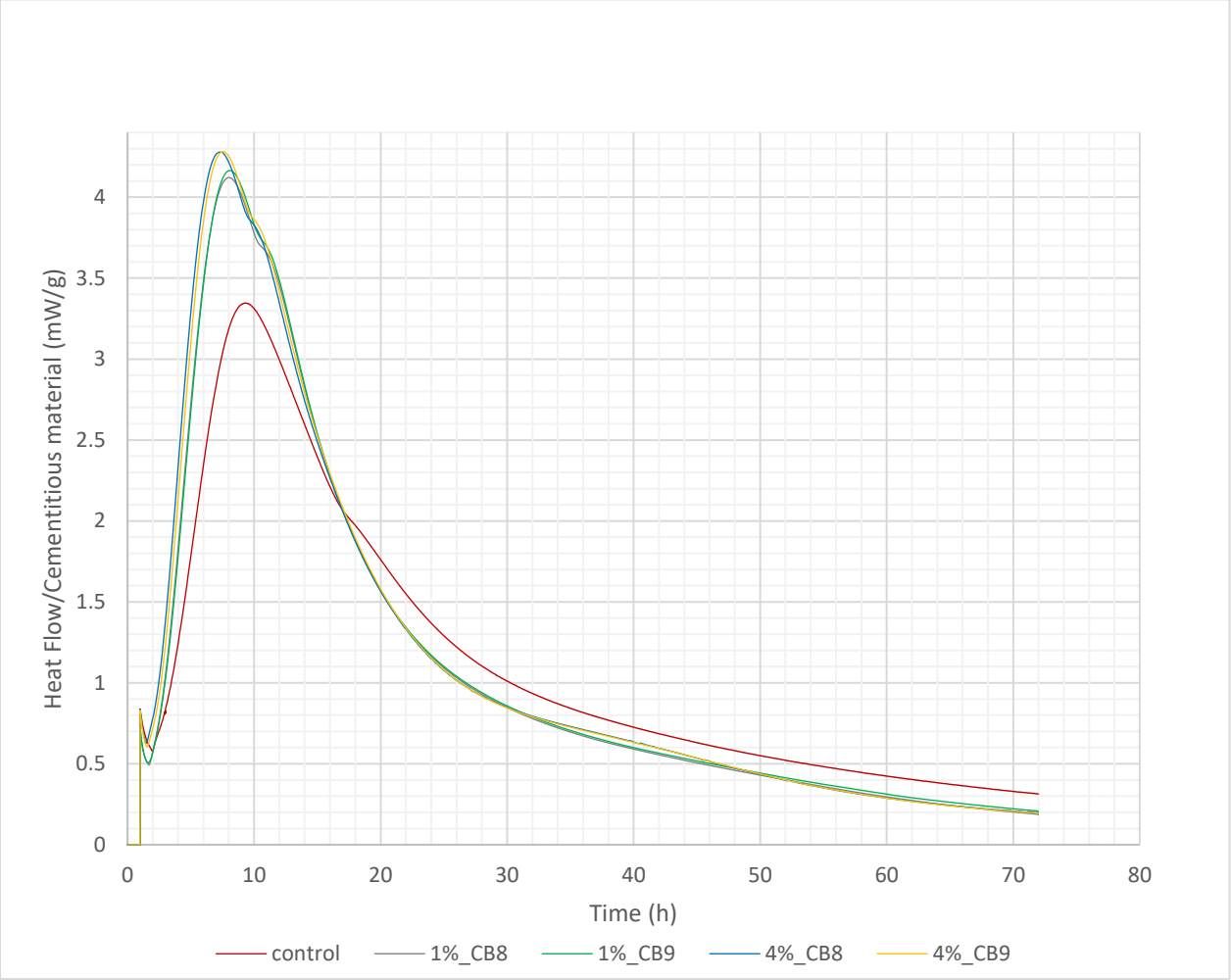


**Figure 4.34: Heat Evolution of CB8 and CB9 silica included cement pastes**

Figure 4.34 shows a comparison of heat evolution of commercially available NS with the normal cement paste. The rates of heat flow show that these two NS types improve the cement hydration. With increasing cement replacement with NS, the rate of hydration increases in these cement pastes. CB9 NS has the particle size 45-47 nm and CB8 has 3-100 nm. However, regardless of the particle size of the two NS, regarding the heat evolution curves for 4% and 1%, both curves of the CB8 and CB9 fitted on top of each other showing a slight difference. The curves have shifted left indicating early hydration in NS included pastes. When considering the maximum heat flow (Figure 4.35) for each curve, the 4% NS included pastes show the highest, control sample shows

the lowest, and the 1% NS is in the middle. Considering 1% NS included pastes, they show their improvements in hydration similar compared to the control sample before around 65 hours. The overall hydration of the 1% NS sample does not show much difference compared to the control sample at 72 hours.

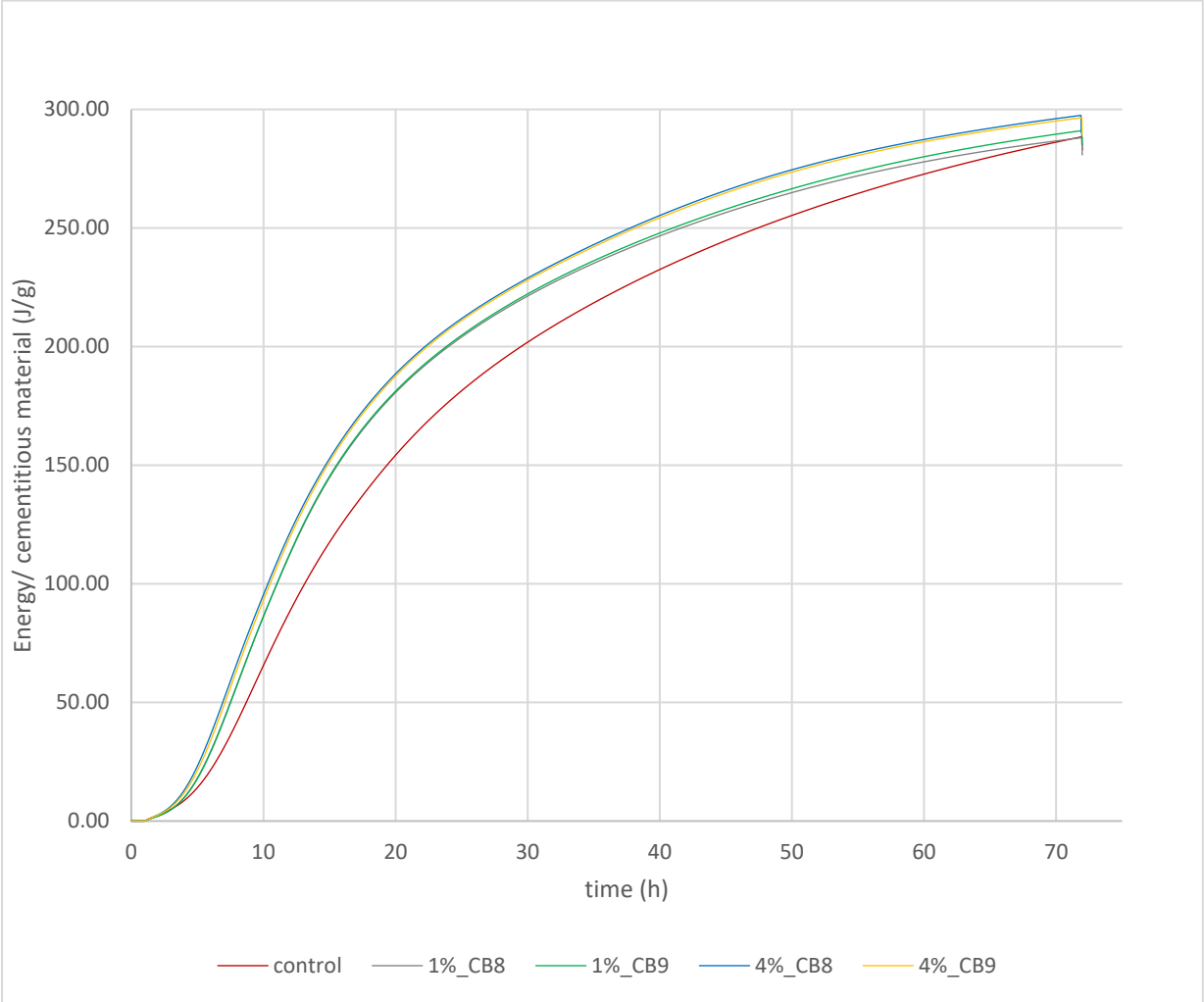


**Figure 4.35: Cumulative energy of CB8 and CB9 silica included cement pastes**

### 4.3.2 Hydration of colloidal silica included cement pastes

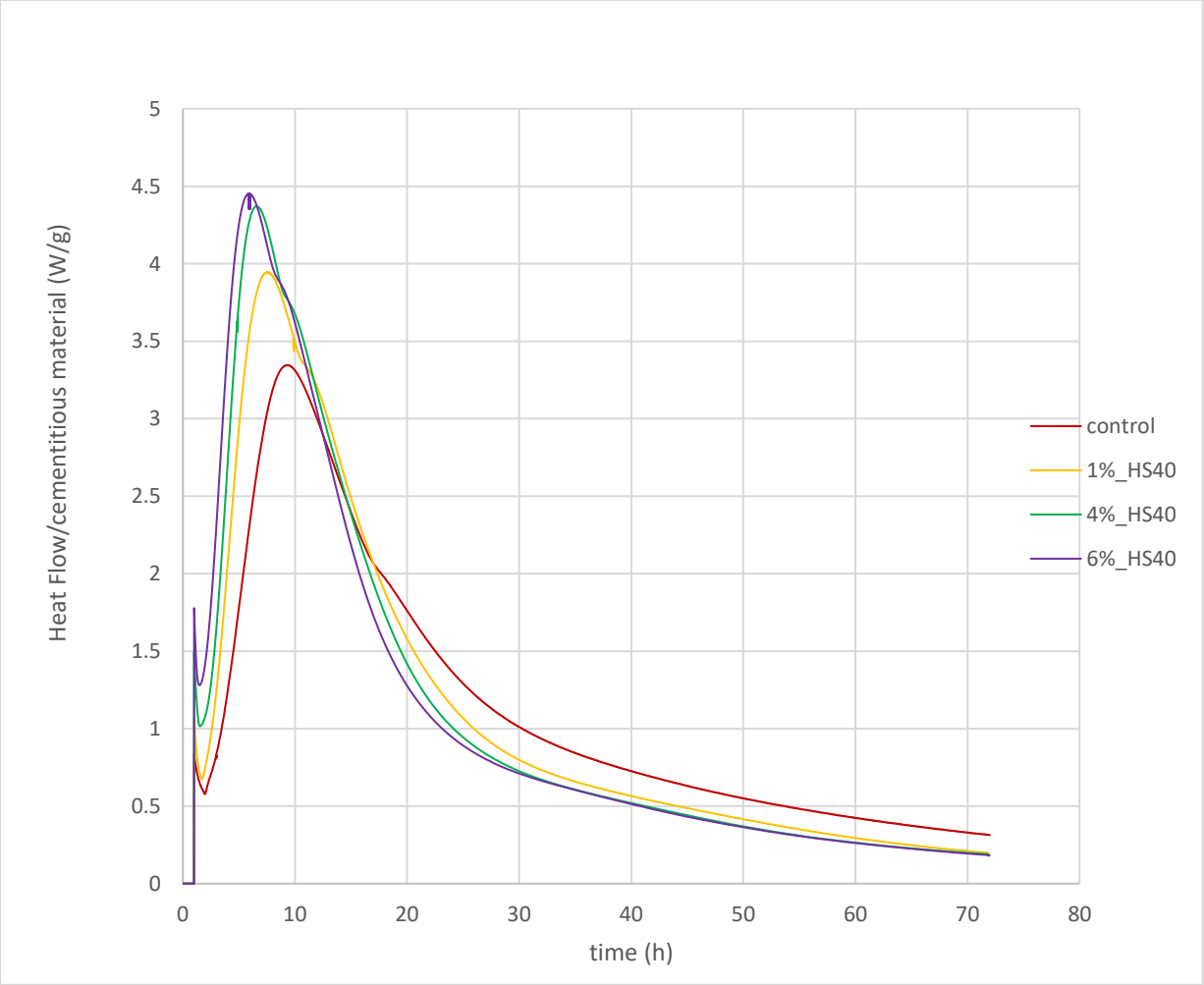


**Figure 4.36: Heat Evolution of colloidal silica included cement pastes**

Figure 4.36 shows the heat flow variation of colloidal NS included cement pastes. The cement replacement levels were 1%, 4%, and 6% by the colloidal silica. As the amount of colloidal silica increased, the curves have been shifted to the left in increasing order. This explains that the hydration reactions occur more rapidly when the colloidal silica is included in the paste than the normal cement paste. The heights of the peaks also show significant increases compared to the normal paste. The power generated by the hydration reactions are maximum at those highest points which means that the reactions occur at their fastest paces. The acceleration period of these curves is related to the nucleation and the growth of the cement hydrates products. Therefore, it can be implied that the colloidal silica improves the rate of reaction and produce more hydration products in a faster manner. However, the mixing 6% colloidal silica was more difficult than the other pastes because the paste had poor workability, requiring more mixing time than the other pastes. Considering the curve for cumulative energy (Figure 4.37), it seemed that the curves of the colloidal silica included pastes have converged at the end of the test (72 hours). This suggests that the quantity of the associated colloidal silica does not affect the total hydration for the 72 hours

and the colloidal silica quantity increase has only affected in improving the hydration within roughly the first 60 hours.

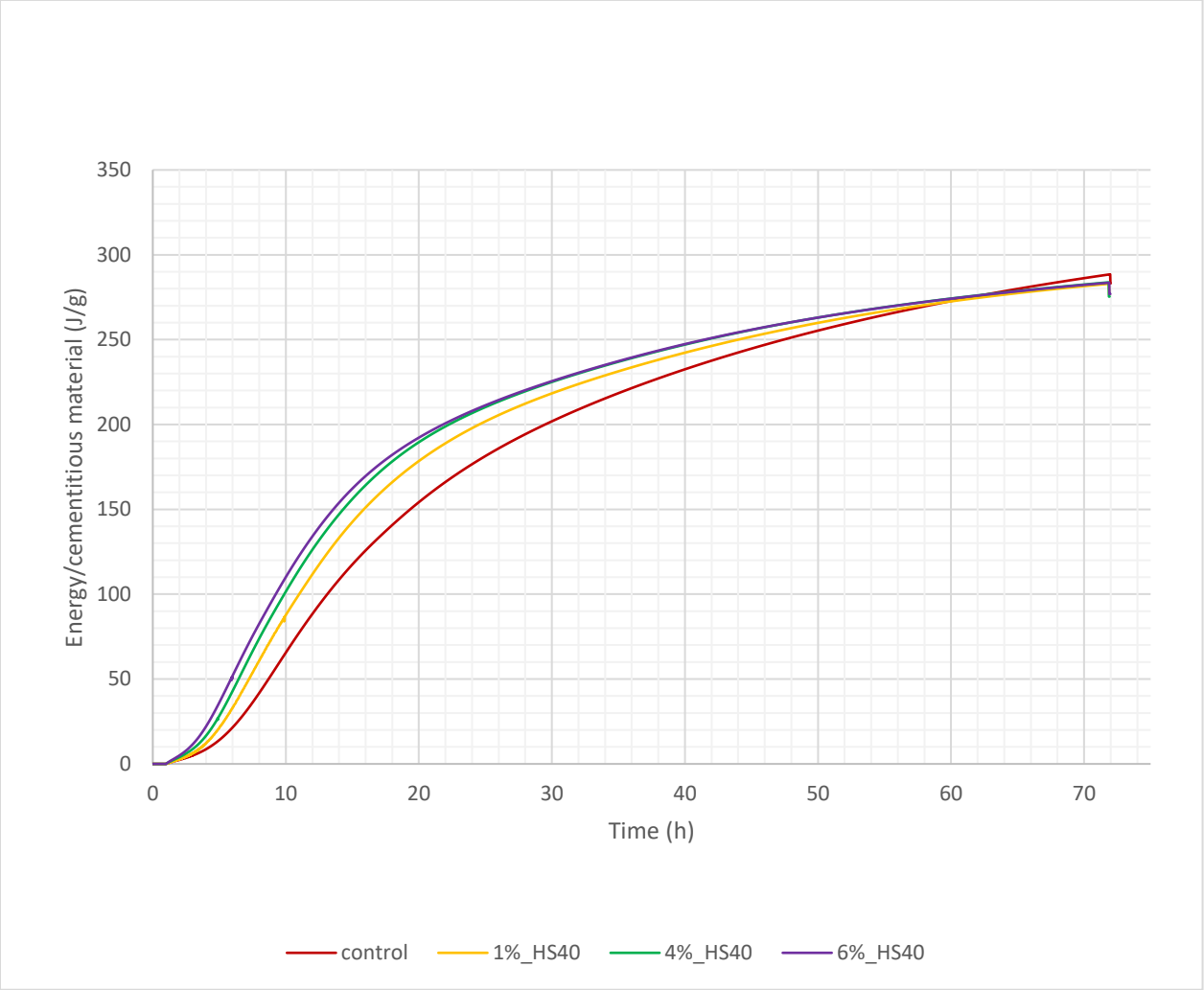


**Figure 4.37: Cumulative energy of colloidal silica included cement pastes**

### 4.3.3 Compressive strength of colloidal silica included cement pastes

Figure 4.38 shows the compressive strength variation of HS-40, colloidal silica (CS) included cement pastes. In this trial, the cement was replaced with 1% and 4% colloidal silica. The 2 days cured pastes show 22% and 25% compressive strength increases for 1% and 4% cement replacements, respectively. The 7 days cured pastes have 11% compressive strength improvement for 1% cement replacement while for the 4% cement replacement the compressive strength change is a 2% drop. This trend is similar in 28 days cured cement pastes which show a slight increase in compressive strength for 1% cement replacement and a drop in the strength for 4% cement replacement.

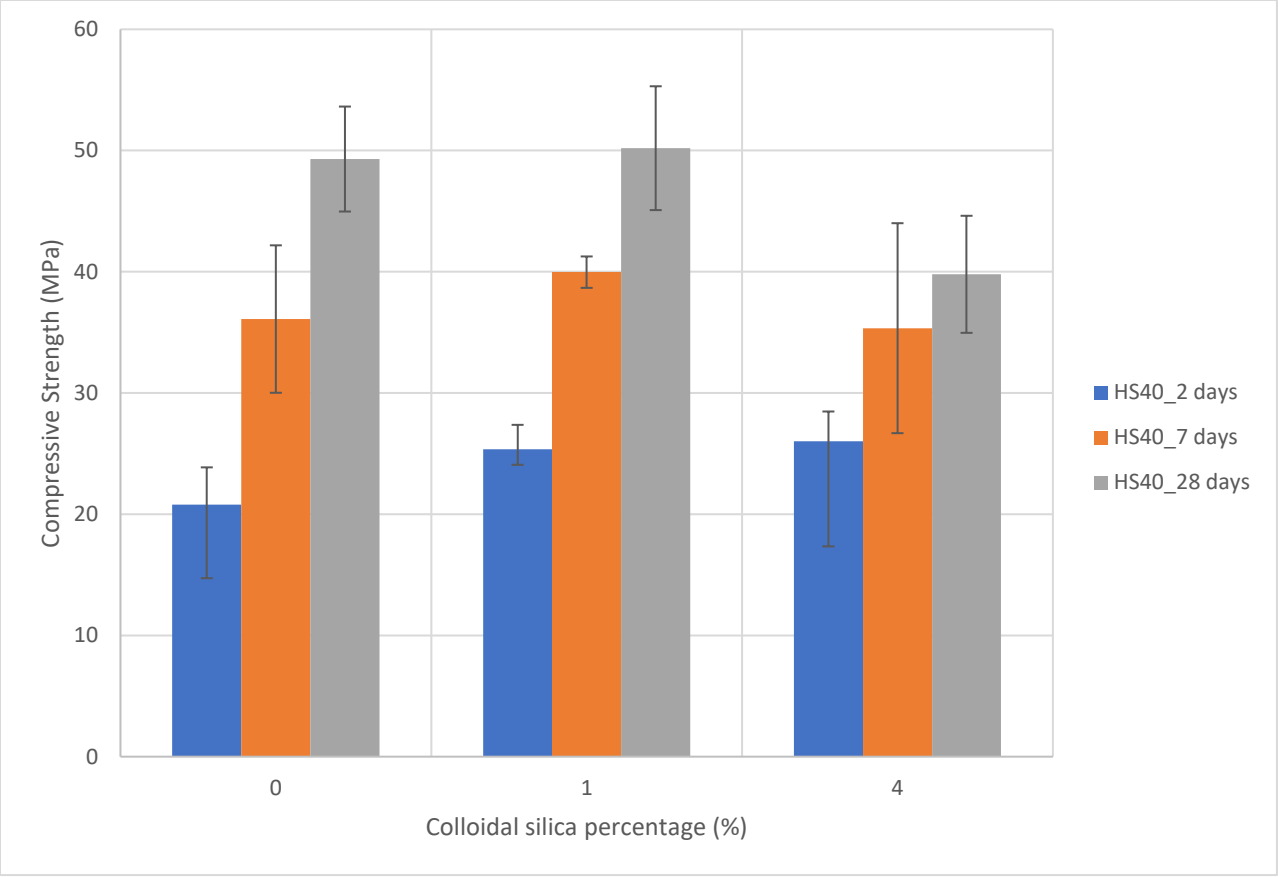


**Figure 4.38: Compressive strength of colloidal silica included cement pastes**

### 4.3.4 XRD analysis of synthesized silica included cement pastes

4.3.4.1.

***XRD analysis of 2 days cured cement pastes***

Figure 4.39 shows the XRD spectra of 2 day cured cement pastes containing NS_U and CB9. The intensity data of the spectra are normalized for the comparison purposes. The utilized silicon amount for the refinement was 9 – 10% of the weight of the sample and its primary intensity peak lies at 28.44° 2-theta. The other identified minerals are CH, $C_3S$, and $C_2S$ in which the primary intensity peaks are at 34.10°, 34.44°, and 32.14° respectively. CH also has a predominant peak at 18.10 2-theta which does not overlap with other peaks. When comparing the primary peaks for the CH for all the samples, the intensity difference of peaks among the samples is insignificant. However, the secondary peaks show some differences in terms of the intensity which are not consistent with NS content. As the quantity measurements depend on several other experimental factors such as crystallite size, strain, absorbance, the Rietveld refinement provides more reasonable fitted quantity measurements.

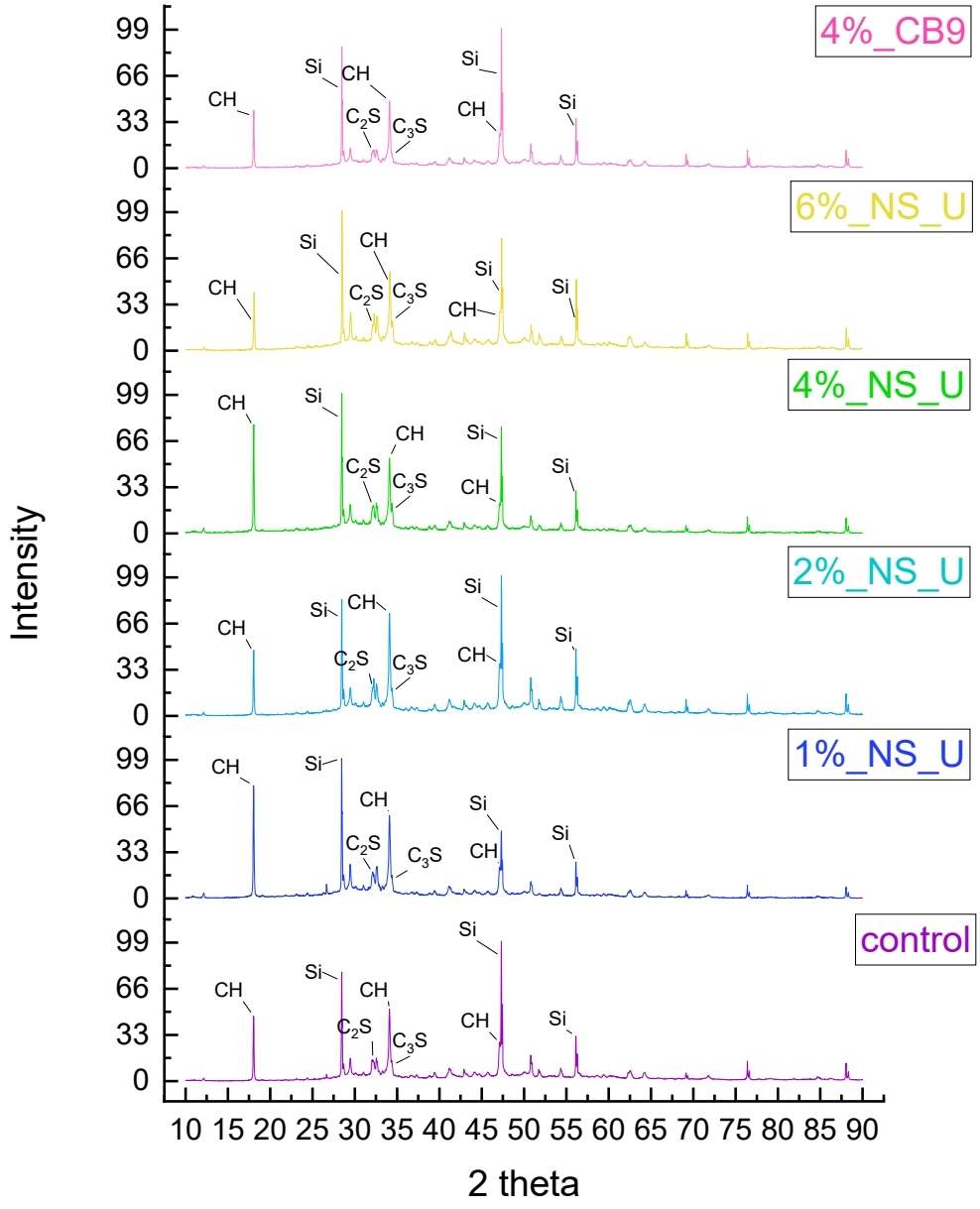


**Figure 4.39: XRD spectra of 2 days cured cement pastes containing NS_U and CB9**

Table 4.8 shows the CH quantities measured by the Rietveld refinement. The CH quantity of the cement pastes containing NS shows a reduction in CH quantity except for the pastes that contain 1% NS_U and 2% NS_U. This suggests that NS_U has improved the cement hydration reactions by the nucleation seeding effect and the pozzolanic effect is not effective in these two samples. The CH quantity reduction in the other samples except the paste containing 6% NS_U, suggests that both nucleation seeding effect and the pozzolanic effect have occurred in them with

the evidence from the calorimetric studies. The paste that contains 6% NS_U shows less CH formation which is visible from its XRD spectrum and the refinement data and it could be due to its low hydration.

**Table 4.8: The CH quantity measured by Rietveld refinement**

| NS percentage | The CH quantity (%) | |
|---|---|---|
| | 2 days | 7 days |
| 0 | 13.9 | 14.3 |
| 1% NS_U | 16.3 | 14.9 |
| 2% NS_U | 14.5 | 14.8 |
| 4% NS_U | 13.7 | 14.6 |
| 6% NS_U | 10.8 | 9.1 |
| 4%_CB9 | 12.9 | N/A |

4.3.4.2. ***XRD analysis of 7 days cured cement pastes***

Figure 4.40 shows the XRD spectra of the 7 days cured cement pastes containing NS_U. The silicon quantity used for the refinement was 9-11% in these samples except the sample containing 2% NS_U which had 19% silicon. Due to that, the normalized data of the cement paste containing 2% NS_U show other peaks shorter when compared with other samples. Due to that and the reasons explained earlier the Rietveld refinement results gives reasonable estimations of the CH quantities which are tabulated in Table 4.8**Error! Reference source not found.**. The results show that very small differences in the CH quantities among the samples. However, the CH quantity is decreasing by very small quantities as the NS_U quantity increases. When considering the pastes that contain 1% NS_U and 6% NS_U, their CH quantities at 7 days are lower than that at two days. This indicates that the pozzolanic action has taken place in these two samples during the period between 3-7 days. The increase of the CH content in the other samples indicate that both hydration improvements and pozzolanic actions have been occurring in them. Also, the calorimetric studies revealed that the pozzolanic effect was taking place after around 40 hours which confirms the pozzolanic action of the cement paste containing NS_U.

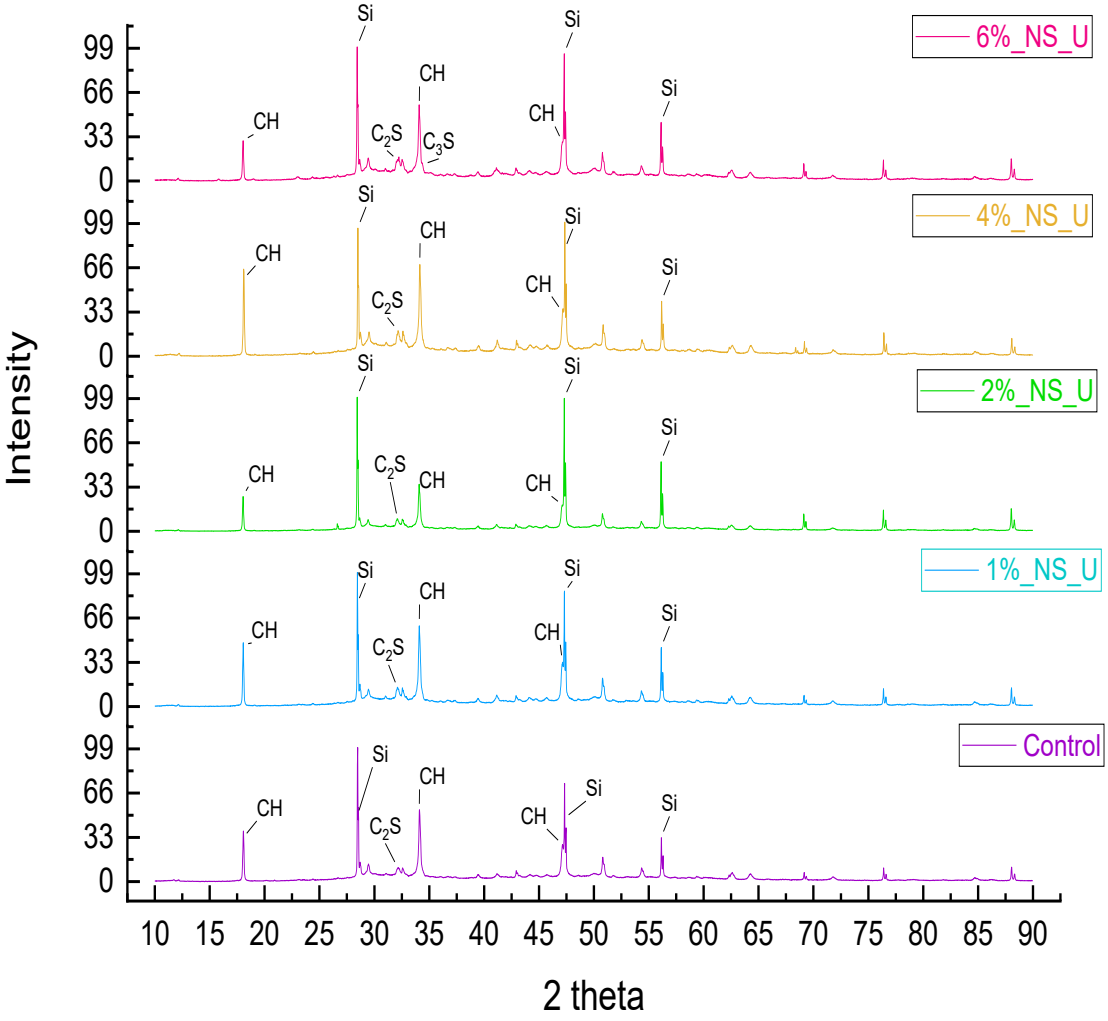


**Figure 4.40: XRD spectra of 7 days cured cement pastes containing NS_U**

# Chapter 5. Discussion

In this chapter, comparisons of results obtained with different materials are presented. The correlations of different results are also discussed.

## 5.1. Effect of NS synthesis method on particle size

**Table 5.1: Particle size of the laboratory synthesized silica**

| Sample ID | Test method / Instrument | Viscosity | Average Particle size |
|---|---|---|---|
| NS_A | Dynamic Light scattering/ Malvern, Zetasizer Nano S90 | 0.93 cP (measured by Ostwald viscometer) | 91 - 109 nm (**Error! Reference source not found.**) |
| NS_U | Dynamic Light scattering/ Malvern, Zetasizer Nano S90 | 1.15 cP (measured by SV-10 vibrating viscometer) | 5.2 - 6.5 nm (**Error! Reference source not found.**) |
| NS_EG | Dynamic Light scattering/ Malvern, Zetasizer Nano S90 | 2.52 cP (measured by SV-10 vibrating viscometer) | 5.7 - 6.1 nm |
| HS-40 | Specified by Fisher | N/A | 12 nm |
| CB-8 | Specified by Levasil | 8.8 cP | 3 – 100 nm |
| CB-9 | Specified by Levasil | N/A | 45 – 47 nm |

The summarized particle size analysis is tabulated in Table 5.1. The particle size measurements were performed with dynamic light scattering. This method is suitable for particle sizes ranging from 0.3 nm to 10 μm [115]. It can be noted that by using ultrasonication at the time of the condensation reaction taking place, the particle size was reduced from approximately 100 nm to below 10 nm. Moreover, ethylene glycol did not affect the particle size of NS as this sample was ultrasonicated as well. While sample 4 and 5 have similar concentrations of NS, the viscosity of the suspension increased as a result of using ethylene glycol indicating that ultrasonification alone is most suitable for incorporation into cementitious materials.

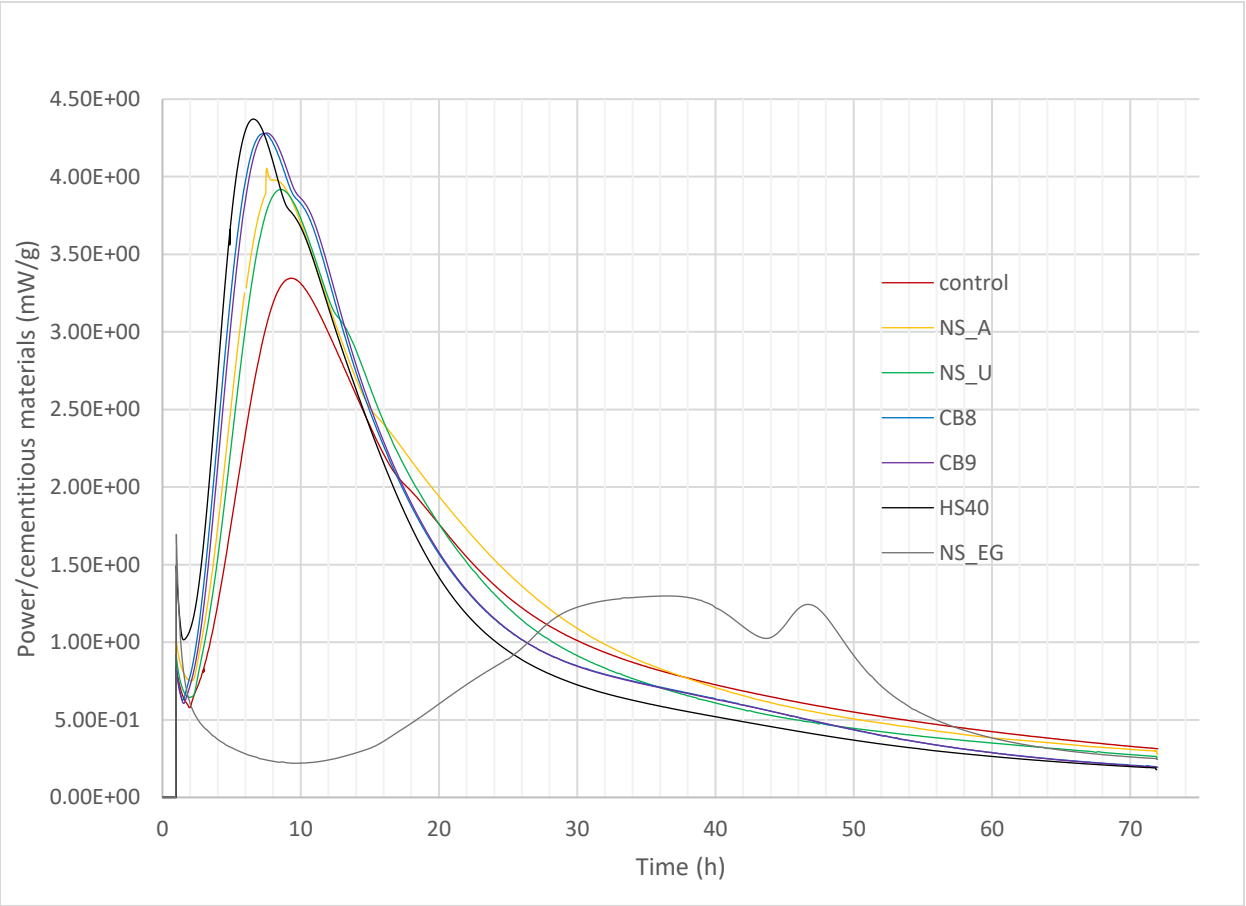


**Figure 5.1: Rate of hydration of the 4% NS included cement pastes**

Figure 5.1 shows the rate of hydration of the 4% NS including cement pastes as measured by isothermal calorimetry. This figure shows that all the NS pastes have a higher rate of hydration (the power value corresponding to a specific point of time) than the control cement paste (the paste without any NS) in the beginning up to about 14 hours except the paste with NS_EG. The paste with NS_EG shows a significant reduction in hydration by shifting its curve to the left and having the shortest peak (which is shorter than half of that of the control sample). This can be attributed to the ethylene glycol in the paste. The behavior of the other curves can be interpreted that the hydration process of the pastes occurs faster than the control sample. The fastest hydration can be observed in the paste that contain colloidal silica (HS40) which has particle size of about 12 nm as per the manufacturer's information. The rapidity of its hydration was observed during the mixing as the paste became less workable than the other pastes. It is possible that the silica could be in the form of the sol or in a form where reactive silicates are present more than silanols on the particle surfaces. CB8 and CB9 cement pastes also showed faster hydrations than the control and the other two pastes that include NS_A and NS_U. After around 20 hours, all the pastes hydrate slower than the control paste except the paste that contain NS_A type NS, indicating a more continuous hydration than the other pastes. This increased rate of hydration of pastes including NS_A was occurring until close to the end of the deceleration period of its curve. It could be

possible that this paste contained some larger particles which would possibly be reacting during the deceleration period. As the SEM images did not show much large sized agglomerates or evidence of the presence of agglomeration in the pastes, it could be assumed that these particles are not so large to be visible at micro levels, and therefore could be sub-micron levels or loosely held nanoparticles. Thus, it is possible that those particles could be consumed during the deceleration period by the formed CH. However, the particles have given beneficial effects to the paste in terms of improvement of hydration and the pore structure, and strength which will be discussed later in this chapter.

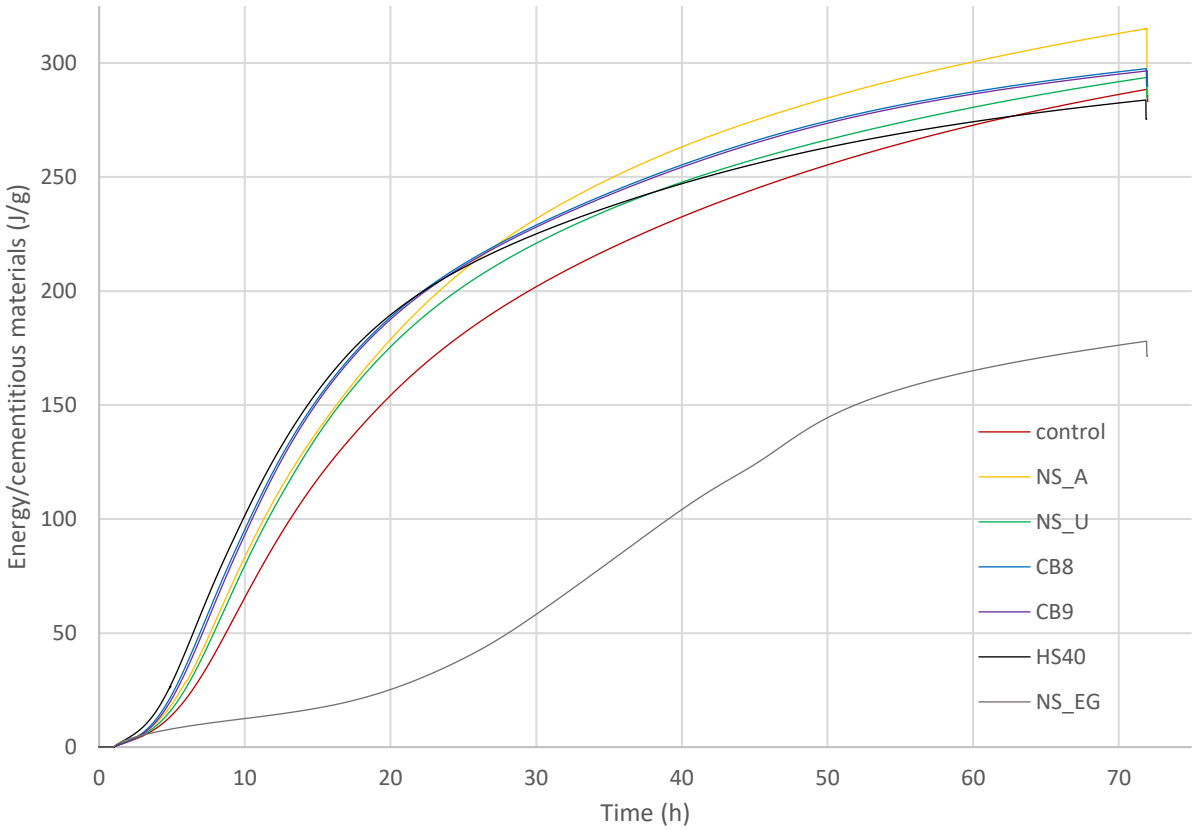


**Figure 5.2: Energy release with time for 4% NS included pastes**

Figure 5.2 shows the energy released with time by cementitious material for the pastes including 4% NS. All the cement pastes display an increased release of energy than the control cement paste until around 62 hours except the paste that contain NS_EG. This indicates that these pastes hydrate more than the control paste up to the mentioned time. After that time, the total amount of energy released by the paste containing colloidal silica becomes lower than the control sample. This suggests that the inclusion of the colloidal silica is effective for a shorter time and that the replacement of cement by this cannot reach the total hydration by the cement itself. Also, it could be exclusively having more seeds of the cement hydration reaction, but not having the pozzolanic reaction. The curve of the NS_U paste also tends to get closer to the curve of the control

paste, which also has 5 -6 nm size NS particles. This could be a result of the fineness of the particles and the presence of more surface silanols.

The progress of hydration of the cement paste including NS_A is more significant than the other pastes due to having a larger difference between the curve of the control sample and that itself for a larger period continuously. This curve keeps increasing at a higher rate than the others. This explains that both the nucleation seeding action and the CH consumption are occurring in that paste.

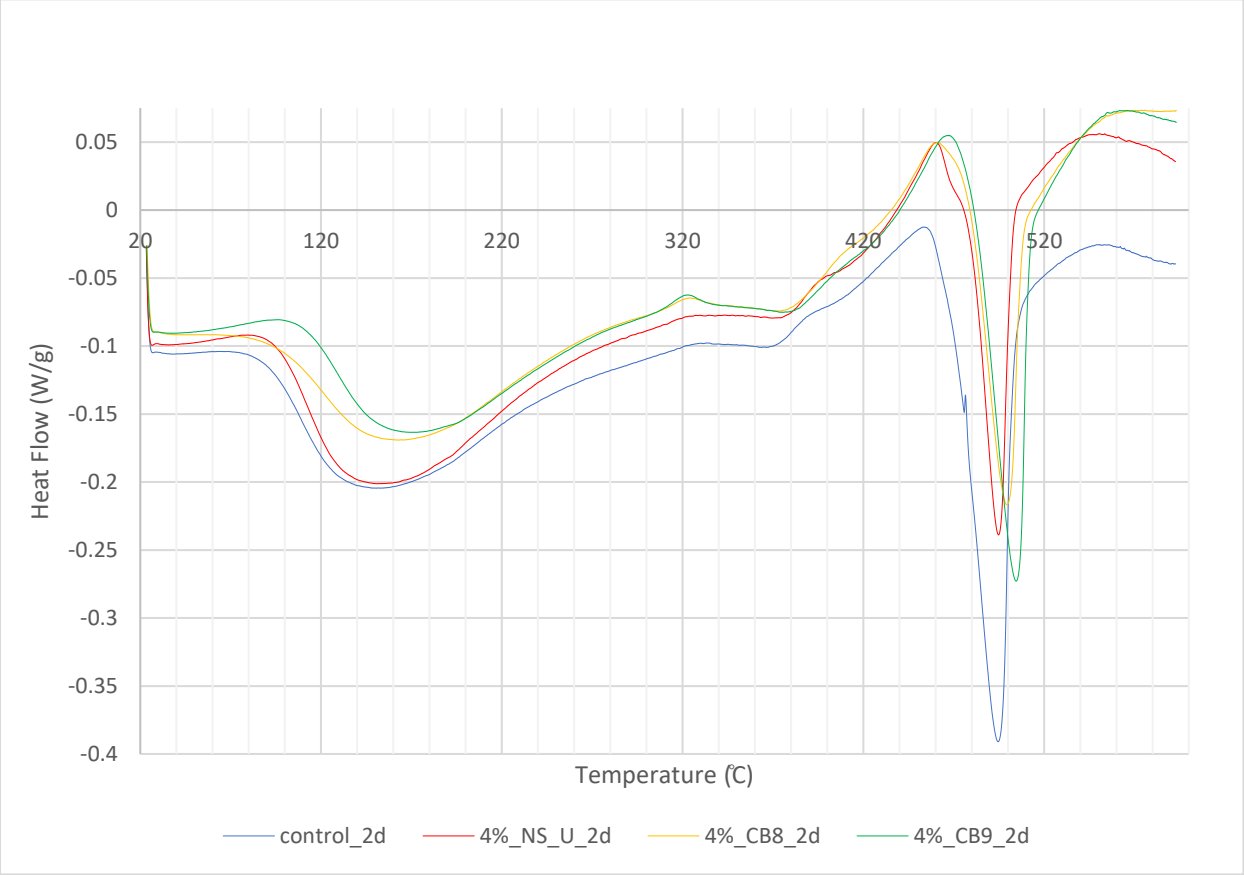


**Figure 5.3: Heat flow of 2 days cured 4% NS included pastes**

Figure 5.3 presents the heat flow of the 2 days cured pastes including 4% NS using DSC upon heating from 23℃ to 600℃. Only cement pastes with NS_U, CB8, CB9 were tested by this technique. The broad peaks which are located around 100℃- 220℃ indicate the dehydration of ettringite and some of the CSH phases. The peaks around the 450℃ -520℃ which are attributable to the decomposition of CH to CaO indicate the quantity of the CH present in the pastes. It is obvious that the pastes that contain 4% NS have less CH (area of the trough: 56.38 J/g, 48.07 J/g, and 64.77 J/g for NS_U, CB8, and CB9 respectively) than the control cement paste (area of the trough: 121.8 J/g). The 4%_CB9_2d paste contains slightly more CH than the other two pastes containing NS. So, it can be confirmed that the NS has consumed the formed CH in the pastes.

Although, these three pastes have similar NS quantities at two days, the cumulative hydration of the pastes at the end of two days (Figure 5.2) are different, with the highest hydrations in the CB8 and CB9 pastes. This suggests that the pastes that have CB8 and CB9 NS could contain more CSH than the paste containing NS_U.

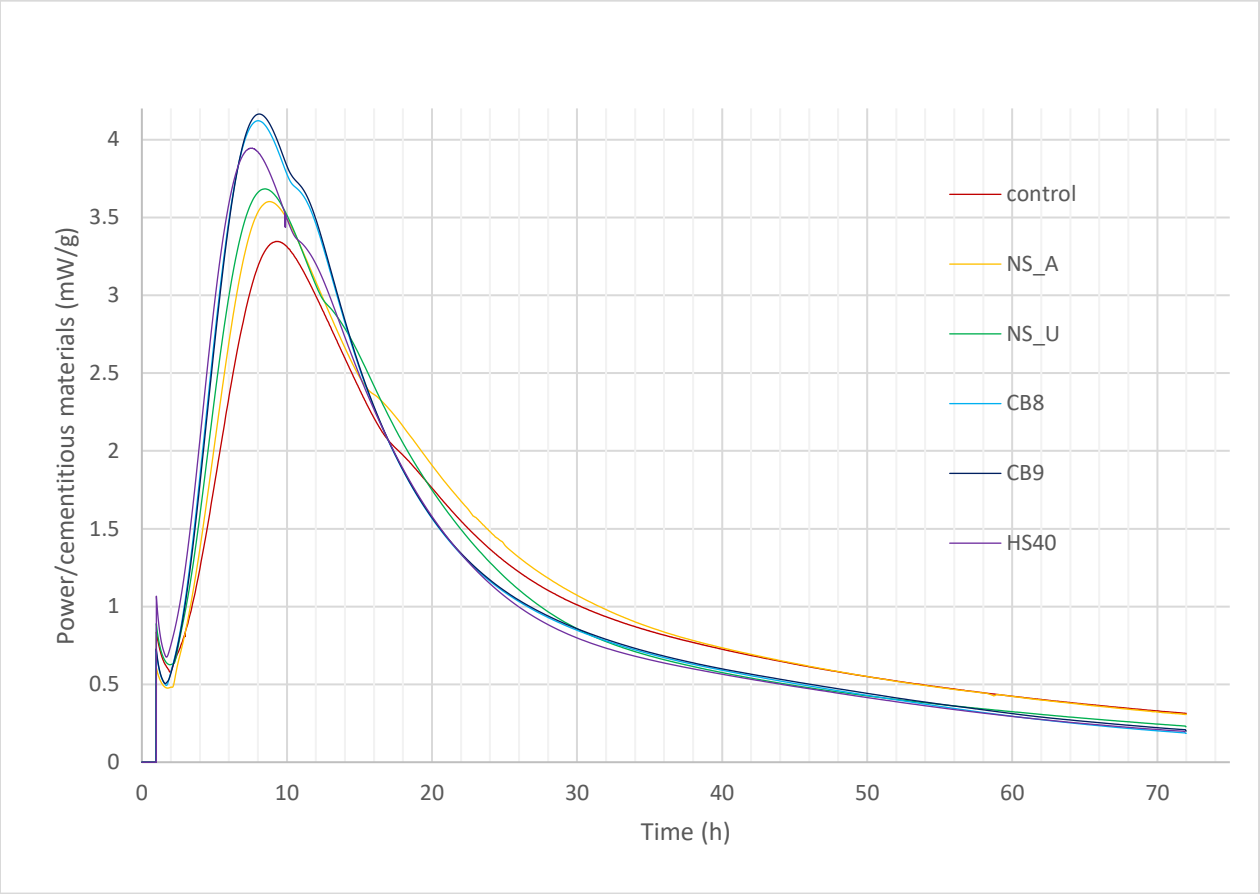


**Figure 5.4: Rate of hydration of 1% NS included pastes**

Figure 5.4 shows the rate of hydration of the cement pastes including 1% NS. Similar to the behavior of the cement pastes containing 4% NS, all the pastes containing 1% NS have more hydration than the control paste. However, the effect of colloidal silica (CS) is less than that of the pastes containing CB8 and CB9 which was the opposite when having 4% NS. If the deceleration period is considered, the NS_A containing paste still shows a higher hydration than the other pastes similar to the case of 4% NS association. This fact is visible in Figure 5.5 which shows the cumulative hydration of pastes containing 1% NS. It also shows that the paste containing NS_A shows the highest overall energy release during from 40 to 72 hours. The total hydration of the paste containing colloidal silica has become the least out of all the pastes similar to the behavior of the pastes including 4% NS.

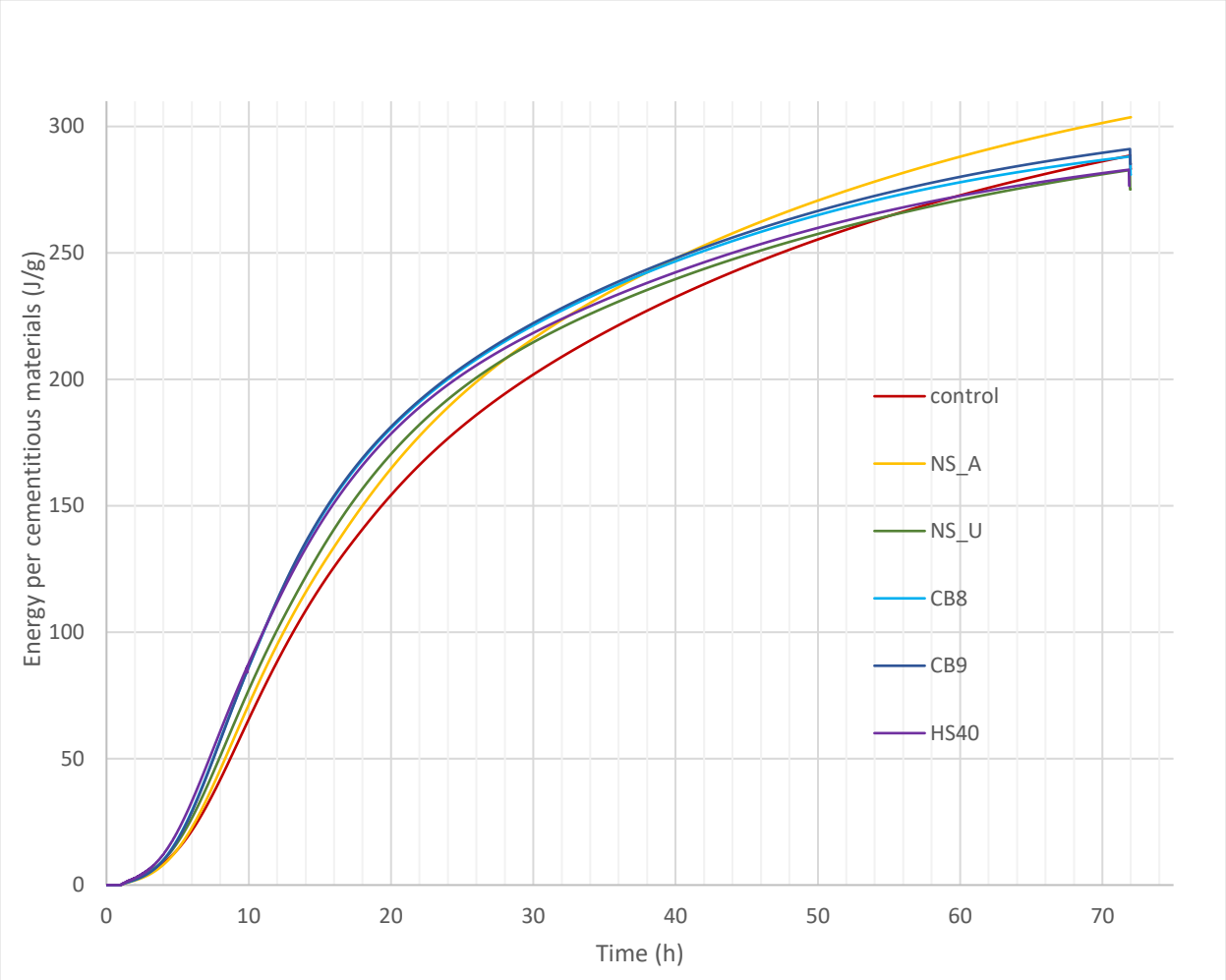


**Figure 5.5: Energy release over time for 1% NS included pastes**

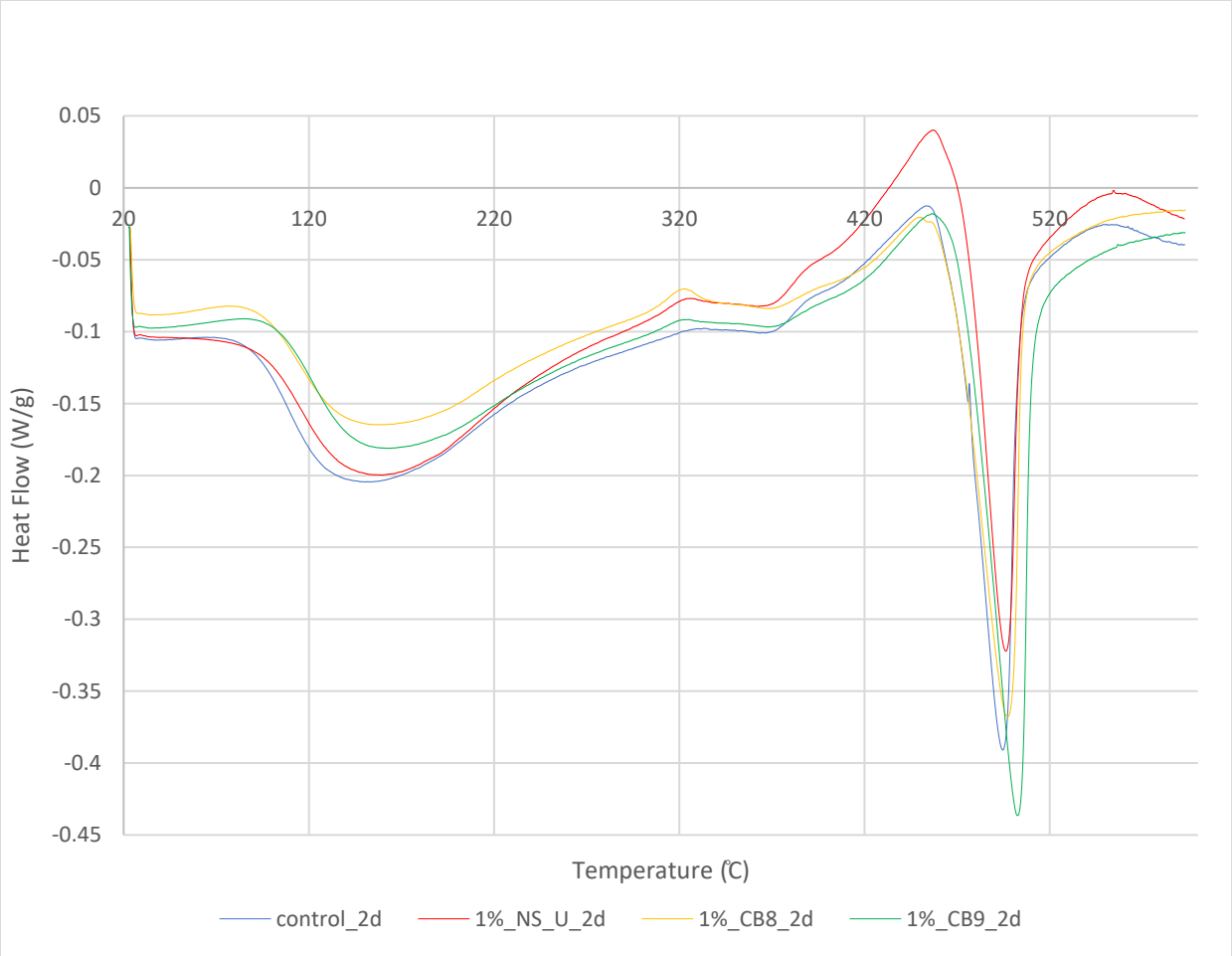


**Figure 5.6: Heat flow of 2 days cured 1% NS included pastes**

Figure 5.6 shows the heat flow variations of the pastes containing 1% NS upon heating. As described before, the endothermic peaks around 450℃ which are pertaining to the CH decomposition have become smaller with the NS addition. In the pastes that contained NS_U, the CH content was observed to be decreasing as the NS percentage increased up to 4% (Figure 4.19). In CB8 and CB9 pastes, this fact was visible by having a smaller peak than that of the control sample. However, if Figure 5.3 was considered, the peaks pertaining to the CH content of the pastes having 4% NS_U, CB8, and CB9 are showing to be comparably same in size, indicating a similar effect by 4% NS. In contrast to that, the size of the peaks (CH decomposition) which contained CB8 and CB9 are in between the size of the peak of the control sample and the 1% NS_U paste which has the lowest CH content out of the graphed curves in Figure 5.6. This implies that it is not only the percentage of NS content which affects the CH content of the hardened paste, but another property relevant to the type of NS. However, in terms of lessening the CH content which is found to not be an indication of less hydration in the results chapter, the cement pastes that contain 1% NS_U are better than pastes containing 1% CB8 and CB9 as it could result in more strength.

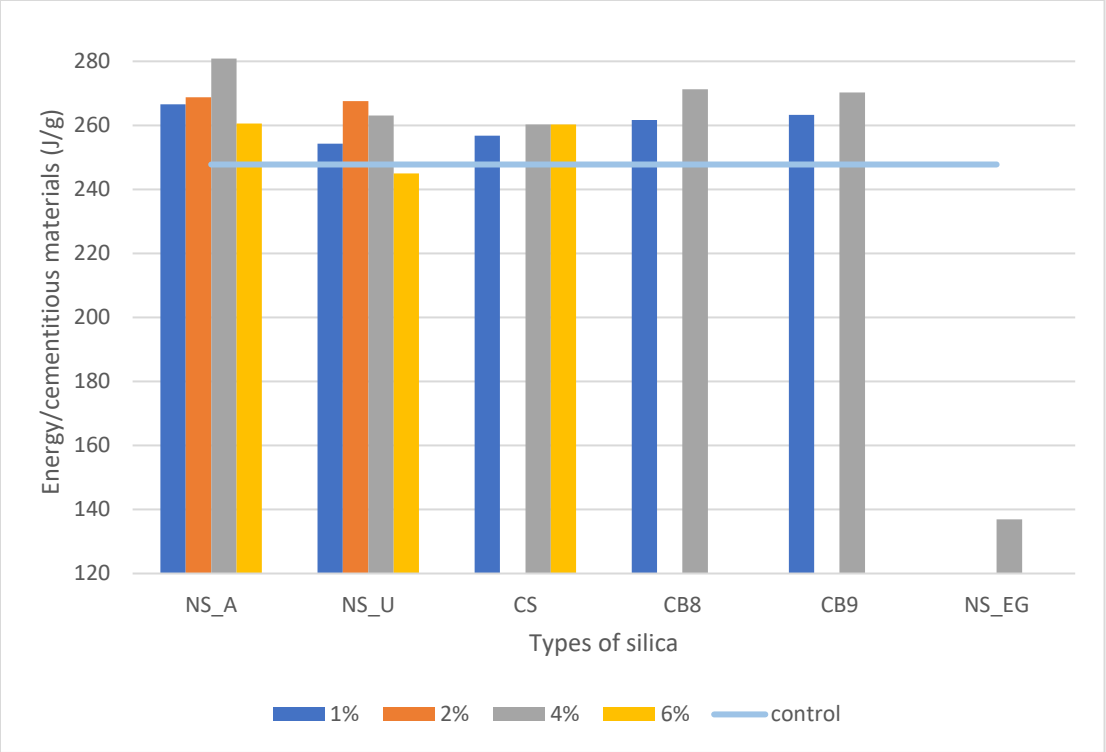


**Figure 5.7: Energy release after 2 days of cement paste**

Figure 5.7 shows the heat energy per cementitious material liberated from different types of cement pastes. Comparing all the pastes, the highest energy liberated are pertaining to the pastes that contain 4% NS. As more energy liberated is an indication of more hydration, it can be considered that this is the best out of the percentages which had been used in this study except NS_U. In the cement pastes with NS_U 2% and 4% show comparable hydration improvements while the 2% has a slightly more hydration than that of the 4%. For the laboratory synthesized NS, the energy seemed to be increasing up to a certain percentage of NS and then decreasing after that. This indicates the maximum NS percentage that could be used for the pastes is around 4%. For NS_A type NS, the best mixture tested is 4% NS; for NS_U type NS, the maximum energy output out of the tested samples is for 2% NS. However, from these two types, the 2 days energy is higher in the cement paste including NS_A type NS batch. Also, it can be noted that the least energy at two days in the NS_U type cement pastes, except for the 4% NS containing paste. Although the average particle size of NS_A is nearly an order of magnitude higher than NS_U, the pastes with the larger sized particles performed better amongst those laboratory synthesised. A similar effect was reported in the work of Haruehansapong et al. [19] where the compressive strength improvements were higher in the cement mortar with 40 nm NS than the mortar with 12 nm or 20 nm. The difference of energy of hydration in the cement paste with NS_A and NS_U could be a size effect similar to their study. In another study [116], also a reduction in effectiveness of CH consumption by NS in the cement paste with the decreasing NS particle size was reported which is similar to the hydration behavior of the cement pastes with NS_A and NS_U (which could be a result of the size effect).

When comparing the laboratory synthesized NS, with the commercial NS, the results of CB8 and CB9 lie between NS_U and NS_A at both 1% and 4% NS additions. CB8 type NS has a particle size range 3-100 nm and CB9 has a very narrow size distribution which is 45-47 nm as per the manufacturer's information. Despite the differences in particle size distribution, CB8 and CB9 have very small differences in energy release. However, regardless of their particle size, the pastes including 1% NS_A, CB8 and CB9 have comparably close energy liberation at two days.

The colloidal silica (HS40) inclusion in 1% has given more hydration than that of the NS_U inclusion. Yet, 4% colloidal silica inclusion has the lowest hydration among all the tested samples. 6% of HS40 inclusion has a similar hydration to that of the NS_A inclusion, but the observations while mixing the paste showed that incorporating colloidal silica had made the paste more viscous than the other pastes that had the same NS addition levels which could be due to the increased amount of surface silanols on the surfaces of silica particles. This was the same with the other NS addition levels where the cement replacements gave more viscous pastes than the other pastes.

**Table 5.2: Comparison of measurements related to the hydration**

| Paste designation | Total energy (J/g) | CH quantity by XRD (%) | CH quantity by TG (%) | CH quantity by DSC (%) | Strength (MPa) | Non-evaporable water content (%) |
|---|---|---|---|---|---|---|
| Control | 247.77 | 13.9 | 11.2 | 33.0 | 20.8 | 10.706 |
| 1%_NS_A | 266.61 | | 11.5 | | 15.0 | 10.850 |
| 2%_NS_A | 268.76 | | 10.7 | | 32.1 | 10.570 |
| 4%_NS_A | 280.88 | | 11.6 | | 26.5 | 11.850 |
| 6%_NS_A | 260.62 | | | | 53.1 | 10.533 |
| 1%_NS_U | 254.33 | 16.3 | | 24.3 | 26.1 | 13.140 |
| 2%_NS_U | 267.54 | 14.5 | | 18.5 | 27.9 | 14.225 |
| 4%_NS_U | 263.06 | 13.7 | | 18.8 | 27.8 | 13.890 |
| 6%_NS_U | 244.96 | 10.8 | | 33.7 | 26.4 | 14.170 |
| 7.2%_NS_U | 245.30 | | | | 27.8 | 12.751 |
| Commercial NS | | | | | | |
| 1%_HS 40 | 256.77 | | | | 25.4 | |
| 4%_HS 40 | 260.23 | | | | 26.0 | |
| 1% CB8 | 261.72 | | | 34.9 | | |
| 4% CB8 | 271.28 | | | 18.7 | | |
| 1% CB9 | 263.26 | | | 36.1 | | |
| 4% CB9 | 270.29 | 12.9 | | 25.1 | | |

Table 5.2 highlights the comparison of the cumulative energy released from the cement pastes with the quantitative measurements related to the hydration. Figure 5.8 illustrates the relationship of cumulative energy with the CH quantity measured by DSC for NS_U, CB8, and CB9 silica. The NS_U inclusion and CB8 and CB9 inclusion show linear relationships separately having coefficient of determinants 0.9432 and 0.9110, respectively. When the trend line for the NS_U inclusion is considered, it shows a good relationship indicating that the CH quantity of the

cement pastes decreases as the energy increases. The other trend line also shows a good relationship with a greater slope than that of the NS_U pastes. This indicates that the CH quantity of the pastes decreases as the energy increases. Though, the control sample did not fit into the relationship of the pastes with CB8 and CB9. The control sample, the pastes with 1% CB8 and 1% CB9 have comparable CH contents with slight differences (Table 5.2). So, it can be deduced that dominant factor of the energy increase of the pastes with 1% CB8 and CB9 is due to the nucleation seeding effect not the pozzolanic effect. Nevertheless, these silica types also show pozzolanic effects which can be seen by their CH quantity reduction as the energy increases (which is due to the increase of CB8 and CB9 content to 4%). By fitting the control sample into the relationship of the NS_U pastes, it suggests that both the pozzolanic action and seeding effect are present in the pastes with NS_U.

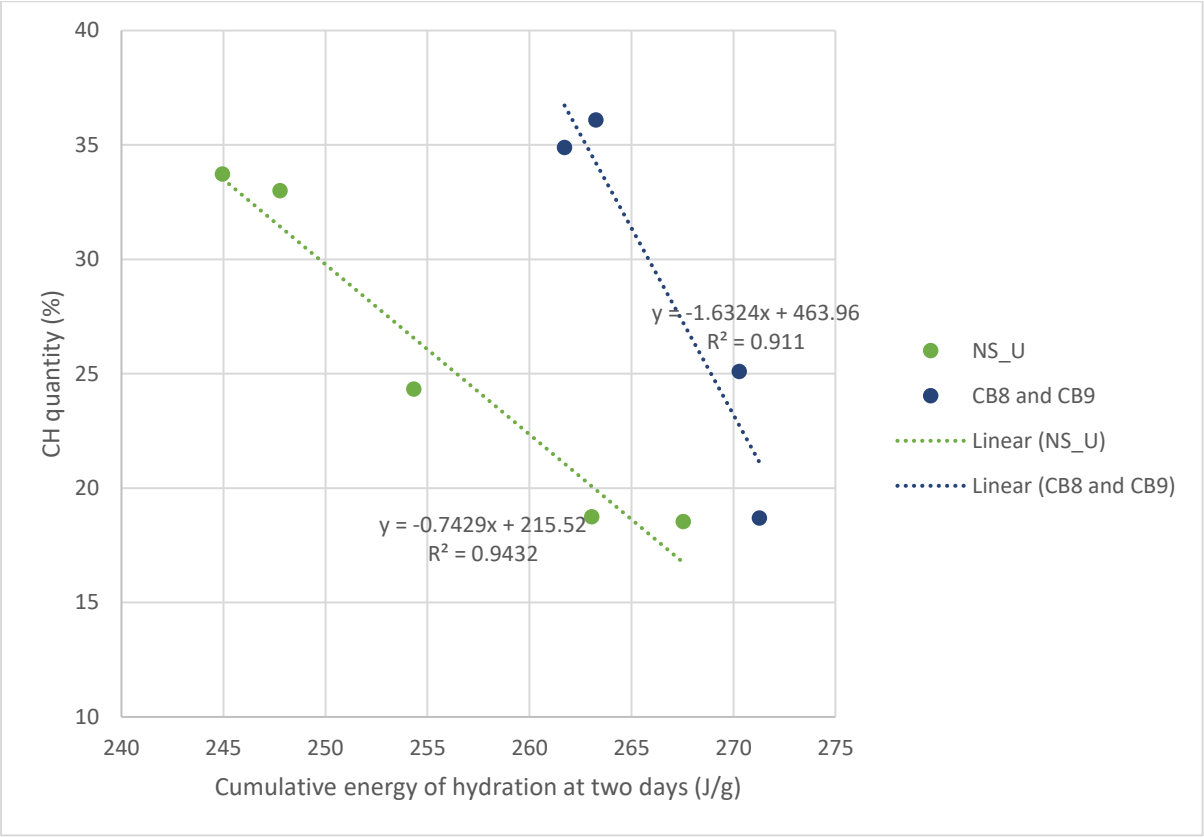


**Figure 5.8: Correlation of the hydration energy at two days with the CH quantity measured by DSC**

Even though, the CH quantity measurements by DSC correlates with the energy, the other measurements show poor correlation in between. This could be due to the sensitivity of the techniques used.

## Effect of NS on Microstructure

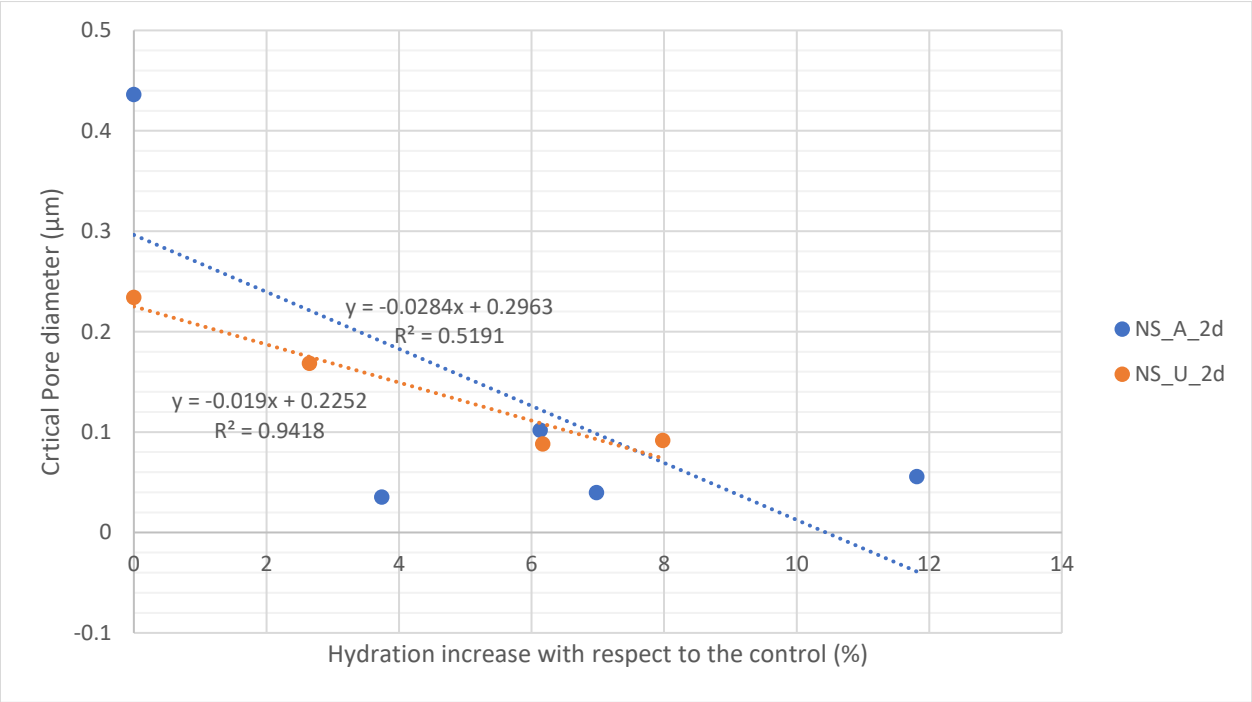


**Figure 5.9: Increase of hydration vs. critical pore diameter of the cement pastes**

Figure 5.9 shows the relationship of the increase in hydration of pastes compared to the control sample at two days and the critical pore diameters of the pastes. Therefore, the hydration increase of the control samples are set at 0. The trend implies that the critical pore diameter of the NS_A pastes decreases as the hydration at two days increases with a linear relationship with a coefficient of determinant of 0.5191. Also, this relationship suggests that regardless of the NS quantity, which was varied, the critical pore diameter can be improved if the two days hydration can be improved. Similar trends of pore diameter improvements with hydration increases were observed by the other researchers [102,117]. Furthermore, one of the researchers mentioned that the critical pore size of hardened cement paste would reach a minimum around 0.025 µm once the hydration of the paste is finished and it is independent of the water/cement ratio of the paste [102]. Also, the pores having sizes below 0.025 µm do not contribute to the permeability of the cement pastes [103]. Two data points of the graph presented here have also reached up to a similar critical pore size and one of these reached this value by two days. These points represent the pastes that had been incorporated with NS and this fact indicates that by using NS, it is possible to reach the possible minimum critical pore size very early such as in two days.

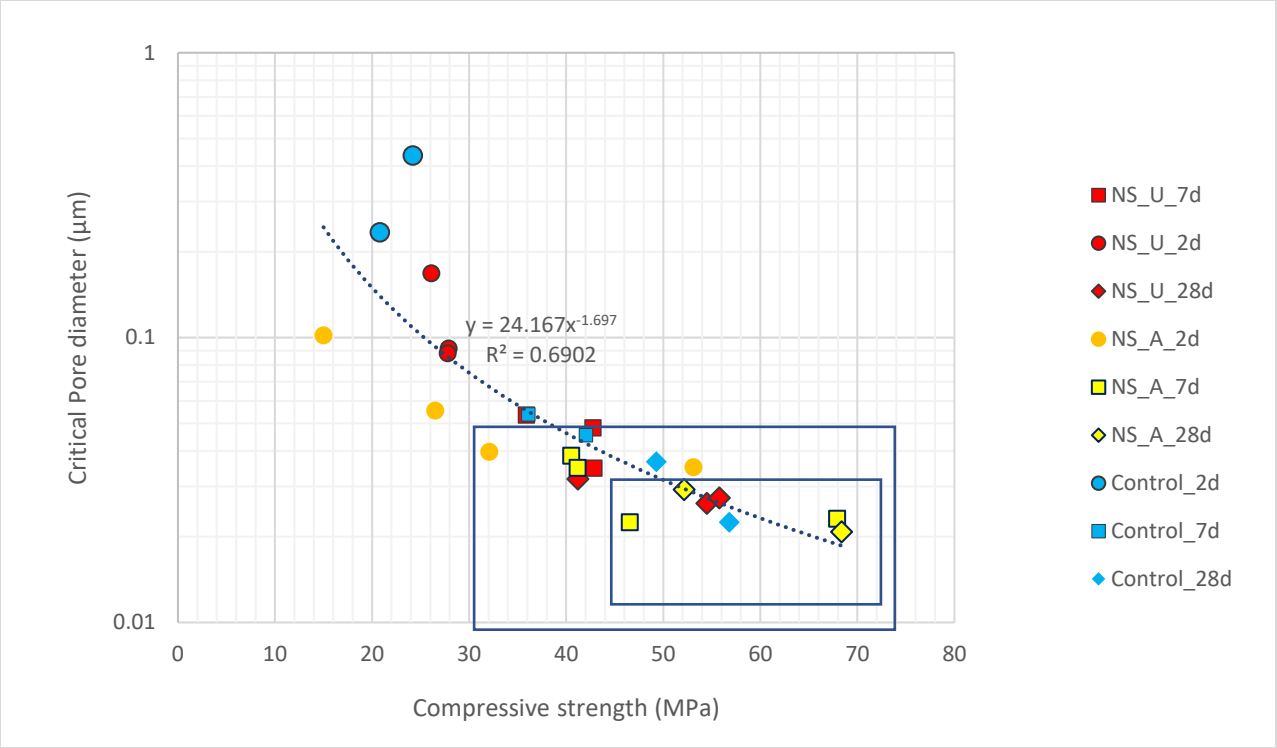


**Figure 5.10: Compressive strength vs. critical pore diameter of the cement pastes**

Figure 5.10 shows the relationship of the critical pore diameter of the cement pastes with the compressive strength of the pastes. The critical pore diameter of the pastes decreases as the compressive strength of the pastes increases. The data can be fitted to a power trendline which has a coefficient of determinant of 0.6902. All the critical pore diameters of the 28 days cured pastes are below 0.04 µm while showing compressive strengths of more than 40 MPa. Both the lowest compressive strength values and the highest critical pore diameter values belong to control samples and samples including 1% NS that had been cured for two days. This indicates that the inclusion of more than 1% of NS_A and NS_U type of NS is beneficial in improving the compressive strength and the pore structure of the pastes.

The data points inside the larger rectangle belong to the pastes that have compressive strengths of more than 30 MPa and the critical pore diameters below 0.5 µm. Most of the points lying in the rectangle are attributable to the pastes that had been cured for 7 days or more. However, there are some points which were from the pastes that had been cured for 2 days and with NS. This again shows that the 2 days cured, and NS included pastes achieved the pore structure and the strength of the 7 days cured control sample by having NS in them. Data from the 28 days cured control sample and data of the pastes including NS that were 7 and 2 days cured are both located inside the small rectangle shown in Figure 5.10. These points are from the pastes that have the compressive strength of more than 42 MPa and the critical pore diameter of less than 0.4 µm.

According to Canut [118], the effect of gel pores which are below 0.04 µm on both permeability and strength is zero or very minimal. Having higher porosity while having lower critical pore diameter indicates that most of the pores of the cement paste are in a range closer to

the critical pore diameter. So, having low critical pore diameter makes the cement paste less permeable and of high strength. Also, this kind of relationship was observed for cement paste by Ma et al. [119] where the relationship was built for the porosity instead of the pore diameter. Yu et al. [120] explained that less porosity usually results in less permeability, but it does not imply that high porosity would always result in higher permeability. The important factor that affects the transport properties of the cement paste is the critical pore size which determines the ingress of water into the pore structure.

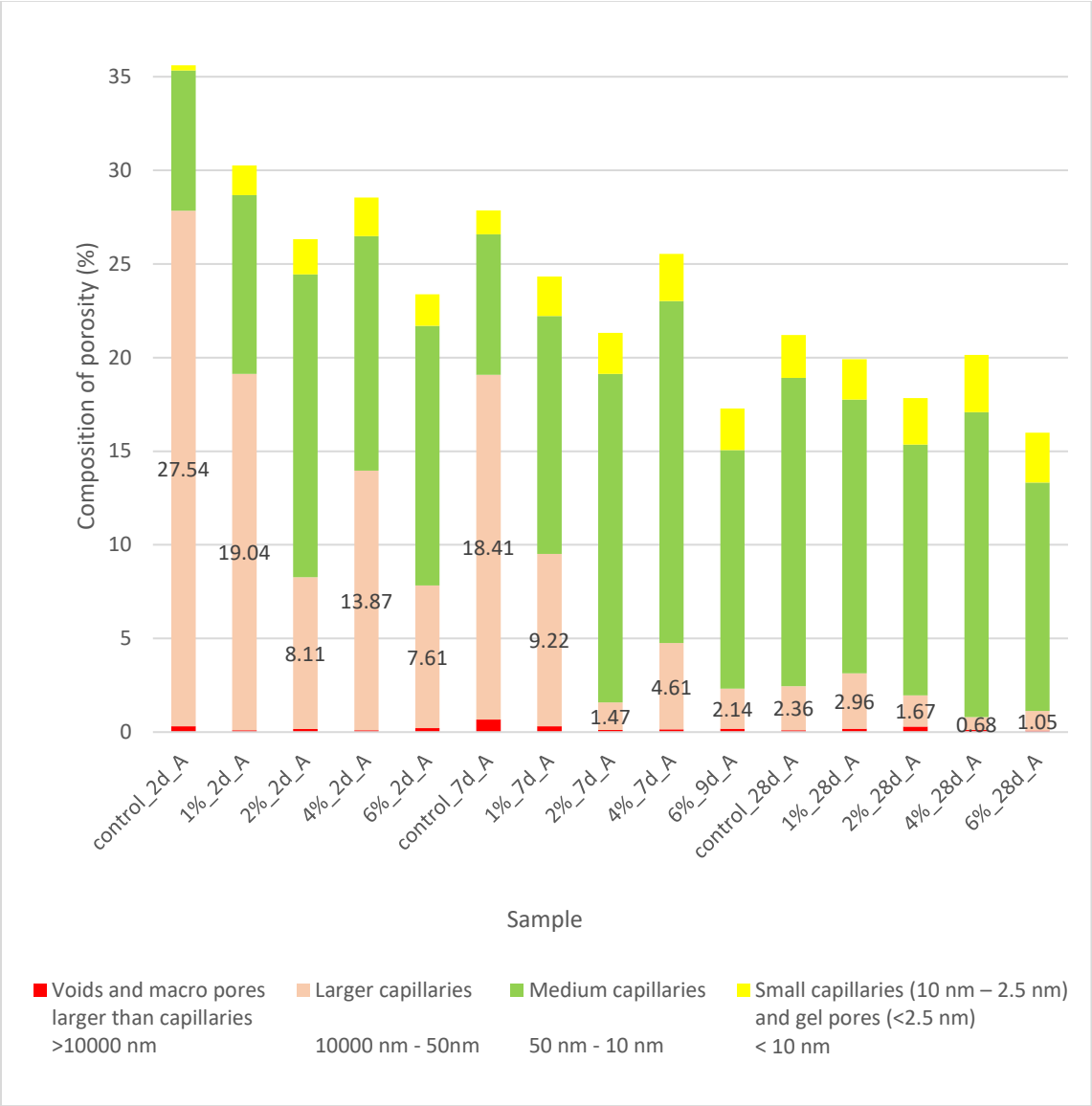


**Figure 5.11: Composition of porosity of cement pastes including NS_A**

Figure 5.11 gives the composition of porosity of cements including NS_A. The porosity of the cement pastes that included NS_A type NS classified according the size ranges namely, voids + macropores larger than capillary pores, large capillaries, medium capillaries and small capillaries + gel pores. From the data obtained, it is apparent that the total porosity of the cement paste

decreases as the curing time increases. As well, it revealed that the porosity composition from medium capillaries, small capillaries and the gel pores increases while the porosity composition from the larger capillaries decreases as the curing time of the cement paste increases. This suggests that larger capillaries are converted into smaller size capillaries or gel pores by hydration during the time of curing.

When considering the cement pastes including NS_A, this process of converting larger capillaries to smaller sized pores seemed to have taken place earlier than that of the control pastes. When considering 2 days cured samples, the expedition of this process is much more visible. The two days cured control sample has a 27.54% porosity from large capillaries, 7.48% porosity from medium capillaries, and 0.28% porosity from small capillaries and gel pores. When NS has been included from 1% to 6%, the porosity from the large capillaries has dropped to 19.04% and further dropped until 7.61% with increasing NS amounts. At the same time, the medium capillaries composition has increased with the NS amount while reducing the total porosity. This process is also visible in critical pore diameter values which have been shifted from the larger capillaries range to the medium capillaries range as the NS amount increases. After taking 7 days cured specimens into account, the same decrease of the porosity composition from the large capillaries while increasing the medium capillaries composition is still noticeable as the NS amount increases in the paste. The porosity of the 7 days cured 2% NS included cement paste shows almost a similar porosity composition of the 28 days cured control sample from large capillaries and medium sized capillaries while the 7 days cured 4% and 6% NS included pastes also show a close porosity composition to that of the 28 days cured control sample. So, the pore structure refinements and more hydration can be possible incorporating this type of NS. These results match with the work of other researchers [121] where they had utilized 0.3% and 0.9% NS in concrete.

Also, some researchers have investigated and characterized the effects of the size of agglomerates of NS on the cement/mortar [68]. In their study, they stated that the agglomerates could be in the size of more than 1 μm by the particle size analysis [68]. If such agglomerates are present in the cement pastes tested in this research, the resulting pores and the voids due to the agglomerates should be visible in the pore size classification plotted in Figure 5.11 in the pastes at later ages. However, such porosity at later ages are not visible indicating that the sol-gel suspensions benefit the cement paste. Also, this study hints about the permeability characteristics of the pastes including NS.

Figure 5.12 presents the porosity classification according to the sizes of the cement pastes that included NS_U type NS. For this batch, the earlier formation of medium capillaries is not observable in 2 days cured specimens with increasing NS. However, the critical pore diameter has slightly decreased with increasing NS amounts in the paste (Table 4.7). However, the 7 days cured specimens exhibit more medium capillaries while having fewer large capillaries with the increasing NS amount in the cement paste. The SEM images (Figure 5.13) of the NS_U type NS included cement pastes also confirms the pore structure variation with NS inclusion. In the 28 days cured cement paste specimens, the more NS containing pastes (2% and 4%) have more porosity from the medium capillaries than that of the control sample and the sample containing 1%_NS.

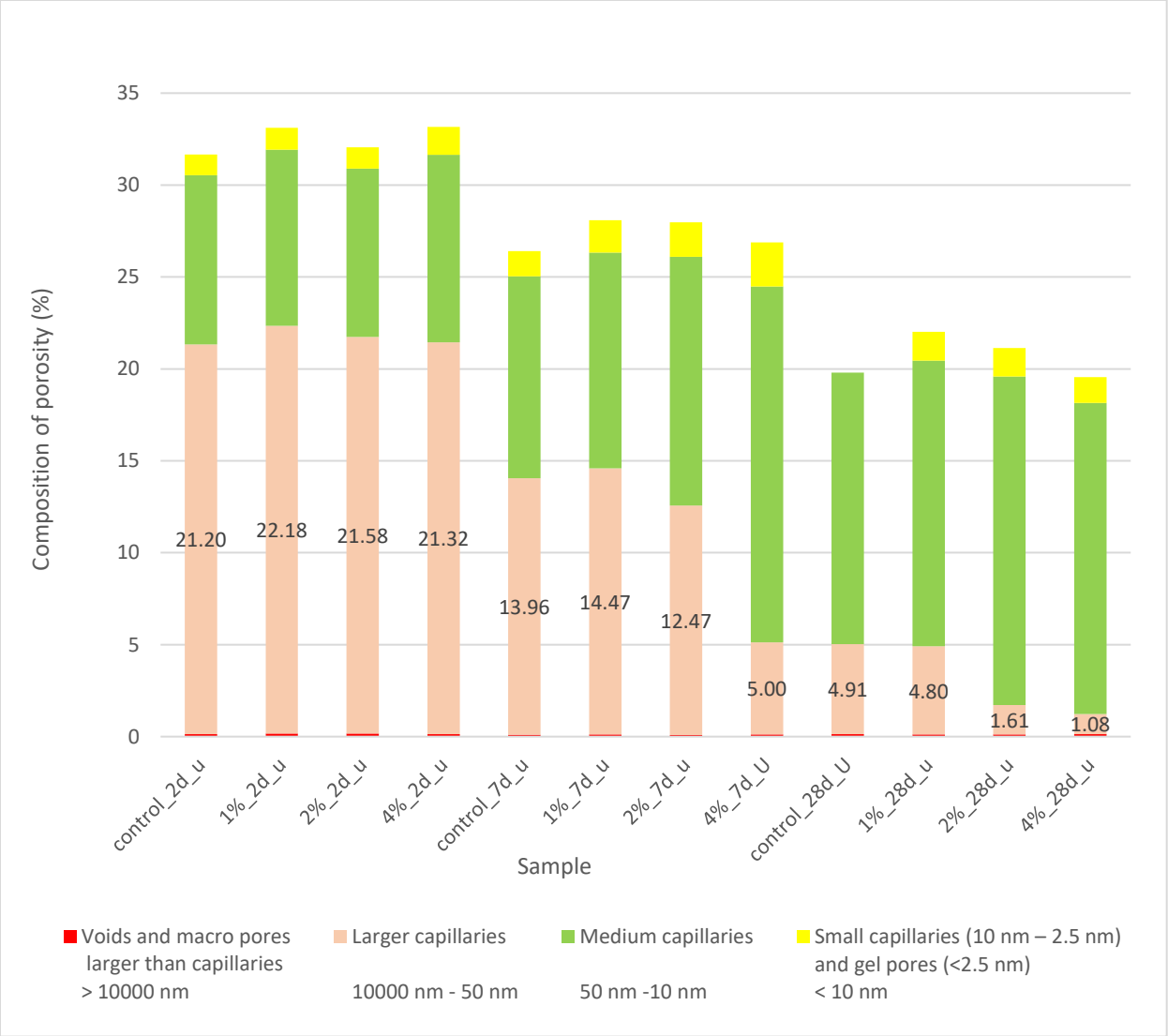


**Figure 5.12: Composition of porosity of cement pastes including NS_U**

Image (a) of **Error! Reference source not found.** is a 1000x magnified image of the 7 days cured control cement which has a total porosity of 26.41%, 13.96% from large capillaries, and 10.99% form medium capillaries. Image (c) of **Error! Reference source not found.** is a 2000x magnified image of the same sample. Images (b) and (c) of **Error! Reference source not found.** are respectively the 1000x and 2000x magnified images of the 7 days cured cement paste including 4% NS_U type NS. This sample has 26.88% total porosity, 5.00% porosity from large capillaries, and 19.36% porosity form medium capillaries. Both samples have almost the same total porosity. The images (a) and (c) of **Error! Reference source not found.** show more visible porosity which could possibly be from the large capillaries than that of the images (b) and (d) of **Error! Reference source not found.** which has more porosity from the medium capillaries (50 nm – 10 nm) and not visible at the magnification used in the images. So, images (b) and (d) show denser structures than the other two. This also shows more hydration achieved by associating NS in cement paste.

| Control_7d | 4%_NS_U_7d |
| --- | --- |
| 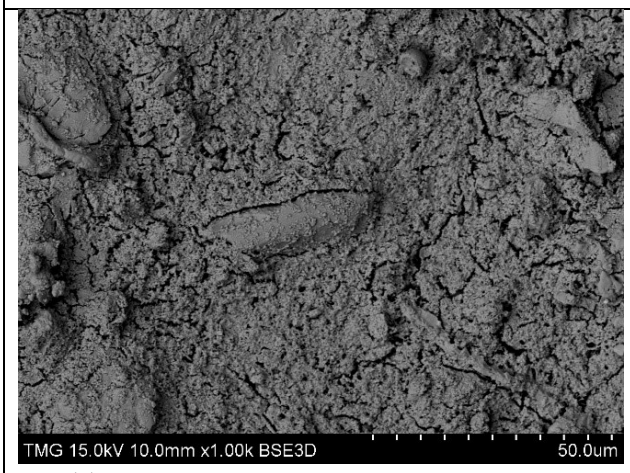  (a) x1000 | 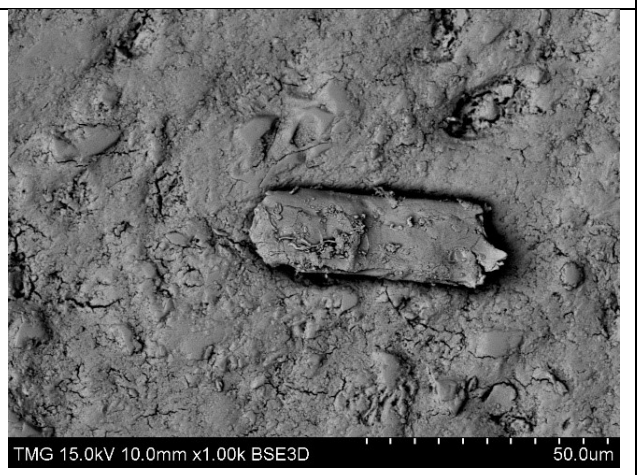  (b) x1000 |
| 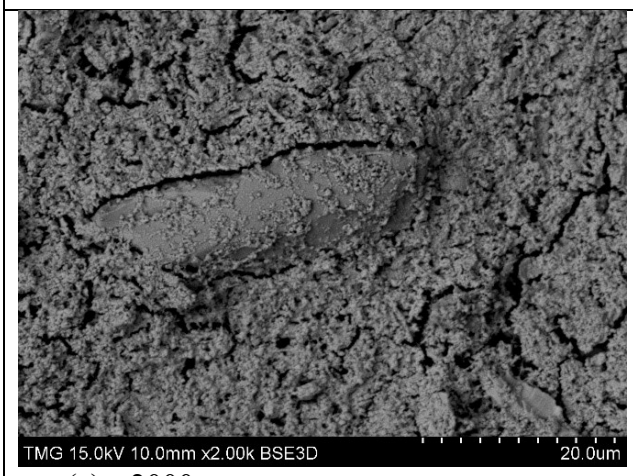  (c) x2000 | 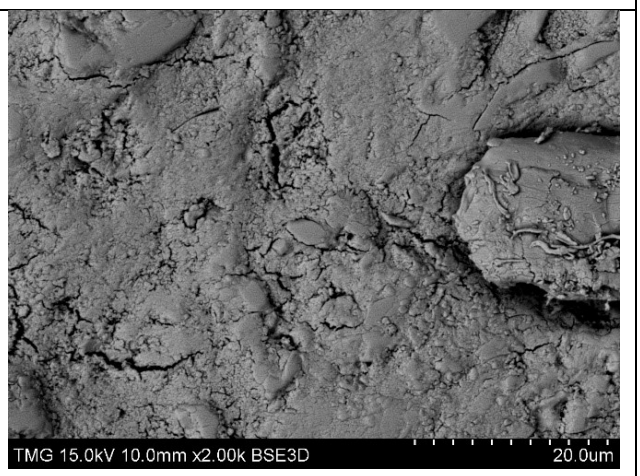  (d) x2000 |

**Figure 5.13: BSE images of control cement paste and NS_U included cement paste**

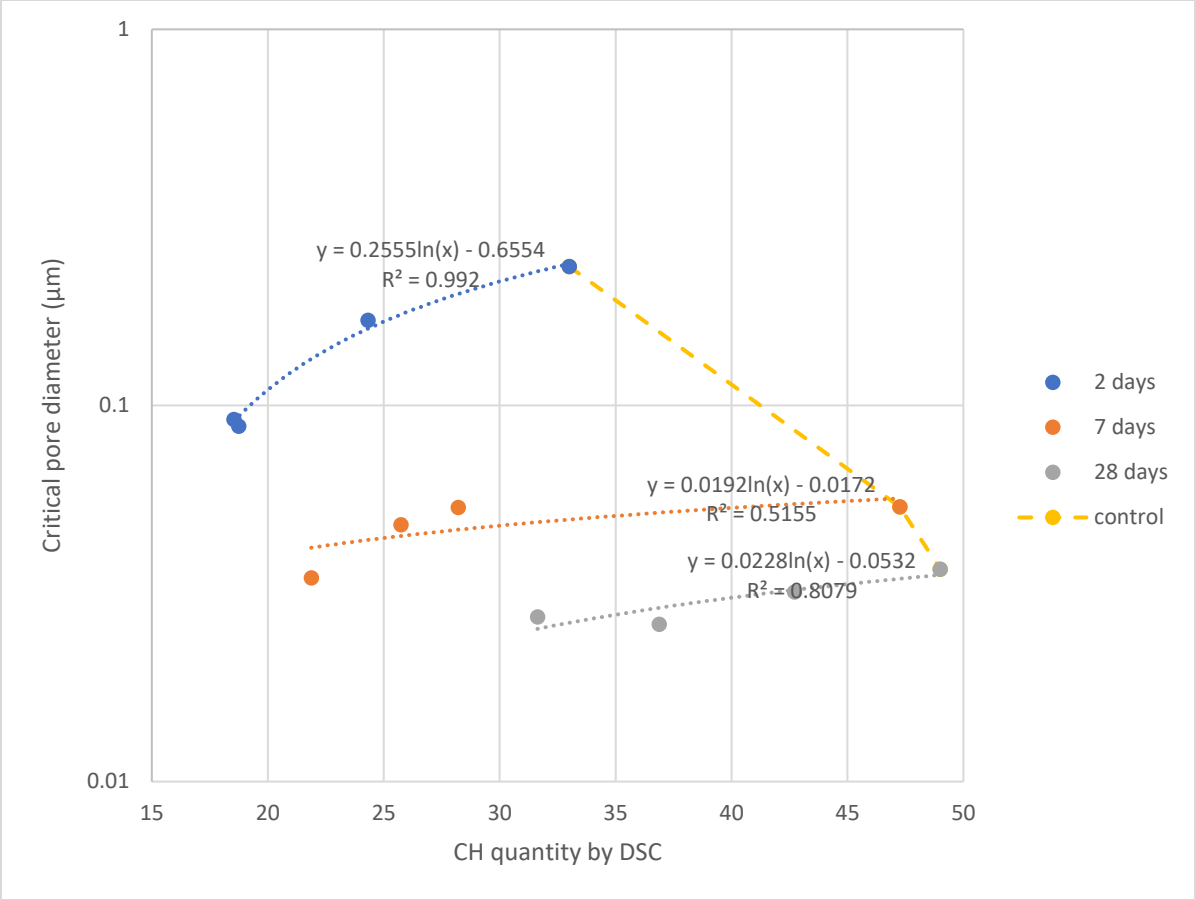


**Figure 5.14: The relationship of CH quantity and the critical pore diameter of NS_U included cement pastes**

Figure 5.14 shows the relationship of the critical pore diameter with CH quantity measured by DSC. The CH quantity at different curing levels are plotted and the curves have moved downward and to the right when the curing time was increasing. The figure also shows that by incorporating the NS_U type NS in the pastes both the CH quantity and the critical pore diameter could be decreased by comparing with the curve for the control pastes which is shifted to the right at the edges of each curves.

The curves which are for different curing times show good logarithmic relationships of their pore sizes with their CH quantity measured by DSC, having 0.99, 0.52, and 0.81 of coefficient of determinants for 2 days, 7 days, and 28 days curves, respectively. The whole figure hints that the curve for the relationship of the critical pore diameter with the CH quantity could become flat as the curing time increases since the curves slant towards a horizontal line with increasing curing time. As having a lower CH percentage implies more strength of the paste, the curves shifting towards the left is beneficial. Thus, having NS in the pastes is beneficial. Also, shifting of curves towards lower critical pore sizes is beneficial.

## Overall Comparison of Results

**Table 5.3: Comparison of 2 days results**

| Mix **5.4.** | Calorimetry (J/g) | CH quantity by TG (%) | CH quantity by XRD (%) | CH quantity by DSC (%) | Non evaporable water content (%) | Critical Pore diameter (μm) | Compressive strength (MPa) |
|---|---|---|---|---|---|---|---|
| Control | 247.77 | 11.24 | 13.9 | 33.0 | 10.706 | 0.234 | 20.8 |
| 1%_NS_A | 266.61 | 11.46 | | | 10.850 | 0.102 | 15.0 |
| 2%_NS_A | 268.76 | 10.74 | | | 10.570 | 0.040 | 32.1 |
| 4%_NS_A | **280.88** | 11.61 | | | 11.850 | 0.056 | 26.5 |
| 6%_NS_A | 260.62 | | | | 10.533 | **0.035** | **53.1** |
| 8%_NS_A | | **10.38** | | | | | |
| 1%_NS_U | 254.33 | | 16.3 | 24.3 | 13.140 | 0.168 | 26.1 |
| 2%_NS_U | 267.54 | | 14.5 | **18.5** | **14.225** | 0.092 | 27.9 |
| 4%_NS_U | 263.06 | | 13.7 | 18.8 | 13.890 | 0.088 | 27.8 |
| 6%_NS_U | 244.96 | | **10.8** | 33.7 | 14.170 | | 26.4 |
| 7.2%_NS_U | 245.30 | | | | 12.751 | | 27.8 |
| 4% NS_EG | 136.97 | | | | | | |
| Commercial NS | | | | | | | |
| 1%_HS 40 | 256.77 | | | | | | 27.3 |
| 2%_HS 40 | | | | | | | 23.3 |
| 4%_HS 40 | 260.23 | | | | | | |
| 6%_HS 40 | 260.27 | | | | | | |
| 1% CB8 | 261.72 | | | 34.9 | | | |
| 4% CB8 | **271.28** | | | **18.7** | | | |
| 1% CB9 | 263.26 | | | 36.1 | | | |
| 4% CB9 | 270.29 | | 12.9 | 25.1 | | | |

Table 5.3 shows the overall two days results of the study. The overall results show that NS_A have the highest cumulative energy measured by the calorimetry, the lowest critical pore size diameter, and the highest compressive strength in two days. The highest non-evaporable water content indicating the most hydrated sample belongs to the cement paste batch with NS_A. When considering the CH content which is dependent on the measurement technique used, both types of NS show pozzolanic activities. As most of the improvements are higher in the cement pastes with NS_A, it can be considered that NS_A is the best out of the laboratory synthesized NS. Considering the commercial NS, CB8 shows the best hydration (cumulative energy) and the best pozzolanic activity. However, the cumulative two days energy released by the paste with CB8 is lower than

that of NS_A. The CH content is comparable with the best of NS_U. This also suggests that NS_A is better in terms of hydration than the best commercial NS tested.

# Chapter 6. Conclusions, contributions, and future research directions

In this chapter the conclusions inferred by this study, the future insights and the contributions are presented.

## 6.1. Conclusions

During the NS synthesis process, the following conclusions were made. The NS formed by this method was discovered to be mainly amorphous with some crystallinity. The crystalline phase of the silica was identified as tridymite. The ratio of TEOS to nitric acid to obtain a good silica composition was found to be 1.95 mL/0.2 mL and the stabilization step was eliminated as it was not useful. The particle size of the NS could be further reduced by ultrasonication during the condensation step of the sol-gel method. Ethylene glycol combined with ultrasonication did not affect the particle size formed.

From associating the silica in cement pastes, the following facts were identified. The ammonium hydroxide in the silica suspensions had detrimental delaying effects on the setting time. Also, with the toxic odor of the ammonium hydroxide, it is impractical to use concrete mixes, and therefore it is necessary to remove it from the suspension. Calcium hydroxide was found to be a good candidate to replace ammonium hydroxide as it could provide the pH which is favourable for both silica particles and the cement paste, and because calcium hydroxide is not harmful for cement pastes. The stability of silica particles in the calcium hydroxide suspension was good, having acceptable zeta potentials on the silica particles. Moreover, changing the suspension media of the NS did not affect the particle size of NS.

Associating NS as a suspension rather than using them as powder was found to be beneficial in improving the setting time. This research implies that the association of NS as suspensions of calcium hydroxide improves the dispersion of NS throughout the hardened cement paste by the particle size distribution of the suspensions. However, it is doubtful about the level of agglomeration of the highly concentrated suspensions in which agglomeration is possible even though they may still be beneficial in terms of early hydration and the strength compared to the cement pastes without NS. Therefore, it is important to limit concentrations to amounts where property improvement can be observed without agglomeration.

The calorimetric studies revealed that incorporating NS increases the rate of hydration of the cement paste during the first 10 hours as the NS content increases up to 7.2%. However, as it continues, the rate of hydration decreases in the cement pastes that have 6% NS or more. The commercial NS has higher rates of hydration (7.5% higher power peak compared to that of NS_A at the maximum level) than the laboratory synthesized NS, but when the total hydration is considered, NS_A type NS has the better performance in terms of the total hydration during the first 2 days (3.4% energy increase compared to the commercial NS) and 3 days (5.6% energy increase compared to the commercial NS). Out of all the percentages tested, 4% NS addition had the best rate of hydration and the total hydration. However, more work is required to confirm this further. Even though the early hydration was visible in all NS included cement pastes, the cumulative heat liberated at 3 days did not increase in all the pastes indicating that some NS types have provided seeds only for improving the rate of reaction and therefore the replacement of cement with them is not as beneficial. The non-evaporable water content measurements also

confirm the early hydration improvements of the cement paste by NS incorporation. Moreover, this test provided evidence about the extent of hydration at 7 days and 28 days and confirmed that it is also beneficial for up to 28 days.

It is clear that the incorporation of NS decreases CH in the hardened cement paste which was inferred from the utilization of NS_U, CB8, and CB9 types of NS. The reduction of CH was not a result of reduced hydration which was confirmed by the calorimetric studies. This CH reduction due to the NS incorporation can be concluded as the actions of NS like nucleation seeds and the consumption of formed CH by the NS to form CSH. The increase in the strength of the cement paste with NS addition also proves this fact.

The critical pore diameter of the cement paste reduces as the amount of NS in the cement paste increases. Furthermore, the study reveals that the composition of the medium sized capillaries increases as the hydration continues and having NS increases this composition while dropping the composition of large sized capillaries compared to the control paste. This behavior is more significant as the NS amount increases up to 4%. The comparison of the SEM images of the pastes including 4% NS and the control pastes also confirmed the pore structure refinement by NS addition. The cement paste including NS_A could achieve a pore structure similar to 28 days hydrated cement paste in two days. Also, out of the two types of laboratory synthesized NS, NS_A was shown to impart a better microstructure to the cement paste than NS_U type.

The strength of the cement paste was shown to be improved by incorporating NS as suspensions. As the amount of NS increases, the strength increases in the cement paste within the range of the percentages of associated NS. In terms of the strength of the cement paste, replacing cement by 6% and 7.2% by NS_U has given strengths exceeding that of the 28 days cured normal cement pastes in just 7 days. So, considering the strength of the cement paste, early strengthening of the cement paste could be seen by using NS.

## 6.2. Contributions

The following main contributions were made within this research.

1. One of the prevailing disadvantages of the NS is the agglomeration, which can be minimized by using the NS suspensions synthesized in a similar way to what was done in this research.
    a. It was found out that the particle size of NS could be reduced by assisting ultrasonication during the condensation step of the sol-gel method.
    b. It was found out that ammonium hydroxide should be removed from the NS suspensions in order to utilize them in cement pastes as it could delay the hydration process.
    c. Calcium hydroxide was found to be a good candidate as the suspension media for NS for utilization in cement paste.
    d. In much of the published literature, NS particles are synthesized and used in various forms which adds processing steps. In this research, the rinsing step with calcium hydroxide proved beneficial from a processing standpoint, a delivery mechanism and improvement of early and hardened properties. The NS suspensions produced in this research was well-dispersed throughout the paste which was confirmed by the pore structure and microstructural analysis of the cement paste.

e. The NS suspensions synthesized in this research were found to improve the strength of the cement paste by reducing the CH content of the paste and improving the microstructure. Also, early hydration is possible with replacing cement by NS.
f. The critical pore size diameter which could indicate that the desired durability of the cement paste could be achieved earlier than usual by using the NS suspensions produced in this research.
g. The NS suspensions synthesized rivaled the results of three commercial NS products.

## 6.3 Future research directions

The following insights were identified as possible modifications to the suspensions produced in this study, in order to improve dispersion and the stability of the particles in the suspensions. As the concentrated NS suspensions tend to settle, an association of surfactants in the suspensions produced by this method will make them more useful in the construction industry. Also, instead of the centrifugation step which was used in this research to separate NS particles and to remove ammonium hydroxide, other nanoparticle separation methods could be investigated. During this step, the particles tend to coagulate which makes ultrasonication necessary in the process of producing the suspension. Freeze drying techniques could also be used to separate the NS from ammonium hydroxide media as reviewed by Rahman et al. [22]. According them, drying NS with the presence of water plays a critical role in the formation of agglomeration which was however avoided in this research. Moreover, other possible suspension media that could offer both stability and non-harmful effects on the cement paste could be investigated to suspend the NS particles synthesized by this method.

As association of NS increases the heat of hydration and improves the gel pore structure in the very early stage of hydration such as 2 days, the shrinkage of the pastes which could impart adverse effects on the cement pastes should be further studied. Also, because the formation of micro cracks is possible in the cement pastes due to the increased hydration at the early stage, the flexural strength of NS associated cement paste should be studied as well.

For some types of NS, it should be investigated whether the addition of NS or the replacement of cement with NS is suitable considering all the properties affected by NS. Association of NS beyond 4% should be further investigated as some properties of the cement paste could be improved while some may not. However, the early strength as well as the strength after 28 days of the cement paste were increased more by the 6% and 7.2% NS inclusion than by 4% NS inclusion. This indicates the possibility of utilizing NS beyond 4%.

The NS synthesized by this method has already shown beneficial effects on the cement paste, and the synthesizing process is simple due to the ambient conditions used. Therefore, if the suspensions are investigated with concrete, it would be very advantageous to bring down the cement usage. As such, the synthesizing NS in bulk and their association in concrete is necessary. Furthermore, how the reactions of the NS synthesized by this method occur with the aggregates and the steel must be investigated prior to utilizing them in concrete.

# References


[1] L.P. Singh, S.R. Karade, S.K. Bhattacharyya, M.M. Yousuf, S. Ahalawat, Beneficial role of nanosilica in cement based materials – A review, Construction and Building Materials. 47 (2013) 1069–1077. https://doi.org/10.1016/j.conbuildmat.2013.05.052.

[2] P.K. Mehta, H. Meryman, Tools for reducing carbon emissions due to cement consumption, Structure. 1 (2009) 11–15.

[3] F. Sanchez, K. Sobolev, Nanotechnology in concrete – A review, Construction and Building Materials. 24 (2010) 2060–2071. https://doi.org/10.1016/j.conbuildmat.2010.03.014.

[4] T. Sato, J.J. Beaudoin, Effect of nano-$CaCO_3$ on hydration of cement containing supplementary cementitious materials, Advances in Cement Research. 23 (2011) 33–43. https://doi.org/10.1680/adcr.9.00016.

[5] J. Chen, S. Kou, C. Poon, Hydration and properties of nano-$TiO_2$ blended cement composites, Cement and Concrete Composites. 34 (2012) 642–649. https://doi.org/10.1016/j.cemconcomp.2012.02.009.

[6] G. Land, D. Stephan, Controlling cement hydration with nanoparticles, Cement and Concrete Composites. 57 (2015) 64–67. https://doi.org/10.1016/j.cemconcomp.2014.12.003.

[7] C. Sauter, M.A. Emin, H.P. Schuchmann, S. Tavman, Influence of hydrostatic pressure and sound amplitude on the ultrasound induced dispersion and de-agglomeration of nanoparticles, Ultrasonics Sonochemistry. 15 (2008) 517–523. https://doi.org/10.1016/j.ultsonch.2007.08.010.

[8] J. Vera-Agullo, V. Chozas-Ligero, D. Portillo-Rico, M.J. García-Casas, A. Gutiérrez-Martínez, J.M. Mieres-Royo, J. Grávalos-Moreno, Mortar and concrete reinforced with nanomaterials, in: Nanotechnology in Construction 3, Springer, 2009: pp. 383–388.

[9] G. Quercia, H.J.H. Brouwers, Application of nano-silica (nS) in concrete mixtures, in: 8th Fib International Ph. D. Symposium in Civil Engineering. Lyngby, 2010: pp. 431–436.

[10] A. Naji Givi, S. Abdul Rashid, F.N.A. Aziz, M.A.M. Salleh, Experimental investigation of the size effects of SiO2 nano-particles on the mechanical properties of binary blended concrete, Composites Part B: Engineering. 41 (2010) 673–677. https://doi.org/10.1016/j.compositesb.2010.08.003.

[11] E. Ghafari, H. Costa, E. Júlio, A. Portugal, L. Durães, The effect of nanosilica addition on flowability, strength and transport properties of ultra high performance concrete, Materials & Design. 59 (2014) 1–9. https://doi.org/10.1016/j.matdes.2014.02.051.

[12] R. Yu, P. Spiesz, H.J.H. Brouwers, Effect of nano-silica on the hydration and microstructure development of Ultra-High Performance Concrete (UHPC) with a low binder amount, Construction and Building Materials. 65 (2014) 140–150. https://doi.org/10.1016/j.conbuildmat.2014.04.063.

[13] M.H. Beigi, J. Berenjian, O. Lotfi Omran, A. Sadeghi Nik, I.M. Nikbin, An experimental survey on combined effects of fibers and nanosilica on the mechanical, rheological, and durability properties of self-compacting concrete, Materials & Design. 50 (2013) 1019–1029. https://doi.org/10.1016/j.matdes.2013.03.046.

[14] R.P. Feynman, There's plenty of room at the bottom, California Institute of Technology, Engineering and Science Magazine. (1960).

[15] P. Iqbal, J.A. Preece, P.M. Mendes, Nanotechnology: The "Top-Down" and "Bottom-Up" Approaches, Supramolecular Chemistry: From Molecules to Nanomaterials. (2012).

[16] P.N. Balaguru, Nanotechnology and concrete: Background, opportunities and challenges, in: Applications of Nanotechnology in Concrete Design: Proceedings of the International Conference Held at the University of Dundee, Scotland, UK on 7 July 2005, Thomas Telford Publishing, 2005: pp. 113–122.
[17] B. Birgisson, P. Taylor, J. Armaghani, S.P. Shah, American road map for research for nanotechnology-based concrete materials, Transportation Research Record. 2142 (2010) 130–137.
[18] U. Sharma, L.P. Singh, B. Zhan, C.S. Poon, Effect of particle size of nanosilica on microstructure of C-S-H and its impact on mechanical strength, Cement and Concrete Composites. 97 (2019) 312–321. https://doi.org/10.1016/j.cemconcomp.2019.01.007.
[19] S. Haruehansapong, T. Pulngern, S. Chucheepsakul, Effect of the particle size of nanosilica on the compressive strength and the optimum replacement content of cement mortar containing nano-SiO2, Construction and Building Materials. 50 (2014) 471–477. https://doi.org/10.1016/j.conbuildmat.2013.10.002.
[20] I. Flores, K. Sobolev, L.M. Torres-Martinez, E.L. Cuellar, P.L. Valdez, E. Zarazua, Performance of Cement Systems with Nano-$SiO_2$ Particles Produced by Using the Sol–Gel Method:, Transportation Research Record. (2010). https://doi.org/10.3141/2141-03.
[21] G. Quercia, H.J.H. Brouwers, Application of nano-silica (nS) in concrete mixtures, in: n.d.
[22] I.A. Rahman, V. Padavettan, Synthesis of silica nanoparticles by sol-gel: size-dependent properties, surface modification, and applications in silica-polymer nanocomposites—a review, Journal of Nanomaterials. 2012 (2012).
[23] M. Sarikaya, T. Depci, R. Aydogmus, A. Yucel, N. Kizilkaya, Production of Nano Amorphous $SiO_2$ from Malatya Pyrophyllite, IOP Conf. Ser.: Earth Environ. Sci. 44 (2016) 052004. https://doi.org/10.1088/1755-1315/44/5/052004.
[24] L.P. Singh, S.K. Bhattacharyya, G. Mishra, S. Ahalawat, Functional role of cationic surfactant to control the nano size of silica powder, Applied Nanoscience. 1 (2011) 117–122.
[25] C. Real, M.D. Alcala, J.M. Criado, Preparation of silica from rice husks, Journal of the American Ceramic Society. 79 (1996) 2012–2016.
[26] A. Lazaro, H.J.H. Brouwers, G. Quercia, J.W. Geus, The properties of amorphous nano-silica synthesized by the dissolution of olivine, Chemical Engineering Journal. 211 (2012) 112–121.
[27] N. Thuadaij, A. Nuntiya, Synthesis and characterization of nanosilica from rice husk ash prepared by precipitation method, J. Nat. Sci. Special Issue on Nanotechnology. 7 (2008) 59–65.
[28] P.K. Jal, M. Sudarshan, A. Saha, S. Patel, B.K. Mishra, Synthesis and characterization of nanosilica prepared by precipitation method, Colloids and Surfaces A: Physicochemical and Engineering Aspects. 240 (2004) 173–178. https://doi.org/10.1016/j.colsurfa.2004.03.021.
[29] Q. Lei, J. Guo, A. Noureddine, A. Wang, S. Wuttke, C.J. Brinker, W. Zhu, Sol–Gel-Based Advanced Porous Silica Materials for Biomedical Applications, Advanced Functional Materials. n/a (n.d.) 1909539. https://doi.org/10.1002/adfm.201909539.
[30] R. Ciriminna, A. Fidalgo, V. Pandarus, F. Béland, L.M. Ilharco, M. Pagliaro, The Sol–Gel Route to Advanced Silica-Based Materials and Recent Applications, (2013). https://doi.org/10.1021/cr300399c.
[31] L.L. Hench, J.K. West, The sol-gel process, Chem. Rev. 90 (1990) 33–72. https://doi.org/10.1021/cr00099a003.

[32] U. Schubert, N. Huesing, A. Lorenz, Hybrid Inorganic-Organic Materials by Sol-Gel Processing of Organofunctional Metal Alkoxides, Chem. Mater. 7 (1995) 2010–2027. https://doi.org/10.1021/cm00059a007.
[33] W. Stöber, A. Fink, E. Bohn, Controlled growth of monodisperse silica spheres in the micron size range, Journal of Colloid and Interface Science. 26 (1968) 62–69. https://doi.org/10.1016/0021-9797(68)90272-5.
[34] G. Land, D. Stephan, The influence of nano-silica on the hydration of ordinary Portland cement, J Mater Sci. 47 (2012) 1011–1017. https://doi.org/10.1007/s10853-011-5881-1.
[35] Noor-ul-Amin, S. Alam, S. Gul, K. Muhammad, Hydration mechanism of tricalcium silicate (alite), Advances in Cement Research. (2015). https://doi.org/10.1680/adcr.11.00061.
[36] J.W. Bullard, H.M. Jennings, R.A. Livingston, A. Nonat, G.W. Scherer, J.S. Schweitzer, K.L. Scrivener, J.J. Thomas, Mechanisms of cement hydration, Cement and Concrete Research. 41 (2011) 1208–1223. https://doi.org/10.1016/j.cemconres.2010.09.011.
[37] S. Brunauer, M. Yudenfreund, I. Odler, J. Skalny, Hardened portland cement pastes of low porosity VI. Mechanism of the hydration process, Cement and Concrete Research. 3 (1973) 129–147. https://doi.org/10.1016/0008-8846(73)90043-4.
[38] B.-W. Jo, C.-H. Kim, G. Tae, J.-B. Park, Characteristics of cement mortar with nano-SiO2 particles, Construction and Building Materials. 21 (2007) 1351–1355. https://doi.org/10.1016/j.conbuildmat.2005.12.020.
[39] L. Wadso, The study of cement hydration by isothermal calorimetry, Building Materials, Lund University, Sweden. (1995).
[40] L.J. Parrott, M. Geiker, W.A. Gutteridge, D. Killoh, Monitoring Portland cement hydration: Comparison of methods, Cement and Concrete Research. 20 (1990) 919–926. https://doi.org/10.1016/0008-8846(90)90054-2.
[41] S. Garrault, E. Finot, E. Lesniewska, A. Nonat, Study of C-S-H growth on C3S surface during its early hydration, Mat. Struct. 38 (2005) 435–442. https://doi.org/10.1007/BF02482139.
[42] S. Lesko, E. Lesniewska, A. Nonat, J.-C. Mutin, J.-P. Goudonnet, Investigation by atomic force microscopy of forces at the origin of cement cohesion, Ultramicroscopy. 86 (2001) 11–21. https://doi.org/10.1016/S0304-3991(00)00091-7.
[43] H.N. Stein, J.M. Stevels, Influence of silica on the hydration of 3CaO, $SiO_2$, Journal of Applied Chemistry. 14 (1964) 338–346.
[44] Y. Reches, Nanoparticles as concrete additives: Review and perspectives, Construction and Building Materials. 175 (2018) 483–495. https://doi.org/10.1016/j.conbuildmat.2018.04.214.
[45] Y. Reches, K. Thomson, M. Helbing, D.S. Kosson, F. Sanchez, Agglomeration and reactivity of nanoparticles of $SiO_2$, $TiO_2$, $Al_2O_3$, $Fe_2O_3$, and clays in cement pastes and effects on compressive strength at ambient and elevated temperatures, Construction and Building Materials. 167 (2018) 860–873. https://doi.org/10.1016/j.conbuildmat.2018.02.032.
[46] T.-P. Chang, J.-Y. Shih, K.-M. Yang, T.-C. Hsiao, Material properties of portland cement paste with nano-montmorillonite, J Mater Sci. 42 (2007) 7478–7487. https://doi.org/10.1007/s10853-006-1462-0.
[47] M. Stefanidou, E.-C. Tsardaka, E. Pavlidou, Influence of nano-silica and nano-alumina in lime-pozzolan and lime-metakaolin binders, Materials Today: Proceedings. 4 (2017) 6908–6922. https://doi.org/10.1016/j.matpr.2017.07.020.
[48] S.M.A. El-Gamal, S.A. Abo-El-Enein, F.I. El-Hosiny, M.S. Amin, M. Ramadan, Thermal resistance, microstructure and mechanical properties of type I Portland cement pastes

containing low-cost nanoparticles, J Therm Anal Calorim. 131 (2018) 949–968. https://doi.org/10.1007/s10973-017-6629-1.
[49] A.K. Santra, P. Boul, X. Pang, Influence of Nanomaterials in Oilwell Cement Hydration and Mechanical Properties, in: Society of Petroleum Engineers, 2012. https://doi.org/10.2118/156937-MS.
[50] A. Bagheri, T. Parhizkar, H. Madani, A.M. Raisghasemi, The influence of different preparation methods on the aggregation status of pyrogenic nanosilicas used in concrete, Mater Struct. 46 (2013) 135–143. https://doi.org/10.1617/s11527-012-9889-z.
[51] G. Quercia, A. Lazaro, J.W. Geus, H.J.H. Brouwers, Characterization of morphology and texture of several amorphous nano-silica particles used in concrete, Cement and Concrete Composites. 44 (2013) 77–92. https://doi.org/10.1016/j.cemconcomp.2013.05.006.
[52] K. Okuyama, I.W. Lenggoro, Preparation of nanoparticles via spray route, Chemical Engineering Science. 58 (2003) 537–547.
[53] B.L. Cushing, V.L. Kolesnichenko, C.J. O'Connor, Recent advances in the liquid-phase syntheses of inorganic nanoparticles, Chemical Reviews. 104 (2004) 3893–3946.
[54] H. Zhang, L. Tang, L. Zhou, C. Eger, Z. Zhang, Comparative study on the optical, surface mechanical and wear resistant properties of transparent coatings filled with pyrogenic and colloidal silica nanoparticles, Composites Science and Technology. 71 (2011) 471–479.
[55] M.A. Akl, H.F. Aly, H.M.A. Soliman, A. El-Rahman, A.I. Abd-Elhamid, Preparation and characterization of silica nanoparticles by wet mechanical attrition of white and yellow sand, J Nanomed Nanotechnol. 4 (2013) 2.
[56] M.N. Rahaman, Ceramic Processing and Sintering. 1995, NY: Marcel Dekker Inc. (1995) 10.
[57] J. Wen, G.L. Wilkes, Organic/Inorganic Hybrid Network Materials by the Sol−Gel Approach, Chem. Mater. 8 (1996) 1667–1681. https://doi.org/10.1021/cm9601143.
[58] H. Schmidt, H. Scholze, A. Kaiser, Principles of hydrolysis and condensation reaction of alkoxysilanes, Journal of Non-Crystalline Solids. 63 (1984) 1–11. https://doi.org/10.1016/0022-3093(84)90381-8.
[59] C.J. Brinker, G.W. Scherer, Sol-gel science: the physics and chemistry of sol-gel processing, Academic press, 2013.
[60] K. Nakanishi, Pore Structure Control of Silica Gels Based on Phase Separation, Journal of Porous Materials. 4 (1997) 67–112. https://doi.org/10.1023/A:1009627216939.
[61] E.J.A. Pope, J.D. Mackenzie, Theoretical modelling of the structural evolution of gels, Journal of Non-Crystalline Solids. 101 (1988) 198–212. https://doi.org/10.1016/0022-3093(88)90155-X.
[62] L. Senff, J.A. Labrincha, V.M. Ferreira, D. Hotza, W.L. Repette, Effect of nano-silica on rheology and fresh properties of cement pastes and mortars, Construction and Building Materials. 23 (2009) 2487–2491. https://doi.org/10.1016/j.conbuildmat.2009.02.005.
[63] M. Berra, F. Carassiti, T. Mangialardi, A.E. Paolini, M. Sebastiani, Effects of nanosilica addition on workability and compressive strength of Portland cement pastes, Construction and Building Materials. 35 (2012) 666–675.
[64] G. Quercia, G. Hüsken, H.J.H. Brouwers, Water demand of amorphous nano silica and its impact on the workability of cement paste, Cement and Concrete Research. 42 (2012) 344–357. https://doi.org/10.1016/j.cemconres.2011.10.008.

[65] J.J. Thomas, H.M. Jennings, J.J. Chen, Influence of nucleation seeding on the hydration mechanisms of tricalcium silicate and cement, The Journal of Physical Chemistry C. 113 (2009) 4327–4334.
[66] J.J. Gaitero, I. Campillo, A. Guerrero, Reduction of the calcium leaching rate of cement paste by addition of silica nanoparticles, Cement and Concrete Research. 38 (2008) 1112–1118.
[67] J. Björnström, A. Martinelli, A. Matic, L. Börjesson, I. Panas, Accelerating effects of colloidal nano-silica for beneficial calcium–silicate–hydrate formation in cement, Chemical Physics Letters. 392 (2004) 242–248.
[68] D. Kong, X. Du, S. Wei, H. Zhang, Y. Yang, S.P. Shah, Influence of nano-silica agglomeration on microstructure and properties of the hardened cement-based materials, Construction and Building Materials. 37 (2012) 707–715. https://doi.org/10.1016/j.conbuildmat.2012.08.006.
[69] F. Torabian Isfahani, E. Redaelli, W. Li, Y. Sun, Effects of Nanosilica on Early Age Stages of Cement Hydration, Journal of Nanomaterials. 2017 (2017) 4687484. https://doi.org/10.1155/2017/4687484.
[70] M. Rupasinghe, R. San Nicolas, P. Mendis, M. Sofi, T. Ngo, Investigation of strength and hydration characteristics in nano-silica incorporated cement paste, Cement and Concrete Composites. 80 (2017) 17–30.
[71] K. Sobolev, I. Flores, L.M. Torres-Martinez, P.L. Valdez, E. Zarazua, E.L. Cuellar, Engineering of SiO 2 nanoparticles for optimal performance in nano cement-based materials, in: Nanotechnology in Construction 3, Springer, 2009: pp. 139–148.
[72] G. Shakhmenko, I. Juhnevica, A. Korjakins, Influence of sol-gel nanosilica on hardening processes and physically-mechanical properties of cement paste, Procedia Engineering. 57 (2013) 1013–1021.
[73] S.A.E. Aleem, M. Heikal, W.M. Morsi, Hydration characteristic, thermal expansion and microstructure of cement containing nano-silica, Construction and Building Materials. 59 (2014) 151–160.
[74] A.M. Said, M.S. Zeidan, M.T. Bassuoni, Y. Tian, Properties of concrete incorporating nano-silica, Construction and Building Materials. 36 (2012) 838–844.
[75] H. Li, H. Xiao, J. Yuan, J. Ou, Microstructure of cement mortar with nano-particles, Composites Part B: Engineering. 35 (2004) 185–189.
[76] A. Nazari, S. Riahi, The effects of $SiO_2$ nanoparticles on physical and mechanical properties of high strength compacting concrete, Composites Part B: Engineering. 42 (2011) 570–578.
[77] P. Hou, S. Kawashima, D. Kong, D.J. Corr, J. Qian, S.P. Shah, Modification effects of colloidal nanoSiO2 on cement hydration and its gel property, Composites Part B: Engineering. 45 (2013) 440–448.
[78] L.P. Singh, S.K. Bhattacharyya, G. Mishra, S. Ahalawat, Reduction of calcium leaching in cement hydration process using nanomaterials, Materials Technology. 27 (2012) 233–238.
[79] H.J. Du, S.D. Pang, Effect of colloidal nano-silica on the mechanical and durability performances of mortar, in: Key Engineering Materials, Trans Tech Publ, 2015: pp. 443–448.
[80] J. Zhang, G.W. Scherer, Comparison of methods for arresting hydration of cement, Cement and Concrete Research. 41 (2011) 1024–1036.
[81] J.M. Makar, T. Sato, The effect of drying method on ordinary Portland cement surfaces during the early stages of hydration, Materials and Structures. 46 (2013) 1–12.

[82] E.M. Johansson, Controlling the pore size and morphology of mesoporous silica, Linköping University Electronic Press, 2010.
[83] C.A. Milea, C. Bogatu, A. Duta, The influence of parameters in silica sol-gel process, Bulletin of the Transilvania University of Brasov. Engineering Sciences. Series I. 4 (2011) 59.
[84] A. Soleimani Dorcheh, M.H. Abbasi, Silica aerogel; synthesis, properties and characterization, Journal of Materials Processing Technology. 199 (2008) 10–26. https://doi.org/10.1016/j.jmatprotec.2007.10.060.
[85] D.A. Donatti, A.I. Ruiz, D.R. Vollet, A dissolution and reaction modeling for hydrolysis of TEOS in heterogeneous TEOS–water–HCl mixtures under ultrasound stimulation, Ultrasonics Sonochemistry. 9 (2002) 133–138. https://doi.org/10.1016/S1350-4177(01)00120-1.
[86] H.D. COGAN, C.A. SETTERSTROM, Properties of Ethyl Silicate, Chem. Eng. News Archive. 24 (1946) 2499–2501. https://doi.org/10.1021/cen-v024n018.p2499.
[87] P. Innocenzi, From a Sol to a Gel, in: P. Innocenzi (Ed.), The Sol-to-Gel Transition, Springer International Publishing, Cham, 2019: pp. 21–37. https://doi.org/10.1007/978-3-030-20030-5_3.
[88] I.A. Rahman, P. Vejayakumaran, C.S. Sipaut, J. Ismail, M.A. Bakar, R. Adnan, C.K. Chee, An optimized sol–gel synthesis of stable primary equivalent silica particles, Colloids and Surfaces A: Physicochemical and Engineering Aspects. 294 (2007) 102–110. https://doi.org/10.1016/j.colsurfa.2006.08.001.
[89] S.K. Park, K.D. Kim, H.T. Kim, Preparation of silica nanoparticles: determination of the optimal synthesis conditions for small and uniform particles, Colloids and Surfaces A: Physicochemical and Engineering Aspects. 197 (2002) 7–17. https://doi.org/10.1016/S0927-7757(01)00683-5.
[90] K.H. Müller, M. Motskin, A.J. Philpott, A.F. Routh, C.M. Shanahan, M.J. Duer, J.N. Skepper, The effect of particle agglomeration on the formation of a surface-connected compartment induced by hydroxyapatite nanoparticles in human monocyte-derived macrophages, Biomaterials. 35 (2014) 1074–1088.
[91] J. Jiang, G. Oberdörster, P. Biswas, Characterization of size, surface charge, and agglomeration state of nanoparticle dispersions for toxicological studies, Journal of Nanoparticle Research. 11 (2009) 77–89.
[92] E. Allen, J. Henshaw, P. Smith, A review of particle agglomeration, AEA Technology plc, 2001.
[93] B. Hanumantha Rao, N. Gangadhara Reddy, Zeta Potential and Particle Size Characteristics of Red Mud Waste, in: G.L. Sivakumar Babu, K.R. Reddy, A. De, M. Datta (Eds.), Geoenvironmental Practices and Sustainability: Linkages and Directions, Springer, Singapore, 2017: pp. 69–89. https://doi.org/10.1007/978-981-10-4077-1_8.
[94] D.P. Kodippili, E. Rezabeigi, M.R. Nokken, R. Drew, Effects of Sol-Gel Derived Nano-Silica Suspensions in Cement Paste, Special Publication. 320 (2017) 5.1-5.10.
[95] R. Bahru, A.R. Mohamed, W.-M. Yeoh, K.A. Yaacob, Electrophoretic Deposition of Carbon Nanotubes on Heat Spreader for Fabrication of Thermal Interface Materials (TIM), Sains Malaysiana. 46 (2017) 1075–1082.
[96] S. Vallar, D. Houivet, J. El Fallah, D. Kervadec, J.-M. Haussonne, Oxide slurries stability and powders dispersion: optimization with zeta potential and rheological measurements, Journal of the European Ceramic Society. 19 (1999) 1017–1021.

[97] ASTM C191-19, Test Methods for Time of Setting of Hydraulic Cement by Vicat Needle, ASTM International, 2019. https://doi.org/10.1520/C0191-19.
[98] K. Wang, Z. Ge, J. Grove, J.M. Ruiz, R. Rasmussen, T. Ferragut, Developing a simple and rapid test for monitoring the heat evolution of concrete mixtures for both laboratory and field applications, (2007).
[99] M. Moukwa, S. Farrington, D. Youn, Determination of $Ca(OH)_2$ in hydrated cement paste by differential scanning calorimetry, Thermochimica Acta. 195 (1992) 231–237.
[100] T. Kim, J. Olek, Effects of sample preparation and interpretation of thermogravimetric curves on calcium hydroxide in hydrated pastes and mortars, Transportation Research Record. 2290 (2012) 10–18.
[101] M.R. Nokken, R.D. Hooton, Using pore parameters to estimate permeability or conductivity of concrete, Materials and Structures. 41 (2008) 1.
[102] H.N. Atahan, O.N. Oktar, M.A. Taşdemir, Effects of water–cement ratio and curing time on the critical pore width of hardened cement paste, Construction and Building Materials. 23 (2009) 1196–1200.
[103] P. Pipilikaki, M. Beazi-Katsioti, The assessment of porosity and pore size distribution of limestone Portland cement pastes, Construction and Building Materials. 23 (2009) 1966–1970. https://doi.org/10.1016/j.conbuildmat.2008.08.028.
[104] M. Edrissi, M. Soleymani, M. Adinehnia, Synthesis of Silica Nanoparticles by Ultrasound-Assisted Sol-Gel Method: Optimized by Taguchi Robust Design, Chemical Engineering & Technology. 34 (2011) 1813–1819. https://doi.org/10.1002/ceat.201100195.
[105] Y.L. Verma, A.K. Gupta, R.K. Singh, S. Chandra, Preparation and characterisation of ionic liquid confined hybrid porous silica derived from ultrasonic assisted non-hydrolytic sol–gel process, Microporous and Mesoporous Materials. 195 (2014) 143–153. https://doi.org/10.1016/j.micromeso.2014.04.026.
[106] Z. Lin, Y. Wu, Y. Bi, Rapid synthesis of $SiO_2$ by ultrasonic-assisted Stober method as controlled and pH-sensitive drug delivery, Journal of Nanoparticle Research. 20 (2018) 304.
[107] T. HIROSE, K. KIHARA, M. OKUNO, S. FUJINAMI, K. SHINODA, X-ray, DTA and Raman studies of monoclinic tridymite and its higher temperature orthorhombic modification with varying temperature, Journal of Mineralogical and Petrological Sciences. 100 (2005) 55–69. https://doi.org/10.2465/jmps.100.55.
[108] Y. Feng, Q. Zhang, Q. Chen, D. Wang, H. Guo, L. Liu, Q. Yang, Hydration and strength development in blended cement with ultrafine granulated copper slag, PloS One. 14 (2019).
[109] D. Marchon, R.J. Flatt, Mechanisms of cement hydration, in: Science and Technology of Concrete Admixtures, Elsevier, 2016: pp. 129–145.
[110] P.E. MOSES, S.B. Perumal, Hydration of Cement and its Mechanisms, IOSR J Mech Civil Eng. 13 (2016) 17–31.
[111] N.C. Collier, Transition and decomposition temperatures of cement phases–a collection of thermal analysis data, Ceramics-Silikaty. 60 (2016).
[112] J.B. Jones, E.R. Segnit, Genesis of cristobalite and tridymite at low temperatures, Journal of the Geological Society of Australia. 18 (1972) 419–422.
[113] W.A. Dollase, The crystal structure at 220 C of orthorhombic high tridymite from the Steinbach meteorite, Acta Crystallographica. 23 (1967) 617–623.
[114] P.C. Schlecht, P.F. O'Connor, Third Supplement to NIOSH Manual of Analytical Methods (NMAM), US National Institute for Occupational Safety and Health, 2003.

[115] U. Foerter-Barth, U. Teipel, Characterization of particles by means of laser light diffraction and dynamic light scattering, in: Developments in Mineral Processing, Elsevier, 2000: pp. C1-1-C1-8.
[116] J.S. Belkowitz, W.B. Belkowitz, K. Nawrocki, F.T. Fisher, Impact of Nanosilica Size and Surface Area on Concrete Properties., ACI Materials Journal. 112 (2015).
[117] P. Halamickova, R.J. Detwiler, D.P. Bentz, E.J. Garboczi, Water permeability and chloride ion diffusion in portland cement mortars: Relationship to sand content and critical pore diameter, Cement and Concrete Research. 25 (1995) 790–802. https://doi.org/10.1016/0008-8846(95)00069-O.
[118] M.M.C. Canut, Pore structure in blended cement pastes, Technical University of Denmark, Department of Civil Engineering, 2011. https://orbit.dtu.dk/en/publications/pore-structure-in-blended-cement-pastes (accessed May 27, 2020).
[119] H. Ma, B. Xu, J. Liu, H. Pei, Z. Li, Effects of water content, magnesia-to-phosphate molar ratio and age on pore structure, strength and permeability of magnesium potassium phosphate cement paste, Materials & Design. 64 (2014) 497–502. https://doi.org/10.1016/j.matdes.2014.07.073.
[120] Z. Yu, G. Ye, The pore structure of cement paste blended with fly ash, Construction and Building Materials. 45 (2013) 30–35. https://doi.org/10.1016/j.conbuildmat.2013.04.012.
[121] H. Du, S. Du, X. Liu, Durability performances of concrete with nano-silica, Construction and Building Materials. 73 (2014) 705–712.